

博士論文

Development of an Expansive Agent Model for Concrete in a Multi-scale
Thermodynamic Platform based on Hydration and Microstructure
Formation (水和反応と空隙構造形成に立脚したマルチスケール型
膨張コンクリートモデルの開発)

ペン コルニアット



東京大学
THE UNIVERSITY OF TOKYO

**Development of an Expansive Agent Model
for Concrete in a Multi-scale
Thermodynamic Platform based on
Hydration and Microstructure Formation**

水和反応と空隙構造形成に立脚したマルチスケール型膨張コンクリートモデルの開発

Pen Kolneath

ペン コルニアット

Student ID: 37-187010

A thesis submitted to The University of Tokyo in partial fulfillment of
the requirements of Degree of Philosophy in Civil Engineering

Concrete Laboratory
Department of Civil Engineering
Graduate School of Engineering
The University of Tokyo

*"This thesis is dedicated to my family, who were always a source of
inspiration and endless support during this journey"*

Acknowledgments

Firstly, I would like to express my sincerest gratefulness to my supervisor, Professor Ishida Tetsuya for giving me the opportunity to conduct research at this prestigious university. Your professional advice, continuous support and consistent encouragement throughout these 5 years of both Master's and Doctoral Course has been a source of great motivation for me to become the person I am today.

Sincere appreciation is extended to the member of my supervising committee: Professor Kishi Toshiharu, Professor Noguchi Takafumi, Assistant Professor Takahashi Yuya, Assistant Professor Sakai Yuya and Assistant Professor Igarashi Go for spending their precious time to provide valuable suggestions, comments and critical ideas to enhance the content of this dissertation. Sincere thank is extended to Research Associate Ohno Motohiro and Wang Tiao for their countless help in discussions. Also, a deep gratitude to Professor Seishi Goto for his kind help in conducting the isothermal calorimetry tests and Mr.Ito Shinya from Denka Company for providing the experimental data on expansive additive to ease with my research experiments.

I also wish to show utmost gratitude to all of my colleagues, whose all names I cannot list, in the Concrete Laboratory as well as Bridge and Wind Laboratory for their freindship, help and moral support, which contributes tremendously in the completion of this dissertation.

I am also indebted to the Ministry of Education, Culture, Sports, Science and Technology of Japan (MEXT) for the provision of a scholarship to financially support myself in pursuit of my degree. I would also like to acknowledge the Denka Company Limited for the provision of necessary finance and experimental datas to support the field investigation of this research.

Last but not the least, my academic life would have been very difficult without the constant support provided by my family, my loved one and friends. Thank you for everything.

Abstract

Concrete structures, which are exposed to external climatic condition, tend to under-go shrinkage. Especially concrete structures with high surface-to-volume ratio experience the highest effect of shrinkage stress. Then, once the tensile strain caused by the shrinkage stress exceed the cracking strain, crack will occur. Consequently, deleterious ions such as chlorides and sulfates could migrate into concrete and cause immense degradation, structurally and aesthetically. This phenomenon is inevitable and has remained a major challenge in the field of civil engineering.

Up until recent times, engineers have been tackling this issue from designing, constructing and material aspects. For example, in the case of designing, structural elements with different shapes have been used. In the case of constructing, sequential constructing has been considered for bridge deck to mitigate the effect of moment distribution on the top surface. From material viewpoints, they have successfully mitigated the effect of shrinkage using shrinkage reducing admixtures, light-weight aggregates and expansive cements or expansive additive. Expansive additive has the capability to offset the shrinkage strain from reaching the cracking strain by enlarging the volume via the existence of expansive hydrates, that could be ettringites (Aft or trisulfoaluminate phase) or portlandites (calcium hydroxide) or magnesium oxide. Two major applications of expansive additives are:

1. To compensate the shrinkage of concrete due to thermal contraction; huge autogenous shrinkage; drying shrinkage.
2. To induce chemical pre-stress on pre-cast concrete elements.

Although a wide range of applications could be done with expansive concrete, there is still a lack of quantitative research to estimate the amount of expansion produced by the complex hydration of expansive additives for engineering applications. Usually, it depends on the conducted trial tests on different mix proportion and experience of engineers who have dealt with expansive concrete to estimate and judge whether the mix design and amount of expansive additive would be applicable for the concrete structures

or not. Hence, estimating the amount of expansive additive to be used without creating harmful cracks in concrete structures could be a difficult task.

On the other hand, the Concrete Laboratory of the University of Tokyo has been developing a multi-scale thermodynamic analytical platform, coded as DuCOM-COM3, with the ultimate goal of being the *lifespan simulator* of concrete structures. This computational platform consists of, first, the material counterpart, that incorporates the hydration of cement particles, micro-pore structure development, transports of multi-species and , second, non-linear structural analysis which deals with macroscopic response of structures. DuCOM[1] covers the thermodynamic multi-chemo-physical modelling part where-by numerous thermodynamic models, such as multicomponent hydration, micropore structure formation and moisture equilibrium/transport. Its counterpart, COM3[2], is a nonlinear structural 3D finite-element analysis that implements constitutive laws of uncracked/cracked and hardening/aging/matured concrete. Time-dependent properties of concrete such as elastic modulus, temperature, pore pressure, creep, moisture status, total porosity of interlayer, gel and capillary pores are calculated consequently after inputting the basic boundary conditions for a structure such as mix proportion, geometry and environmental conditions based on the micromodels of materials in-side the DuCOM system. The calculation sequence starts from multi-component heat of hydration model whereby the degree of hydration is determined through the amount of heat release by each phase in the system based on modified Arrhenius' equations. Then, the degree of hydration and mass of phases information retrieved from heat of hydration model would in turn be utilized to determine the volumetric balance and moisture status in the microstructure. Then, based on the solidification theory, time-dependent deformations such as creep and shrinkage would be superimposed to represent all the stresses existing in the cement paste matrix. Finally, models of concrete mechanics will deal with macroscopic structural responses based on the space-averaged constitutive laws on the fixed four-way cracked concrete model[2]. Verification of the analytical models to real structures have been performed throughout the years. Due to the unstable nature of expansive additive, its practice in civil engineering field is quite limited as intended advantage of shrinkage compensating could not be attained if improper usage was conducted. Thus, the authors set out to extend a multi-scale thermodynamic analytical platform, coded as DuCOM-COM3, by incorporating an expansive additive model based on crystallization pressure theory.

The first part of the study involves the experiments to investigate the behavior of expansive additive from its hydration to its volumetric expansion. In addition to that, these experimental results were also used for developing and verification of the model. Preliminarily, hydration study of both CSA and free-lime type expansive study with

100% replacement ratio of ordinary Portland cement was done through XRD-Rietveld and TGA method. Such replacement ratio was decided in order to limit the parameters under investigation and to develop the reference heat rate for hydration model. After that, the hydration degree of each reactant phase, mass of both reactant and resultant phases inside the system was determined. Furthermore, isothermal calorimetry of different replacement ratio was also conducted and its results were specifically used to verify the heat model developed based on the multi-component heat of hydration model concept. Then, expansion behavior of cement paste bars and concrete with system of ordinary Portland cement and expansive additives at different replacement ratios was studied. As the very first step towards making the expansive additive model, this study aimed at tackling the effect of expansive additive at shrinkage compensating level, which is approximately 6 percents of addition into ordinary Portland cement mix.

The second part of the study is the development of the expansive additive model from its hydration to its volumetric expansion. Based on the combined XRD-Rietveld and TGA method to determine the degree of hydration of the phases in expansive additive, the reference heat rate for respective phases were determined and implemented as an extension on the multi-component heat of hydration model. Based on the hydration degree, the microstructure of cement matrix is formed whereby fractional volume of expansive hydrates, calcium hydroxide and ettringites, could be determined. However, not all of the volume of the expansive hydrates are accounted for expansion. In fact, only the volume of expansive hydrates after adjacent particle contacts have been made would contribute in expansion. Then, as an initial step, the macroscopic expansive stress was expressed as linear isotropic pressure based upon upscaling through poromechanics from the local crystallization pressure of the expansive additive hydrates' crystals. Superimposing with the existing solidification model, which determines the creep and shrinkage of both cement paste and aggregates, this system of calculation could capture the behavior of both expansion and shrinkage of cement matrix based on the initial chemical composition of the binder. However, there was a limitation in this isotropic model as it could not capture the behavior of expansive cement pastes or concretes under restraints properly. Therefore, an investigation into using the ASR poromechanical model based on 2-phase Biot theorem was done.

The third part of the study is the implementation of ASR poromechanical model to simulate the effect of both restrained and unrestrained condition of expansive additive concrete. Due to the similar nature of expansion between ASR and expansive additive, as the scale of reaction and mechanism of expansion is closely related, it could be reasonably feasible to apply the ASR poromechanical model for expansive additives. By adapting the ASR poromechanical model to reflect the anisotropic behavior due to precipitation

space when system is restrained, the model could capture the restrained effect in a more appropriate manner in uniaxial condition.

List of Symbol

The following abbreviations have been used in this thesis: $C = \text{CaO}$; $A = \text{Al}_2\text{O}_3$; $S = \text{SiO}_2$; $\bar{S} = \text{SO}_3$; $F = \text{Fe}_2\text{O}_3$; $H = \text{H}_2\text{O}$

OPC	= Ordinary Portland cement
CSA	= Calcium sulfoaluminate
$3\text{CaO} \cdot \text{Al}_2\text{O}_3 \cdot 3\text{CaSO}_4 \cdot 32\text{H}_2\text{O}$	= Ettringite
$3\text{CaO} \cdot \text{Al}_2\text{O}_3 \cdot \text{CaSO}_4 \cdot 12\text{H}_2\text{O}$	= Monosulfate
$C\bar{S}H_2$	= Gypsum
$C\bar{S}H_{0.5}$	= Hemihydrate
$C\bar{S}$	= Anhydrite
CaO	= Free lime
$C_4A_3\bar{S}$	= $4\text{CaO} \cdot 3\text{Al}_2\text{O}_3 \cdot \text{SO}_3$
C_3S	= $3\text{CaO} \cdot \text{SiO}_2$
C_2S	= $2\text{CaO} \cdot \text{SiO}_2$
C_3A	= $3\text{CaO} \cdot \text{Al}_2\text{O}_3$
C_4AF	= $4\text{CaO} \cdot \text{Al}_2\text{O}_3 \cdot \text{Fe}_2\text{O}_3$

Contents

Abstract	ii
List of Symbol	vii
Contents	ix
List of Figures	xiii
List of Tables	xviii
1 Introduction	2
1.1 Research Background	2
1.2 Research objectives	4
1.3 Organization of thesis	4
2 Literature Review	6
2.1 Introduction	6
2.2 Background information on expansive additives	6
2.3 Factors involving macroscopic expansion of expansive additive system	7
2.3.1 Hydration mechanism	7
2.3.2 Expansion mechanism	9
2.3.3 Other worth-mentioning phenomena relating to ettringite and port- landite formation in $C_4A_3\bar{S} - C - C\bar{S}H_2$ system	11
2.3.4 Current existing models for expansive additives	11
2.4 Conclusion	12
3 Overview of thermodynamic analytical platform - DuCOM-COM3	13
3.1 Durability COConcrete Model (DuCOM)	14
3.1.1 Overview of the computational system - DuCOM	14
3.1.2 Multi-component hydration model	14

3.1.3	Pore-structure development model	18
3.1.4	Model of moisture transport and thermodynamic equilibrium	23
3.1.5	Multi-scale constitutive model	28
3.2	Nonlinear mechanics of reinforced concrete computational system (COM3)	50
3.2.1	Overall composition of the model including cracks	51
4	Experimental Investigation on Expansive Additives	53
4.1	Introduction	53
4.2	Experimental Programme	54
4.2.1	Materials	54
4.2.2	X-ray Diffraction and Thermogravimetric Experiment	54
4.2.3	Isothermal conduction calorimetry	59
4.2.4	Unrestrained expansion of expansive cement paste	65
4.3	Conclusion	67
5	Thermodynamic Modeling of Expansive Additives	69
5.1	Introduction	69
5.2	Overview of expansive additive modeling framework	70
5.3	Hydration of expansive phases	70
5.3.1	Thermal activity of expansive additive phases	71
5.3.2	Reference heat rate of expansive additive phases	71
5.3.3	Results based on the newly installed hydration model for expansive	
	additives	75
5.4	Micro-structure formation of expansive additives and OPC system	77
5.5	Local crystallization pressure	78
5.5.1	Determination of Saturation Index (SI)	79
5.6	Upscaling of local crystallization pressure to macroscopic crystallization stress	81
5.7	Analyses of macroscopic expansion based on crystallization pressure	82
5.8	Limitation of the current linear isotropic model of crystallization pressure	84
5.9	Conclusion	85
6	Poromechanical model to express anisotropic behavior	87
6.1	Introduction	87
6.2	Expansion from Alkali-silica reaction versus Expansive additive	88
6.3	Current model in DuCOM regarding Alkali-silica reaction	88
6.4	Adaptation of Alkali-silica reaction poromechanical model for Expansive	
	additive expansion model	90

6.4.1	A factor expressing the free precipitation space of expansive hy-	
	drates under external restraint, β	90
6.4.2	Analytical results	93
6.5	Conclusion	98
7	Conclusion	99
8	Appendix	103
8.1	Effect of temperature	103
8.2	Chemical prestress	105
8.3	Interaction between expansive additive and cement phases	106
	Bibliography	109

List of Figures

1.1 Schematic illustrating the moment of cracking due to tensile strain development	3
2.1 Schematic diagram of the expansion process of $C_4A_3\bar{S}$ phase by Ogawa and Roy [12]	10
3.1 Reference heat rate of each mineral	16
3.2 Solidifying clusters of cement paste and aging	34
3.3 Effects of temperature and moisture status in gel pores on visco-plastic strain	39
3.4 Driving force of shrinkage under low and high RH	43
3.5 Effect of cement particle distribution by w/c and its contribution to hydration shrinkage	45
3.6 Relationship between aggregate shrinkage and aggregate saturation	46
3.7 Conceptual diagram of cracks in RC from the constitutive modeling	51
4.1 Experimental results for expansive additives: PCSA with replacement ratio of 100%	57
4.2 Experimental results for expansive additives: #20 with replacement ratio of 100%	57
4.3 Experimental results for expansive additives: PCSA-OPC system with replacement ratio of 50%	58
4.4 Experimental results for expansive additives: #20-OPC system with replacement ratio of 50%	59
4.5 Isothermal calorimetry results after 30 minutes from the specimens inserting moment; (a) Heat rate & (b) Accumulated heat & (c) Degree of hydration by diving with the theoretical maximum heat release of HyperExpanded binders	62

4.6	Isothermal calorimetry results after 30 minutes from the specimens inserting moment; (a) Heat rate & (b) Accumulated heat & (c) Degree of hydration by diving with the theoretical maximum heat release of pcsa-blended binders	63
4.7	Isothermal calorimetry results after 30 minutes from the specimens inserting moment; (a) Heat rate & (b) Accumulated heat & (c) Degree of hydration by diving with the theoretical maximum heat release of #20-blended binders	64
4.8	Unrestrained $4 \times 4 \times 16$ cm ³ cement paste of ordinary Portland cement and Taiheyo HyperExpan expansive additive system	66
4.9	Unrestrained $4 \times 4 \times 16$ cm ³ cement paste of ordinary Portland cement and Denka #20 expansive additive system	67
5.1	Proposed expansive additive modeling framework	70
5.2	Hydration degree of expansive additive phases in 100% replacement ratio of Denka PCSA	72
5.3	Process of determining reference heat rate for expansive additive phases	73
5.4	Reference heat rate of expansive additive phases installed in the multi-component hydration heat model	74
5.5	Verification of XRD results versus the analytical results from DuCOM	75
5.6	Verification of XRD results [(1) and (2) from Morioka [21]; (3) and (4) from Denka internal report] versus the analytical results from DuCOM	76
5.7	Verification of isothermal calorimetric results versus the analytical results from DuCOM	77
5.8	Original and proposed microstructure model of ordinary Portland cement and expansive additive system	78
5.9	Dissolution and precipitation process of cement clinker and expansive additive phases	79
5.10	Mass of unhydrated and hydrated phase in OPC-CSA system with: a) 0% CSA (0% Hauyne) b) 7% CSA (1.4% Hauyne) c) 15% CSA (3% Hauyne) and d) 30% CSA (6% Hauyne) [from Chaunsali and Mondal [56]]	80
5.11	(a) Saturation Index of ettringites based on different contents of Hauyne [from Chaunsali and Mondal [56]] (b) Fictitious Saturation Index of Ettringites (c) Fictitious Saturation Index of CH	81
5.12	Superimposition of crystallization stress on the expansive cement matrix	82

5.13 Analytical and experimental results on unrestrained $4 \times 4 \times 16$ cm ³ cement paste of ordinary Portland cement and Taiheyo HyperExpan expansive additive system	83
5.14 Analytical and experimental results on unrestrained $4 \times 4 \times 16$ cm ³ cement paste of ordinary Portland cement and Denka #20 expansive additive system	83
5.15 Analytical and experimental results on concrete under JIS-A-6202 Standard ($10 \times 10 \times 40$ cm ³ with 0.97% of reinforcement ratio)	84
5.16 Effect of reinforcement on restrained expansion at different replacement ratio based on Expan expansive additive[60]	85
6.1 Analytical results to display the effect of β parameter, redrawn from Taka- hashi et al. [69]	89
6.2 Overview calculation scheme of ASR gel generations and stress formations [68], [69, 70, 71]	90
6.3 Anisotropy model expression for expansive additive system	91
6.4 Tentative β parameter to express the anisotropic behavior	92
6.5 Analytical and experimental results on unrestrained $4 \times 4 \times 16$ cm ³ cement paste of ordinary Portland cement and Taiheyo HyperExpan expansive additive system (Poromechanical Model)	93
6.6 Analytical and experimental results on unrestrained $4 \times 4 \times 16$ cm ³ cement paste of ordinary Portland cement and Denka #20 expansive additive sys- tem (Poromechanical Model)	93
6.7 Analytical and experimental results on concrete under JIS-A-6202 Standard ($10 \times 10 \times 40$ cm ³ with 0.97% of reinforcement ratio (Poromechanical)) . . .	94
6.8 Analytical and experimental results on concrete under JIS-A-6202 Stan- dard ($10 \times 10 \times 40$ cm ³ with 0.97% of reinforcement ratio with water curing condition at different temperatures (Poromechanical))	95
6.9 Analytical and experimental results on lime-based expansive additive by Tsuji no et al. [74] (Poromechanical Model)	96
6.10 Analytical and experimental results on Denka#20 expansive additive by NGUYEN et al. [75] (Poromechanical Model)	97
6.11 Effect of reinforcement on restrained expansion at different replacement ratio based on Expan expansive additive[60] (PoromechanicalModel)	97
7.1 Overall modeling framework of expansive additives	102

8.1	(a) Total volume of expansive hydrates focusing on modified heat rate for 10°C; (b) Total volume of expansive additive at 10, 20 and 30°C; (c) Effective expansive hydrates i.e. expansive hydrates after particle contact; (d) Effective expansive hydrates i.e. expansive hydrates after particle contact with the modified heat rate increment for 10°C	103
8.2	(a) Current simulated results due to the effect of temperature based on current expansive additive model (b) Modified simulated results due to the effect of temperature based on current expansive additive model (by increasing the heat rate of expansive additive hydration at lower temperature)	105
8.3	Simulated versus experimental chemical prestress based on experiment conducted by Oshio et al. [78]	106
8.4	Interaction between cement and expansive additive phases. (a) and (b) are experimental results redrawn from Morioka [21]; (c) and (d) are analytical results from DuCOM's simulations	108

List of Tables

2.1	Stoichiometric equations for Aft formation by Hauyne	7
2.2	Stoichiometric equations for Afm formation by Hauyne	7
2.3	Stoichiometric equations for Afm formation by Hauyne(sulfate source depletion)	8
2.4	Stoichiometric equations for Aft formation by Hauyne (non-expansive)	8
2.5	Stoichiometric equations for Portlandite formation from Free-lime	8
2.6	Stoichiometric equations for hydration of C_3S	9
3.1	Summary of the calculated solid phase volume change	48
4.1	Chemical composition in - (1) Power-CSA (pcsa) & (2) #20	54
4.2	Mineral composition in - (1) Power-CSA (pcsa) & (2) #20 & (3) OPC	54
4.3	Standard enthalpies of formation of clinker phases (J/g)	60
8.1	Mineral composition in - (1) CSA & (2) FL Expansive additive	107

Chapter 1

Introduction

Contents

1.1 Research Background	2
1.2 Research objectives	4
1.3 Organization of thesis	4

1.1 Research Background

Concrete structures, which are exposed to external climatic condition, tend to undergo shrinkage. Especially concrete structures with high surface-to-volume ratio experience the highest effect of shrinkage stress. Then, once the tensile strain caused by the shrinkage stress exceed the cracking strain, crack will occur as shown in [Figure 1.1](#). Consequently, deleterious ions such as chlorides and sulfates could migrate into concrete and cause immense degradation, structurally and aesthetically. This phenomenon is inevitable and has remained a major challenge in the field of civil engineering.

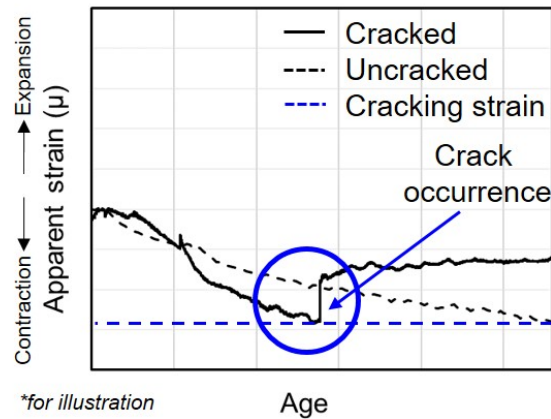


Figure 1.1: Schematic illustrating the moment of cracking due to tensile strain development

Up until recent times, engineers have been tackling this issue from designing, constructing and material aspects. For example, in the case of designing, structural elements with different shapes have been used. In the case of constructing, sequential constructing have been considered for bridge deck to mitigate the effect of moment distribution on the top surface. From material viewpoints, they have successfully mitigate the effect of shrinkage through the use of shrinkage reducing admixtures, light-weight aggregates and expansive cements.

Some expansive cements have been studied in the form of sustainable cements, which have been in the spotlight for the past few decades due to our concerns of massive CO_2 emission from ordinary Portland cement. Around 5% of global man-made CO_2 emission is produced by combustion of fuels for clinkering process to manufacture Portland cement. Tremendous efforts have been invested in the development and undermining the various mechanism of calcium sulfoaluminate (CSA) cement in the last few decades. Its mechanism to create shrinkage compensating effect from early-age volume change have been exploited and heavily studied. As a matter of fact, it has been generally accepted that the expansion mechanism is dependent on the development of compressive stress in its early-age hydration under both external and internal restraints. Even with all these benefits, doubts still exist regarding the its usage mostly due to its unstable nature once overdose of expansive additives have been used, which could instead cause harmful delayed expansion to the structures. Practically, there have been cases with the use of expansive additives in real structures. However, the usage still requires extensive experimental resources to ensure the maximum safety from crack occurrence by the delayed expansion. Thus, we need an analytical model that could ease and promote the usage of expansive additives to their full capability without expressing too much of their drawbacks.

1.2 Research objectives

To achieve the rational design, construction and maintenance of concrete structures, prediction of the performance of structures throughout their lifespan is crucial, which starts from the beginning of the hydration reaction to the end of their service life, with consideration of various material and mix proportions, structural dimensions and curing and environmental conditions. On the other hand, aiming for a unified approach to the evaluation of the behaviour of concrete structures in various conditions, the Concrete Laboratory of the University of Tokyo has been working to develop a multiscale integrated analysis platform, DuCOM-COM3 [1]. The platform consists of two systems: a thermodynamic coupled analysis system, DuCOM, which integrates various micro-physical-chemical-based models of cementitious composites, and a nonlinear dynamic RC structure analysis system COM3, which deals with macroscopic mechanical responses and damage to RC structures. With using only simple inputs such as such as mix proportions, structural geometry and boundary conditions in terms of history of environmental exposure of the structure, DuCOM-COM3 attempts to tackle the physio-chemical properties of concrete structures from its young age onward while also incorporate various ion transport phenomena for future performance-based durability design. The main objectives of this study are unfolded into three main part: hydration, microstructure and expansive stress.

1.3 Organization of thesis

This thesis aims to investigate the chemo-mechanical factors influencing the early-age volume change of cement systems with expansive additives. Broadly speaking, the thesis is organized into three major parts: hydration, microstructure and expansive pressure of ordinary Portland cement and expansive additive paste system. A in-depth literature review on early-age hydration and expansion mechanism of expansive additive system is delivered in Chapter 2. Chemo-mechanical phenomena involving the expansion action and modeling of expansive stress are discussed. Since the motivation behind this study was to extend the capability of the current thermodynamic platform of calculation, DuCOM-COM3, by incorporating an expansive additive model to estimate the amount of expansion in a system of cement paste and expansive additives, it is necessary to present an overview of the state-of-the-art analytical models in Chapter 3. In a more specific explanation, the hydration, microstructure, moisture equilibrium, cement paste solidification and constitutive lawas of non-linear reinforced concrete are discussed in a summarized manner. In order to see the hydration and expansion behavior of expansive additive and ordinary Portland cement behavior, numerous experiments were conducted ranging from

X-Ray Diffraction, Thermogravimetric analysis, Rietveld analysis, Isothermal calorimetry and Strain Measurement via embedded strain gages, which are presented in Chapter 4. Chapter 5 marks the beginning of the discussion of expansive additive model, extension of multi-component of hydration and microstructure model, originally proposed by Kishi and Maekawa [3], by adding the expansive additive phases, namely, Free-lime, Hauyne and Anhydrite. The application of crystallization stress via crystallization pressure based on Poromechanics is also presented in Chapter 5. As linear isotropic crystallization stress could not represent the distribution of stress under anisotropy, Chapter 6 shows that application of poromechanical model based on 2-phase Biot theorem, which have been used to model ASR expansion, could be applicable for anisotropic expression of expansive concrete under restrained conditions. Finally, Chapter 7 presents the conclusions and propose the future work.

Chapter 2

Literature Review

Contents

2.1 Introduction	6
2.2 Background information on expansive additives	6
2.3 Factors involving macroscopic expansion of expansive additive system	7
2.3.1 Hydration mechanism	7
2.3.2 Expansion mechanism	9
2.3.3 Other worth-mentioning phenomena relating to ettringite and portlandite formation in $C_4A_3\bar{S} - C - C\bar{S}H_2$ system	11
2.3.4 Current existing models for expansive additives	11
2.4 Conclusion	12

2.1 Introduction

This chapter aims to provide the necessary background information on expansive additives starting with its origin and current application in construction industry as well as other applications. Then, thorough literature reviews on its hydration mechanism, microstructural formation and expansive characteristics would be provided. These literature reviews would provide us with a strong base that leads to various assumptions for modeling the expansive additives.

2.2 Background information on expansive additives

The story of expansive additive dates back to the late 1900s with the origin from the study of ettringite in cement. It was noted by Michaelis that the expansive destruction of Portland cement concrete in the presence of sulfate content was accounted by formation of ettringites [4]. Then, Lossier and Caguol [5] took the first leap in exploiting the benefits of ettringite by purposefully introducing chemical prestress via external expansive agent intergrinding with Portland cement blended concrete in the 1930s. Then, through investigating Lossier's study, Lafuma [6] concluded that it was not necessary to produce such an expansive component for expansion as the development of ettringite could be done through hydration of Portland cement clinkers and anhydrite or gypsum as sulfate source as well. Finally, Klein and Troxell [7] succeeded in clinkering anhydrous expansive cement that could be managed in a similar manner as that of Portland cement whereby desired expansion intensity could be regulated through adjusting the amount of added to the regular Portland cement.

In Japan, instead of expansive cement, expansive additives, which are mixed additionally to ordinary or blended cement concrete, are practically utilized. As a method of inhibiting cracks from occurring in concrete structures, expansive additives in Japan have gained quite a lot of popularity in the recent years [8].

2.3 Factors involving macroscopic expansion of expansive additive system

2.3.1 Hydration mechanism

Table 2.1: Stoichiometric equations for Aft formation by Hauyne

	$C_4A_3\bar{S}$	$+8C\bar{S}$	$+6C$	$+96H$	\rightarrow	$3C_6A\bar{S}_3H_{32}$
Weight(g)	610	1088	336	1728		3762
Specific gravity	2.61	2.96	3.34	1		1.73
Volume (cm ³)	234	368	101	1728	2431	2175

Rate of volume change for Aft hydrate series: $\frac{2175 - 2431}{2431} \times 100 = -10.5\%$ Rate of
 volume change for $C_4A_3\bar{S}$ particle: $\frac{2175}{235} = 9.3$ times

Table 2.2: Stoichiometric equations for Afm formation by Hauyne

	$C_4A_3\bar{S}$	$+2C\bar{S}$	$+6C$	$+36H$	\rightarrow	$3C_4A\bar{S}H_{12}$
Weight(g)	610	272	336	648		1866
Specific gravity	2.61	2.96	3.34	1		1.95
Volume (cm ³)	234	92	101	648	1075	957

Rate of volume change for Afm hydrate series: $\frac{957 - 1075}{1075} \times 100 = -10.9\%$ Rate of volume change for $C_4A_3\bar{S}$ particle: $\frac{957}{235} = 4.1$ times

Table 2.3: Stoichiometric equations for Afm formation by Hauyne(sulfate source depletion)

	$C_4A_3\bar{S}$	$+18H$	\rightarrow	$C_4A\bar{S}H_{12}$	$2AH_3$
Weight(g)	610	324		622	156
Specific gravity	2.61	1		1.95	2.24
Volume (cm ³)	234	324	558	319	64

Rate of volume change for Afm hydrate series: $\frac{383 - 558}{558} \times 100 = -31.36\%$ Rate of volume change for $C_4A_3\bar{S}$ particle: $\frac{319}{235} = 1.36$ times

Table 2.4: Stoichiometric equations for Aft formation by Hauyne (non-expansive)

	$C_4A_3\bar{S}$	$+2C\bar{S}$	$+38H$	\rightarrow	$3C_6A\bar{S}_3H_{32}$	$+2AH_3$
Weight(g)	610	272	684		1254	156
Specific gravity	2.61	2.96	1		1.73	2.42
Volume (cm ³)	234	92	684	1010	725	64

Rate of volume change for Aft hydrate series (non-expansive): $\frac{789 - 1010}{1010} \times 100 = -21.9\%$
 Rate of volume change for $C_4A_3\bar{S}$ particle: $\frac{725}{235} = 3.1$ times

Table 2.5: Stoichiometric equations for Portlandite formation from Free-lime

	C	$+H$	\rightarrow	CH
Weight(g)	56	18		74
Specific gravity	3.34	1		2.24
Volume (cm ³)	17	18	35	33

Rate of volume change for Portlandite hydrates series (non-expansive): $\frac{33 - 35}{35} \times 100 = -5.7\%$
 Rate of volume change for C particle: $\frac{33}{17} = 1.9$ times

Table 2.6: Stoichiometric equations for hydration of C_3S

	$2C_3S$	$+6H$	\rightarrow	$C_3S_2H_3$	$3CH$
Weight(g)	457	108		342	222
Specific gravity	3.06	1		2.6	1.73
Volume (cm ³)	149	108	257	131	128

Rate of volume change for C particle: $\frac{259}{149} = 1.74$ times
 Contribution of C-S-H in the volume change from C_3S : $\frac{131}{149} = 0.88 \approx 50.6\%$
 Contribution of CH in the volume change from C_3S : $\frac{131}{149} = 0.86 \approx 49.4\%$

Based on the information displayed from Table 2.1 to chpt2-tab:calc-aft-f-lime relating the total volume change of the hydrates from the stoichiometric equations, it appears that there is a reduction in total volume instead for both cases. However, if attention is turned towards the volume change of the solid particles, it could be seen that $C_4A_3\bar{S}$ changes its volume by 9.3 times to form ettringites whereby C changes its volume by 1.9 times, compared to original particle volumes. Due to this matter, some researchers [9, 10, 11] believed that the expansion was associated with the increase of solid volume during the hydration of their parent unhydrated particles, hard-burnt lime or $C_4A_3\bar{S}$ or C3A. This hypothesis seems not to be the only contribution and plausible for every case. Hydration of a Portland cement clinker always accompanies a large increase of solid volume but no expansion occurs. As can be seen, the volume of C-S-H gels is fairly the same as CH. Thus, if the increase in solid volume was to be the main reason, then even a Portland cement clinker would cause expansion given that the amount of C-S-H inside is large compared to that of CH. Thus, it is sound to conclude that expansion is not only dependent on the ‘increase of solid volume’ during hydration process. There must be further mechanisms, which triggers the expansion phenomena.

2.3.2 Expansion mechanism

Imagine that an unhydrated particle is staying in a restricted place, once volume increase happens, pressure would be applied and the hardened cement matrix would expand just like that of a cardboardbox full of books.

Two schools of thoughts have been raised regarding the mechanism of pressure development. The first one is the crystal growth or crystallization pressure – when pore solution is saturated, precipitation of ettringites with their long needles pushes the nearby hydrates and cause the increase in pressure. As can be seen from the SEM images of Ogawa and Roy [12], when expansion initiates, the needle lengths appeared to be longer than in image A and B when expansion was not seen.

The second hypothesis is the swelling pressure as proposed by Mehta [13]. He believes that it was due to the reason that the expansive hydrates would adsorb or imbibe water on its high surface area and increase its volume. In the wet cured specimens, it could be observed that the needles' volume seems to be larger and thicker than that of dry cured. However, Deng et al. [9] suggested that this swelling force was weak and did not contribute to much expansion. Rossetti et al. [14] also demonstrated that the effect of the swelling pressure was apparently exhausted in the interval of 0 - 0.1MPa restraint. In addition to that, Taylor et al. [15] raise an argument with that fact that C-S-H gels with larger specific surface area would have attracted more water than ettringite crystals. Thus, we could deduce that the main expansive mechanism could not be from 'Swelling pressure'.

On the contrary, Deng et al. [9] has found that, due to its high solubility, recrystallization of ettringites could occur easily in a solution while the in-situ precipitation of ettringites on the surface of aluminum-bearing grains would confine the ettringite crystals, consequently producing higher expansive pressure. Komatsu et al. [16] has also found in-situ precipitation of ettringite on the surface of aluminum-bearing grains. Additionally, crystallization pressure also happen in the same manner for the Portlandite formation from free-lime or hard-burnt lime [17]. Therefore, how concrete expands could be explained by this 'crystallization pressure' theory. Then, the next question is: when does this crystallization pressure initiate?

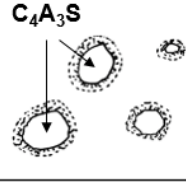


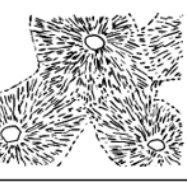
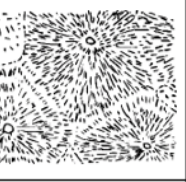
Stage	1	2	3	4	5
As observed in SEM images					
Expansion	0	0	0	0-20%	20%
α (DoH)	0-50%	50%-70%	70%-75%	75%-90%	> 90%
	Formation of <u>ettringites</u>	Radially arranged without contact	Start of expansion at min. stiffness	Repulsion at contact points	Expansion halts. Unreacted left.

Figure 2.1: Schematic diagram of the expansion process of $C_4A_3\bar{S}$ phase by Ogawa and Roy [12]

Based on the study by Ogawa and Roy [12] and schematic representation in Figure , he proposed the expansion mechanism as follows:

1. Precipitation of ettringites would initiate around the particles.
2. More ettringites precipitate whereas the previously precipitated starts to radially expand as needles.
3. Two criterias are needed to be met here for expansion to occur, (1) ettringites start to contact (2) minimum stiffness of the microstructure is achieved.
4. The expansive action starts to act at the contact points of hydrates.
5. Unreacted particles were left and expansion stops.

2.3.3 Other worth-mentioning phenomena relating to ettringite and portlandite formation in $C_4A_3\bar{S} - C - C\bar{S}H_2$ system

The reaction of hauyne to form ettringite itself is rather complicated. As mentioned in Table 2.1 and Table 2.4, even though the resultants would be ettringites, there have been reports that mentioned the non-expansive behavior of ettringites without lime source in the system [10, 13, 18, 19]. The non-expansive ettringites as shown in Table 2.4 possesses the characteristics of large prismatic ettringite crystals that contributes to mechanical strength, but not expansion. On the other hand, the expansive ettringites are small in size, more like colloidal, and formed in stellar formation instead [11, 12, 13, 18, 20].

Morioka [21] studied the interaction between ordinary Portland cement clinker phases with hauyne-based expansive additives. Hydration of the main components of the expansive additive phases, namely hauyne, free-lime and anhydrite shows an elevated reaction

rate when they are blended with alite and aluminate phases as compared to that of reacting alone.

Regarding the stoichiometric equations from Table 2.1 to 2.4, it is usually accepted that formation of monosulfates would initialize once $C\bar{S}H_2$ has depleted [11, 20]. This information is very crucial for modeling as it heavily affects the production of ettringites that would be the expansive hydrates in $C_4A_3\bar{S} - C - C\bar{S}H_2$ system.

Another interesting finding by Chen et al. [22] regarding the behavior of expansive additive was that limiting access to reactants at early age would subsequentially increase expansion, e.g., lower temperature or low water-to-binder ratio.

2.3.4 Current existing models for expansive additives

Cohen [19] was probably one of the first to start tackling with modeling of $C_4A_3\bar{S}$ -based expansive cements. His model consists of three subsystems: the solution, expansive particles and matrix. The main purpose is to express the hydration kinetics, ettringite formation and expansion characteristics. His model was done based on the assumption that reacted $C\bar{S}H_2$ would cause the ettringite crystals to form on the surface and radially increasing its volume in a rod-like state. Even though the results were spectacular, but such an assumption might be controversial with the findings of other researchers that expansive ettringites have stellar and colloidal features instead [11, 12, 13, 18, 20].

Choi et al. [23, 24, 25, 26] proposed a model of concrete using expansive additive, which could predict the volumetric stability in both expansion and shrinkage. His model comprises of hydration, mechanical properties, volume change and time-dependent behavior. However, regarding the hydration part of the model [23], to express the effect of temperature on the relationship between the mineral compositions, the model parameters are modified in numerous counts to express the interactions.

2.4 Conclusion

This chapter described the state-of-the-art literatures which are crucial for making the expansive additive model a reality. Various investigations conducted by many researchers with the aim to understand the behavior of different types of expansive additives from its hydration stage to its mechanically volumetric expansion stage were presented. The followings could be concluded from this chapter:

- The expansion intensity is not solely dependent upon the total amount of parent expansive hydrate particles, which are free-lime and hauyne, reacted.

- Unless the cement matrix possess a minimum stiffness i.e. when the particles start to make contact with each other, expansion would initiate. Prior to particle contact phenomenon, the hydrated particles would just fill in the pore space without any contribution to the expansion intensity.
- For Hauyne hydration, formation of ettringites is the most favorable under the condition that calcium hydroxide and calcium sulfate are sufficiently present in the system.

Chapter 3

Overview of thermodynamic analytical platform - DuCOM-COM3

Contents

3.1 Durability COncrete Model (DuCOM)	14
3.1.1 Overview of the computational system - DuCOM	14
3.1.2 Multi-component hydration model	14
3.1.3 Pore-structure development model	18
3.1.4 Model of moisture transport and thermodynamic equilibrium .	23
3.1.5 Multi-scale constitutive model	28
3.2 Nonlinear mechanics of reinforced concrete computational	
system (COM3)	50
3.2.1 Overall composition of the model including cracks	51

3.1 Durability COncrete Model (DuCOM)

3.1.1 Overview of the computational system - DuCOM

The aging process in young or early-age concrete consists of mutual influence of hydration, pore structure development and moisture migration inside those pores. DuCOM was initialized in consideration of the interaction based on three fundamental models: hydration reaction, pore structure development, and moisture equilibrium and transport. With regards to the calculation scheme, initial temperature, mix proportion, curing condition and environmental boundary condition are necessary as inputs. First and foremost, the

temperature and degree of hydration of each clinker components are computed based on the proposed heat of hydration model in second-scale time difference. Then, the degree of hydration and amount of chemically bound water would be inserted into the pore structure development model to obtain the pore structure properties of hardened cement paste, to put it simply, porosity of capillary and gel pores, pore distribution and void ratio. The pore water pressure, relative humidity and moisture distribution in the pores are achieved from moisture migration characteristics in the pore structures from the moisture equilibrium and transport model. The water consumption via hydration is based on the law of conservation of mass as reflected in the governing equation of equilibrium below:

$$\frac{\partial S(\theta_i)}{\partial t} + \text{div} J_i(\theta_i, \nabla \theta_i) - Q_i(\theta_i) = 0 \quad (3.1)$$

where $\frac{\partial S(\theta_i)}{\partial t}$ is the potential term, $\text{div} J_i(\theta_i, \nabla \theta_i)$ is the flux term and $Q_i(\theta_i)$ is the sink term. Then, we would be able to achieve the governing equation for heat and moisture, respectively as:

$$\text{Heat: } \rho_c \frac{\partial T}{\partial t} + \text{div} J_i(-K_H \nabla T) - Q_H = 0 \quad (3.2)$$

$$\text{Moisture: } \frac{\partial \rho_i \phi S}{\partial t} + \text{div} J_i(-(K_L + K_V) \nabla P) - Q_H = 0 \quad (3.3)$$

3.1.2 Multi-component hydration model

3.1.2.1 Multi-mineral hydration concept

In the multi-component model developed by Kishi and Maekawa [1], the cement's heat generation from hydration is computed by the summation of individual component's heat generation rate corresponding to their individual properties. The cement minerals which are covered in this model include alite (C_3S), belite (C_2S), aluminate phase (C_3A), ferrite phase (C_4AF) and gypsum ($C\bar{S}H_2$). The exothermic reaction for all of these phases are individually calculated for superposition. The mineral admixtures such as blast furnace slag, fly ash and silica fume are treated as individual components since only the amorphous phase of the admixtures react, which requires no need for constituent separation. Therefore, the heat rate for the cement as a whole, H_C :

$$H_C = \sum \rho_i H_i$$

$$H_C = \rho_{C_3A} (H_{C_3AET} + H_{C_3A}) + \rho_{C_4AF} (H_{C_4AFET} + H_{C_4AF})$$

$$+ \rho_{C_3S} H_{C_3S} + \rho_{C_2S} H_{C_2S} + \rho_{SG} H_{SG} + \rho_{FA} H_{FA} + \rho_{SF} H_{SF} \quad (3.4)$$

Based on the Arrhenius equation, which considers the effect of thermal activity on reaction rates and reference heat rate which provides the heat rate of individual clinker components at a specified temperature, the hydration heat rate of each component, H_i , could be obtained as:

$$H_C = \gamma_i \beta_i \lambda_i \mu_i H_{i,T_0} (Q_i) \exp \left[-\frac{E_i}{R} \left(\frac{1}{T} - \frac{1}{T_0} \right) \right] \quad (3.5)$$

where γ_i is the coefficient expressing the delaying effect of the chemical admixture and fly ash in the initial hydration process, β_i coefficient expressing the reduction in heat generation rate due to reduction in free water availability, i.e. space for gel deposition, λ_i is the coefficient expressing the change in heat rate of the powder admixture, μ_i is the coefficient expressing the change in heat rate due to interdependency of alite and belite, H_{i,T_0} is the reference heat generation rate of component i at constant temperature T_0 and Q_i is the accumulated heat. The temperature distribution and hydration could then be obtained through the thermal equilibrium governing equation [3.2](#) and total heat generation [3.5](#).

Degree of hydration is defined as the ratio between the generated calorific heat of individual cement component and the total cement, which is a dimensionless value between 0 and 1, represented by equation below:

$$\varphi_t = \frac{Q(t)}{Q_\infty} \quad (3.6)$$

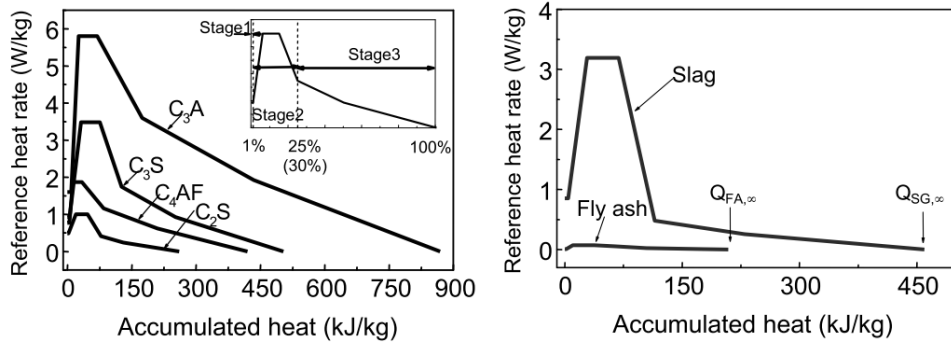
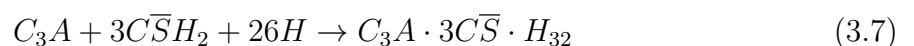


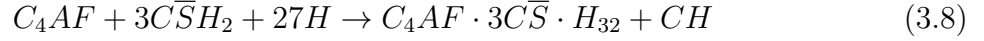
Figure 3.1: Reference heat rate of each mineral

3.1.2.2 Interdependency among cement clinker minerals

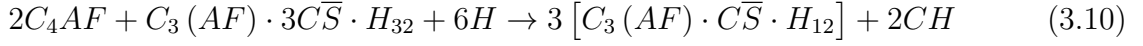
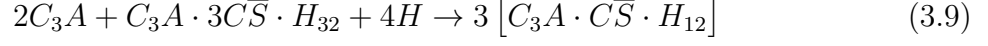
Ettringite formation and monosulfate conversion model

Stoichiometric equations for Aft formation:





Stoichiometric equations for Afm formation:



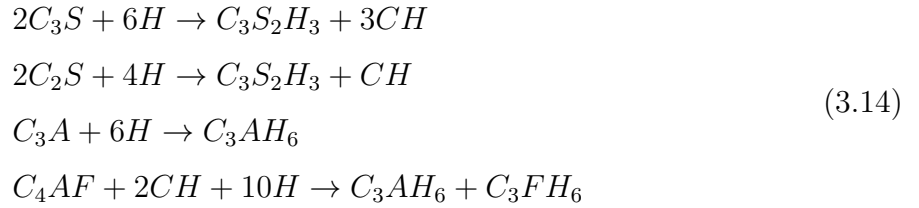
3.1.2.2.1 Gel precipitation model – free water as the deposit space

$$\beta_i = 1 - \exp \left\{ -r \cdot \left[\frac{\omega_{free}}{100 \cdot \nu_i} \right]^s \right\} \quad (3.11)$$

$$\omega_{free} = \frac{W_{total} - \sum W_i}{C \cdot (\rho_{pc} + m_{SG} \cdot \rho_{SG} + m_{FA} \cdot \rho_{FA})} \quad (3.12)$$

$$\eta_i = 1 - \left(1 - \frac{Q_i}{Q_{i,\infty}} \right)^{\frac{1}{3}} \quad (3.13)$$

The amount of chemically bound water from each reaction could be computed by the multiplication of bound water ratio obtained from the reaction equation of each mineral by the degree of hydration as calculated by Equation [3.6](#).



As a matter of fact, hydration does not only consume the chemically bound water. The physically trapped water would also be constrained by the hydrated pore volume corresponding to a value about 15% of the total cement weight. Therefore, water consumption, W_i , is the computed chemically bound water volume plus the extra 15%.

3.1.2.2.2 Interdependency of alite and belite reaction

In ordinary Portland cement or moderate-heat Portland cement, due to the temperature dependence of the reaction, the adiabatic temperature rise indicates that there seems to be a rapid rise in temperature even when Stage 3 of hydration process has taken place.

On the contrary, for low-heat Portland cement, the adiabatic temperature rise indicates a slow rise which coherently relates with the initial period of Stage 2. This difference is accounted by the ratio between C_2S and C_3S , which is integrated into the model through the usage of μ_i .

$$\mu = 1.4 \cdot \left\{ 1 - \exp \left(-0.48 \left(\frac{\rho_{C_3S}}{\rho_{C_2S}} \right)^{1.4} \right) \right\} + 0.1 \quad (3.15)$$

This modification would be applied for C_2S and C_3S reference heat generation whereas, for other components, this μ factor will be constant, i.e. $\mu = 1$.

3.1.2.2.3 Supply of calcium hydroxide by portland cement hydration for reactions of mineral admixtures

As hydration proceeds, CH will be produced from the reactions of clinker's minerals. Subsequently, consumption of CH is required for either pozzolanic reaction (FA and SF) or latent hydraulic reaction (BFS) to further hydrate the cement. Therefore, to reflect the decrease in hydration due to insufficient CH content, λ is incorporated into the model.

$$\lambda = 1 - \exp \left\{ -2.0 \cdot \left(\frac{F_{CH}}{R_{SGCH} + R_{FACH}} \right)^{5.0} \right\} \quad (3.16)$$

The consumption ratios of BFS, FA and SF are 22%, 100% and 200% respectively. However, in ternary blended cement, aqueous CH is assumed to be entirely consumed by BFS since FA reaction is slower than that of BFS.

3.1.3 Pore-structure development model

As the hydration progresses, the solid resultants from various clinker, pozzolanic and hydraulic reactions could not be mutually connected without leaving spaces and pores. These pore structure is an indispensable constituent which associates with the quality of the concrete such as strength, permeability, moisture migration and other various factors.

3.1.3.1 Initial state of cement particle spatial distribution

In this model, at the initial state right after mixing, the powder material is idealized as spherical particle with uniform colloidal size of about 150 μm . From practical WB ratio encountered, the interparticle distance is about the same order of magnitude as the average size of the powder particles itself, which is implemented into the model as such. Then, once the initial average size of the powder particles is known, the homogenous and

uniformly dispersed system of spherical particles with radius of r_0 , the average volumetric concentration G , and the average spacing between outer surfaces of two particles s is mutually associated by:

$$G = \frac{G_0}{\left(1 + \frac{s}{2r_0}\right)^3} \quad (3.17)$$

$$G_0 = 0.79 \left(\frac{BF}{350}\right)^{0.1} \quad G_0 \leq 0.91 \quad (3.18)$$

$$s = 2r_0 \left\{ \left[G_0 (1 + \rho_p \omega_0)^{\frac{1}{3}} \right] - 1 \right\} \quad (3.19)$$

In this uniformly dispersed system of spherical particles, each particle has a free cubical volume of l^3 for cluster deposit. When the outer clusters of each particle is in physical contact with one another, further expansion and merging would be done in the empty spaces in the cubical volume. To simplify the analytical process, the initial volume of the cubic cell is transformed into a representative spherical cell of radius, r_{eq} :

$$l^3 = \frac{4\pi r_{eq}^3}{3} \quad (3.20)$$

$$r_{eq} = \left(\frac{3}{4\pi}\right)^{\frac{1}{3}} l = \chi \cdot l \quad (3.21)$$

When the thickness of the expanding cluster has reached δ_{max} , it would represent a complete filling of the cubic cell or the equivalent representative spherical cell, in which:

$$\delta_{max} = r_{eq} - r_0 = r_0 \left\{ 2\chi \left[G_0 (1 + \rho_p \omega_0)^{\frac{1}{3}} \right] - 1 \right\} \quad (3.22)$$

3.1.3.2 Macroscopic volumetric balance of hydration products

Disregarding the effect of bleeding or contraction in plastic state concrete and the small change in volume once the concrete is set, various compounds exist in the hydrate matrix such as gel, unreacted powder, CH crystals, other mineral compounds and partially water-filled voids. Pore spaces are subdivided into three different categories depending on the scales. Firstly, capillary pores, which is the largest among the three categories, act as the deposit spots between the powder particles for new hydrates as hydration proceeds. Secondly, gel pores exist between the interstitial spaces of the hydrated gel products, C-S-H. Lastly, interlayer pores exist between the layers of C-S-H. Therefore, the water which would be available for hydration to consume is limited to only the water residing

in capillary pores. C-S-H gels, which are assumed to possess a layer structure with an interlayer spacing of a single water molecule, hold a constant value of 0.28 for characteristic porosity ϕ_{ch} throughout the whole hydration process. Therefore, volume V_s of C-S-H in a unit volume of paste could be computed from the following formula:

$$V_s = \frac{\varphi \cdot W_p}{1 - \phi_{ch}} \left(\frac{1}{\rho_p} + \frac{\beta}{\rho_w} \right) \quad (3.23)$$

where W_p is the weight of powder materials per unit paste volume, ρ_p is the density of powder, ρ_w is the density of chemically combined water (around 1.25 g/cm³).

$$\phi_l = \frac{t_w s_l \rho_g}{2} \quad (3.24)$$

$$\phi_g = \phi_{ch} V_s - \phi_l \quad (3.25)$$

$$\rho_g = \frac{(1 + \beta)(1 - \phi_{ch})}{\rho_w + \beta/\rho_p} \quad (3.26)$$

$$s_l = 510f_{pc} + 1500f_{sg} + 3100f_{fa} \quad (3.27)$$

where t_w is the interlayer thickness (2.8Å), s_l is the specific surface area of the interlayer, ρ_g is the dry density of gel products and f_{pc} , f_{sg} and f_{fa} are the weight fractions of the Portland cement, blast furnace slag and fly ash, respectively.

Subsequently, the capillary porosity ϕ_c is obtained through volumetric balance from the equation below:

$$\phi_c = 1 - V_s - (1 - \varphi) \left(\frac{W_p}{\rho_p} \right) \quad (3.28)$$

3.1.3.3 Cluster expansion model

As the hydrated gel products would deposit outside the initial particle boundary with assumedly similar characteristics as the inner products, the density ρ_δ at any point in the cluster is associated with the mass of the gel and the bulk porosity at that point, represented by:

$$\rho_\delta = \frac{(1 + \beta)(1 - \phi_\delta)}{\left(\frac{1}{\rho_p} + \frac{\beta}{\rho_u} \right)} \quad (3.29)$$

where ϕ_δ is the bulk porosity at any point in the outer product and ρ_u the specific gravity of the chemically combined water. The bulk porosity distribution in the outer products is modeled by:

$$\phi_\delta = (\phi_{ou} - \phi_{in}) \left(\frac{\delta}{\delta_m} \right)^n + \phi_{in} \quad (3.30)$$

where δ is the distance of any point in the cluster from the outer boundary of the particle, δ_m is the cluster thickness at the instant of hydration, ϕ_{in} the porosity of inner product, which is equivalent to ϕ_{ch} , ϕ_{ou} is the porosity at the outermost boundary of the expanding cluster and equals to unity before the cluster reaching the outermost surface of the representative spherical cell of the particle and n is the power-function parameter for the consideration of gel products depositional pattern around the particle, which is also applicable for inclusion of temperature effect.

Regarding this computational platform, n is adopted as unity. Then, rearranging the bulk porosity, ϕ_δ , distribution formula:

$$\phi_\delta = (\phi_{ou} - \phi_{in}) \left(\frac{\delta}{\delta_m} \right) + \phi_{ch} \quad (3.31)$$

In this cluster model, two different cases of cluster expansion are taken into consideration. The first case concerns with an unobstructed expansion, which correspondingly means ϕ_{ou} is equivalent to unity. The second case concerns with a state that cluster thickness equals to free space available for expansion.

$$\phi_{ou} = 1 - \frac{X - Y}{Z} \quad (3.32)$$

$$X = -n(1 - \phi_{in}) \left[\frac{k^3}{3(n+3)} + \frac{k^2}{(n+2)} + \frac{k}{(n+1)} \right] \quad (3.33)$$

$$Y = \frac{\alpha}{3} \left(\phi_{in} + \beta \frac{\rho_p}{\rho_u} \right) \quad (3.34)$$

$$X = \frac{k^3}{3(n+3)} + \frac{k^2}{(n+2)} + \frac{k}{(n+1)} \quad (3.35)$$

$$\delta_{max} = 2\chi \left[G_0 (1 + \rho_p \omega_0)^{\frac{1}{3}} \right] - 1 \quad (3.36)$$

3.1.3.4 Surface area of capillary and gel components

Based on the implicit assumption that development of the inner mass occurs within the boundary of original particle with uniform properties throughout the entire hydration process and the outer products of constant and uniform properties, i.e representative hydrate crystals, would deposit in the outer pore solution phase as concrete matures, the outer and inner microstructural properties would attain almost a homogeneous state. In other words, the distinction between the inner and outer microstructural properties would decline as hydration proceeds. Thus, capillary surface area in the outer products could be obtained once the bulk porosity of the outer products is determined. By considering

a region of thickness located from the center of the particle, if dV_g and ρ_g represent the real volume and dry density of hydrates in this zone, and ϕ_r is the bulk porosity of the expanding cluster at r , then through mass equilibrium of hydrates exist in the region:

$$\rho_g dV_g = 4\pi r^2 dr \frac{(1 + \beta)(1 - \phi_r)}{\rho_p + \frac{\beta}{\rho_u}} \quad (3.37)$$

where ζ represents the volume-to-surface ratio of the solid grains of hydrates exist in the region above. This ratio is actually proportional to the average size of C-S-H gels, since the hydration products are majorly contributed by C-S-H gels. In the model, the value of ζ is assumed to be constant during the entire process of hydration, which is approximately $0.01 \mu\text{m}$ to $0.015 \mu\text{m}$ based on the average gel particle size as reported by Powers and Brownyard [27]. In case of blended powders, an empirical formula would be calculated as:

$$\zeta = 30.0f_{pc} + 1.5f_{sg} + 1.0f_{fa} \quad (3.38)$$

Then, through applying the chain rule of differential equation to dV_g and further simplification, the capillary surface area dS_c occupied in the region dr is:

$$dS_c = \frac{dS_c}{dV_g} dV_g = \frac{4\pi r^2}{\zeta} \left(\frac{1 - \phi_r}{1 - \phi_{in}} \right) dr \quad (3.39)$$

Integrating the differential equation above over all of the cluster thickness and then normalizing it to the volume of spherical REV, S_c will be obtained. Furthermore, the surface area of gel S_g could be calculated by simply multiplying with the mass of gel products.

$$S_g = W_g s_g \frac{\zeta_1}{\zeta} \quad (3.40)$$

where s_g is the internal specific surface area of C-S-H gel particle, which is currently assumed to be a constant value of $30000 \text{ m}^2/\text{kg}$.

3.1.3.5 Porosity distribution function

Using the calculated porosity and surface area, the total porosity distribution of the cement paste as a function of the pore radius could be obtained as the superposition of all the pores by the following expression:

$$\phi(r) = \phi_{cp} V_{cp}(r) + \phi_{gl} V_{gl}(r) + \phi_{lr} \quad (3.41)$$

$$V_{cp}(r) = 1 - \exp(-B_{cp}r) \quad 0 \leq V_{cp}(r) \leq 1 \quad (3.42)$$

$$V_{gl}(r) = 1 - \exp(-B_{gl}r) \quad 0 \leq V_{gl}(r) \leq 1 \quad (3.43)$$

$$dV_{cp} = B_{cp}r \exp(-B_{cp}r) \quad (3.44)$$

$$dV_{gl} = B_{gl}r \exp(-B_{gl}r) \quad (3.45)$$

where $V_{cp}(r)$ and $V_{gl}(r)$ represent fractional pore volume of the distribution up to pore radius, r , of capillary and gel pores, respectively. B_{cp} and B_{gl} represent the sole porosity function parameter for capillary and gel pores, respectively. Assuming a cylindrical pore shape in the distribution, the B parameter could be calculated by this relationship:

$$S_i = 2\phi \int r^{-1} dV = 2\phi \int_{r_{min}}^{\infty} B_i \exp(-B_i r) d \ln r \quad i = cp, gl \quad (3.46)$$

where r_{min} represents the minimum pore radius.

Due to the matter that the above equation could not be solved as a closed-form expression, an explicit relationship was proposed by fitting the accurate numerical evaluation of the above integral to a finitely large amount of dataset in which B is mutually linked by a function of S/ϕ .

$$B_i = \exp \left[\frac{\log \left(\frac{S_i}{\phi_i} \right) + 3.72633}{4.59715} \right] \quad (3.47)$$

3.1.4 Model of moisture transport and thermodynamic equilibrium

In the model, only liquid and gas phases are assumed to fill up the network of pores per representative elementary volume. The moisture phases inside the pores are divided into adsorbed water, condensed water and interlayer water, which ubiquitously exist throughout the pore distributions. Based on the thermodynamic equilibrium at the surface of liquid and gaseous phase, the pore size distribution and pore structure development model, the total moisture content in the pores could be obtained from the modified B.E.T theory for adsorbed water and condensed water. Interlayer water, which is strongly bound to the solid particle, is disregarded since it could not be simply removed under normal pressure gradient.

3.1.4.1 Thermodynamic equilibrium of condensed phase

The liquid-vapor equilibrium surface is assumed to be formed when the vapor pressure in the capillary and gel voids is smaller than the saturated vapor pressure, i.e. there is a difference in the pore pressure due to the formed meniscus surface and capillary tension force. Assuming a cylindrical pore radius of size, r , the vapor pressure could be determined from the Kelvin equation as:

$$P_v \ln \left(\frac{P_v}{P_{v0}} \right) = -\frac{1}{r} \cdot \frac{2\gamma V_m \cos \theta}{RT} \quad (3.48)$$

where P_v is the vapor pressure (Pa), P_{v0} is the saturated vapor pressure (Pa), γ is the surface tension of liquid (N/m), V_m is the molar volume of liquid (m^3/mol), θ is the contact angle of liquid and solid (rad), $\cos \theta = 1$ when cement is hydrophilic meaning the contact angle is 0° , R is the the gas constant ($= 8.314 \text{ J/mol/K}$), T is the absolute temperature (K) and r is the assumed cylindrical pore radius (m). Assuming that the maximum pore radius in which liquid can reside in is r_s and all the voids with radius below r_s are entirely filled with water, the degree of saturation S could be defined as:

$$r_s = -\frac{2\gamma}{RT} \cdot \frac{M_w}{\rho_l} \cdot \frac{1}{\ln h} \quad (3.49)$$

$$S_i = \int_0^{r_s} dV = 1 - \exp(-B_i r_s) \quad (3.50)$$

where r_s is the maximum pore radius in which liquid water is present (m), h is the relative humidity (%), M_w is the molecular weight of water (kg/mol) and ρ_l is the density of liquid water (kg/m^3)

3.1.4.2 Adsorbed water model

In the pores that are not fully filled with water, adsorbed water would be present on the surfaces of solid walls whereby the thickness of this adsorbed water could be determined from B.E.T theory as:

$$t_a = \frac{k_1 V_m h}{\left(1 - \frac{h}{h_m}\right) \left(1 - \frac{h}{h_m} + k_1 h\right)} \quad (3.51)$$

where t_a is the thickness of physically adsorbed water layer (m), V_m is the thickness of a single molecular layer (0.35 nm), h is the relative humidity (%), h_m is the relative humidity required for the pores to be completely filled with water and k_1 is a coefficient with a value of 15. Assuming that the pores are in cylindrical shape with actual interface

pore radius of r_l, h_m could be defined as:

$$h_m = \exp\left(\frac{-2\gamma M_w}{RT \rho_l r_l}\right) \quad (3.52)$$

Thus, the degree of saturation of the pores which is not saturated could be given as:

$$S_r = 1 - \left(\frac{r - t_0}{r}\right)^2 \quad (3.53)$$

Then, the saturation degree of adsorbed water is obtained via integration of S_r from r_c to infinity is defined as:

$$S_{ads} = \int_{r_c}^{\infty} S_r dV \quad (3.54)$$

$$r_c = C \cdot r_s \quad (3.55)$$

where r_c is the pore radius at the interface where liquid and vapor are in equilibrium, i.e. if $r > r_c$, the pores will be completely saturated and if $r < r_c$, these larger pores are only partially saturated. It should be noted that $r_c > r_s$, C is a coefficient that takes the thickness of adsorbed water layer into account, which is analytically set to 2.15. The summation of the degree of saturation from condensed phase and adsorbed water would give the total saturation degree of the whole pore structure.

$$S = S_c + S_{ads} = \int_0^{r_s} dV + \int_{r_c}^{\infty} S_r dV \quad (3.56)$$

3.1.4.3 Model of hysteretic behavior in capillary and gel pores

Only under ideal isotherm, the moisture capacity and equilibrium in the pores follow a single path under drying-wetting conditions. As a matter of fact, the hysteresis loop exists as numerous experiments have shown whereby, during the desorption process, pores tend to retain more water than the adsorption process. This hysteresis loop is accounted by the inkbottle effect, which refers to a state that, due to the complex microstructural network of pores and gels, water would be trapped in the inkbottle-shaped pores during drying process. Thus, to accurately determine the desorption-adsorption behavior, the inkbottle effect and entrapped water must be taken into consideration. In this model, the saturation due to this inkbottle effect is added to the total saturation as:

$$S_{total} = S_c + kS_{ink} + S_{ads} = S_c + (-kS_c \ln(S_c)) + S_{ads} \quad 0 \leq k \leq 1 \quad (3.57)$$

where S_{total} is the total saturation occupied by the condensed water and adsorbed water, S_c

is the saturation due to the condensed water in the pores which have radii smaller than r_c , S_{ink} is the saturation due to the inkbottle effect, S_{ads} is the saturation due to the adsorbed water at the solid walls of partially water-filled voids and k is the coefficient representing the water escaped from inkbottle pores which depends on the ambient temperature. At the early stage of the drying process, the value of k is equivalent to 1 which would be decreased as the drying process proceeds further until k reaches 0 which define as a state that no moisture is contained in the inkbottle pores. Through performing inverse analysis from experimental values, the inkbottle water dissipation coefficient is defined as:

$$\frac{dk}{dt} = -C \cdot a_{ink}^T \cdot a_{ink}^h \cdot k \quad (3.58)$$

$$a_{ink}^T = \exp\left(\frac{-1.5 \times 10^4}{T}\right) \quad (3.59)$$

$$a_{ink}^h = 0.05 \cdot (100.0 - 100.0 \cdot h)^{0.81} \quad (3.60)$$

where C is the constant which is equivalent to 3.0×10^{13} /sec, a_{ink}^T is the coefficient denoting influence by temperature, a_{ink}^h is the coefficient denoting influence by relative humidity, T is the temperature (K) and h is the relative humidity

$$S_{ink} = -S_c \ln(S_c) \quad (3.61)$$

The formula for S_{ink} above signifies a monotonous drying from a complete wetting state only. However, in reality, structures will undergo various wetting-drying cycles. Therefore, S_{ink} when wetting occurs during the drying process should be expressed as:

$$S_{ink} = \ln(S_{max}) - S_c \ln(S_c) \quad (3.62)$$

Regarding wetting process which structures alter from dry state to the wet state, liquid water is gradually filled from the pores with smallest radii. Since $k = 0$ in a complete dry state, the degree of saturation could be defined as:

$$S_{total} = S_c + S_{ads} \quad (3.63)$$

However, in a similar manner to drying process, the formula above could not represent the case, when drying comes into play during the wetting. In such case, S_{ink} could be expressed as:

$$S_{ink} = -S_{min} \ln(S_c) \quad (3.64)$$

To summarize, the degree of saturation for drying and wetting process is:

$$\text{Drying: } S_{total} = S_c + kS_{ink} + S_{ads} = S_c + (-kS_c \ln(S_c)) + S_{ads} \quad 0 \leq k \leq 1 \quad (3.65)$$

$$\text{Wetting: } S_{total} = S_c + S_{ads} - S_{min} \ln(S_c) \quad (3.66)$$

3.1.4.4 Interlayer water

Interlayer water could be defined as the water molecules which reside between the C-S-H layers with thickness of a water molecule. The moisture state in interlayer water is different from that of condensed water and vapor since most of the interlayer water molecules can only be dried out at relative humidity of 10% and below only. The degree of saturation of the interlayer pores could be determined from the equation below:

$$S_{lr}^{env} = \begin{cases} a \cdot h^{n_2} + b, & \text{if } h \geq 0.8 \\ h^{n_1} + c, & \text{if } h < 0.8 \end{cases} \quad (3.67)$$

$$a = \frac{1.0 - h_t^{env}}{1.0 - 0.8^{n_1}} \quad (3.68)$$

$$b = \frac{-0.8^{n_1} + h_t^{env}}{1.0 - 0.8^{n_1}} \quad (3.69)$$

$$c = h_t^{env} - 0.8^{n_1} \quad (3.70)$$

$$h_t^{env} = -1.5 \times 10^{-2} \cdot T + 5.4 \quad (3.71)$$

$$n_1 = 25.0, \quad n_2 = 0.05 \quad (3.72)$$

where h is the relative humidity (%), and h_t^{env} is the coefficient which determine temperature dependency on the equilibrium in interlayer space. Additionally, to account for the transition state of interlayer water when the ambient temperature fluctuates, the following equations are introduced as:

$$\frac{dh_t}{dt} = -C \cdot a_{lr}^T \cdot a_{lr}^h \cdot (h_t - h_t^{env}) \quad (3.73)$$

$$a_{lr}^T = 3.0 \cdot \exp\left(\frac{-1.5 \times 10^4}{T}\right) \quad (3.74)$$

$$a_{lr}^h = \begin{cases} \exp(8.0 \cdot h), & \text{if } h_t \leq h_t^{env} \\ 0.05(100.0 - 100.0 \cdot h)^{0.81}, & \text{if } h_t > h_t^{env} \end{cases} \quad (3.75)$$

where a_{lr}^T is the coefficient denoting influence by temperature, a_{lr}^h is the coefficient denoting

influence by relative humidity, T is the temperature (K) and h is the relative humidity. At a certain time of hydration, relative humidity could be obtained. Then, the interlayer humidity could be further obtained from the above equations.

3.1.4.5 Moisture transport model

It is generally considered that, in porous materials, the moisture transport is driven by both pressure and temperature gradient. Assuming that all the capillary and gel pores possess cylindrical shape; consequently, the total moisture flux in the moisture transport model could be defined in the following model.

3.1.4.5.1 Vapor transport model

Based on Fick's second law of diffusion, which describes the diffusion effects on concentration within time and Knudsen diffusion, which considers the diffusion of vapor molecules through very small capillary pores, the vapor flux could be computed by:

$$q_v = -\frac{\phi D_0(T)}{\Omega} \int_{r_c}^{\infty} \frac{dV}{1 + N_k} \nabla \rho_v = -D_v \nabla \rho_v \quad (3.76)$$

where ϕ is the porosity (excluding the interlayer pores), D_0 is the vapor diffusion coefficient (m^2/s), Ω is the coefficient which relate molecular diffusion to different temperatures, ρ_v is the density of saturated vapor (kg/m^3) and N_k is the Knudsen number. Knudsen number could be calculated from below equation:

$$N_k = \frac{l_m}{2(r - t_a)} \quad (3.77)$$

where r is the pore diameter (m), t_a is the thickness of adsorbed water layer and l_m is the mean free path of a water molecule (m). At atmospheric pressure, 20°C and 0.3 nm of water molecule, l_m is assumed to be 100 nm.

3.1.4.5.2 Liquid water transport model

Disregarding the movement of adsorbed water attached on the pore walls, gel and capillary pores of cylindrical shape are assumed to be the transport medium whereby the total liquid flux could be determined as the integration of liquid flux over the pore

distribution as:

$$q_l = -\frac{\rho_l \phi^2}{50\eta} \left(\int_0^{r_c} r dV \right)^2 \nabla \rho_l = -K_l \nabla \rho_l \quad (3.78)$$

where ϕ is the porosity (excluding the interlayer pores), ρ_l is the density of liquid water (kg/m^3), K_l is the liquid water transfer coefficient and η is the fluid viscosity in non-ideal condition (Pa.s).

$$\eta = \eta_0 \exp\left(\frac{G_e}{RT}\right) \quad (3.79)$$

where η_0 is the viscosity of liquid water in ideal condition, G_e is the free energy of activation of flow in non-ideal condition (J/mol), R is the gas constant and T is the absolute temperature. Through summation of the liquid and vapor flux, the total moisture flux in the water-vapor system can be obtained by the equation:

$$\begin{aligned} J &= -(D_v \nabla \rho_v + K_l \nabla P_l + K_T \nabla T) \\ &= -\left\{ \left(D_v \frac{\partial \rho_v}{\partial P_l} \nabla P_l + D_v \frac{\partial \rho_v}{\partial T} \nabla T \right) + K_l \nabla P_l + K_T \nabla T \right\} \\ &= -\left(D_v \frac{\partial \rho_v}{\partial P_l} + K_l \right) \nabla P_l - \left(D_v \frac{\partial \rho_v}{\partial T} + K_T \right) \nabla T \end{aligned} \quad (3.80)$$

3.1.5 Multi-scale constitutive model

3.1.5.1 Introduction

Crack initialization has a lot to do with time-dependent deformation, including shrinkage and creep, which will significantly affect the durability and structural performance of concrete. Based on previous reviews on the mechanism of drying shrinkage, many have shown that, under high or moderate relative humidity, pore pressure due to surface tension of water molecules governs whereas, under low relative humidity, the increase in surface energy of C-S-H gels governs. Therefore, based on the thermodynamic states of micro-pore moisture with different scales, the multi-scale solidification model of concrete shrinkage and creep is developed.

3.1.5.2 Two-phase model (aggregate-cement paste)

Concrete is assumed to be a two-phase composite material composed aggregates and cement paste with macroscopic deformation expressed by the following equations. Additionally, aggregate is considered to be rigid including its elastic deformation and shrinkage. Hardened cement paste is considered as a group of fictitious clusters in which amount of clusters increases as hydration proceeds referring to the solidification theory.

Stress-strain constitutive equations:

$$\sigma_0 = \frac{1}{3}(\sigma_{xx} + \sigma_{yy} + \sigma_{zz}) \quad (3.81)$$

$$\varepsilon_0 = \frac{1}{3}(\varepsilon_{xx} + \varepsilon_{yy} + \varepsilon_{zz}) \quad (3.82)$$

$$S_{ij} = \sigma_{ij} - \sigma_0 \delta_{ij} \quad (3.83)$$

$$e_{ij} = \varepsilon_{ij} - \varepsilon_0 \delta_{ij} \quad (3.84)$$

$$\sigma_{ij} = \begin{bmatrix} \sigma_{xx} & \sigma_{xy} & \sigma_{xz} \\ \sigma_{yx} & \sigma_{yy} & \sigma_{yz} \\ \sigma_{zx} & \sigma_{zy} & \sigma_{zz} \end{bmatrix} \quad (3.85)$$

$$\varepsilon_{ij} = \begin{bmatrix} \varepsilon_{xx} & \varepsilon_{xy} & \varepsilon_{xz} \\ \varepsilon_{yx} & \varepsilon_{yy} & \varepsilon_{yz} \\ \varepsilon_{zx} & \varepsilon_{zy} & \varepsilon_{zz} \end{bmatrix} \quad (3.86)$$

$$\delta_{ij} = \begin{cases} 1.0, & \text{if } i = j \\ 0.0, & \text{if } i \neq j \end{cases} \quad (3.87)$$

where σ_0 is the volumetric stress, ε_0 is the volumetric strain, S_{ij} is the deviatoric stress tensor, e_{ij} is the deviatoric strain tensor, σ_{ij} is the total stress tensor, ε_{ij} is the total strain tensor and δ_{ij} is the Kronecker delta.

Volumetric stress-strain:

$$\sigma_0 = V_{ag}\sigma_{ag} + V_{cp}\sigma_{cp} \quad (3.88)$$

$$\varepsilon_0 = V_{ag}\varepsilon_{ag} + V_{cp}\varepsilon_{cp} \quad (3.89)$$

$$\varepsilon_{ag} = \frac{1}{3K_{ag}}\sigma_{ag} \quad (3.90)$$

$$\varepsilon_{cp} = f(\sigma_{cp}) \quad (3.91)$$

where σ_{ag} is the volumetric stress of aggregate, σ_{cp} is the volumetric stress of cement paste, ε_{ag} is the volumetric strain of aggregate, ε_{cp} is the volumetric strain of cement paste, V_{ag} is the unit volume of aggregate, V_{cp} is the unit volume of cement paste, K_{ag} is the volumetric stiffness of aggregate. The total strain ε_{ij} is obtained from the thermodynamic stress-strain as discussed above. Since ε_0 is known, the parameters which are left are σ_0 , σ_{ag} , σ_{cp} , ε_{ag} and ε_{cp} . To entirely account for the deformation phenomenon, shear stiffness denoted by G_{cp} must be added. This viscoelastic deformation behavior, assuming contribution from aggregate as well, could be defined as a combination of Maxwell and Kelvin model.

If the cement paste acts like a viscous fluid, i.e. possess no shear stiffness, the uniform pressure condition $\sigma_{cp} = \sigma_{ag}$ must hold true. In this case, Maxwell model in series which expresses the relaxation of stress and corresponding deformation is used. On the other hand, when the cement paste hardens, if the shear stiffness of the cement paste does not permit change in shape, i.e the shear stiffness is infinitely large, aggregate and cement paste will hold the same deformation and $\varepsilon_{cp} = \varepsilon_{ag}$. In this case, Kelvin model including creep deformation will be implemented. Since the shear rigidity of the actual hardened cement paste lies between these two extreme cases, generalizing this method would provide the following restraint condition.

$$\left(\frac{\sigma_{ag} - \sigma_{cp}}{f(G_{cp})} \right) + (\varepsilon_{ag} - \varepsilon_{cp}) = 0 \quad (3.92)$$

where G_{cp} is the shear stiffness of hardened cement paste. The ratio g of volumetric strain of composite body could be defined as:

$$g = \frac{3K_1 + 4G_1}{3K_2 + 4G_1} \quad (3.93)$$

where K_1 is the bulk modulus of the base material, K_2 is the bulk modulus of the secibd material and G_1 is the shear modulus of the base material.

In concrete composite body, it is considered that the base material is equivalent to the interfacial transition zone. Then, the shear stiffness of cement paste is formulated as:

$$f(G_{cp}) = 4G_{cp} \quad (3.94)$$

The shear modulus and bulk modulus of cement paste and aggregate are determined from the following equations:

$$K_{cp} = \frac{E_{cp}}{3(1 - 2\nu_{cp})} \quad (3.95)$$

$$G_{cp} = \frac{E_{cp}}{2(1 + \nu_{cp})} \quad (3.96)$$

$$K_{ag} = \frac{E_{ag}}{3(1 - 2\nu_{ag})} \quad (3.97)$$

$$G_{ag} = \frac{E_{ag}}{2(1 + \nu_{ag})} \quad (3.98)$$

where K_{cp} and K_{ag} are the bulk modulus of hardened cement paste and aggregate, G_{cp} and G_{ag} are the shear modulus of hardened cement paste and aggregate, E_{cp} and E_{ag} are the elastic modulus of hardened cement paste and aggregate, and ν_{cp} and ν_{ag} are the

shear modulus of hardened cement paste and aggregate.

Elastic modulus of cement paste is calculated from compressive strength of hydrated cement whereas elastic modulus of aggregate is calculated based on the density of the aggregate.

$$E_{cp} = 716f_{cp}^{0.785} \quad (3.99)$$

$$f_{cp} = 820f(\psi)\exp(-0.05 \times W/B) \quad (3.100)$$

$$f(\psi) = 1.5 - \sqrt{2.47 - 2.22\psi} \quad \psi \geq 0.1 \quad (3.101)$$

$$E_{ag} = (23.5\gamma_{ag} - 57.8) \times 10^4 \quad (3.102)$$

where f_{cp} is the compressive strength of hydrated cement, ψ is the degree of hydration and γ_{ag} is the density of aggregate.

The Poisson's ratio of aggregate is assumed to be a constant of 0.2. On the other hand, the Poisson's ratio of cement paste is determined by incorporating the effect of dispersed aggregates and expressed as effective Poisson's ratio.

$$\nu_{cp} = \{1 - y(x_p)\} \cdot \nu_{cp,pure} \quad (3.103)$$

$$y(x_p) = 0.98(1 - x_p)^{1.8} + 0.02 \quad (3.104)$$

$$x_p = V_{cp} + \frac{E_{cp}}{E_{ag}} \cdot V_{ag} \quad (3.105)$$

where $\nu_{cp,pure}$ is the effective Poisson's ratio of hardened cement paste (around 0.25), x_p is the specific volume of concrete that has been hydrated into hardened concrete and $y(x_p)$ is the degree of restraint from aggregate to hardened cement paste.

The volumetric stress, σ_{cp} , of hardened cement paste is obtained as the summation between the stress from the gel skeletons and the shrinkage stress from driving force.

$$\sigma_{cp} = \dot{\sigma}_{cp} + \sigma_s \quad (3.106)$$

where $\dot{\sigma}_{cp}$ is the volumetric stress generated by hardened cement skeleton and σ_s is the shrinkage stress. $\dot{\sigma}_{cp}$ is computed based on solidification theory which is considered through the following equation:

$$\dot{\sigma}_{cp}(t) = \int_{\dot{t}=0}^t \sigma_{ly}(t, \dot{t}) d\psi(\dot{t}) \quad (3.107)$$

where $\dot{\sigma}_{cp}(t)$ is the volumetric stress generated from hardened cement paste skeleton, $\sigma_{ly}(t, \dot{t})$ is the volumetric stress in each cluster, t is the current time and \dot{t} is the time at

which each cluster has been formed.

Generally, shear stiffness due to contact between the dispersed aggregates can be ignored. Based on this generalization, the shear stiffness of the two-phase composite is roughly equivalent to the shear stiffness of the hardened cement paste matrix. Two additional factors should be put into consideration. The first one is the stiffness of interfacial transition zones, formed at the surface between aggregate and cement paste, is very low, which is assumed to hold a value of 30-50% of the stiffness of cement paste. The second point is that, as aggregate density increases, the degree of restraint on free rotation of aggregate particles increases sharply. The model is expressed as below.

$$S_{ij} = (S_{ij})_{cp} = f \left((e_{ij})_{cp} \right) \quad (3.108)$$

$$(e_{ij})_{cp} = h(x_d) \cdot e_{ij} \quad (3.109)$$

where S_{ij} is the deviatoric stress tensor in a two-phase composite, $(S_{ij})_{cp}$ is the deviatoric stress tensor for the cement paste, e_{ij} is the deviatoric strain tensor in a two-phase composite and $(e_{ij})_{cp}$ is the deviatoric strain tensor for the cement paste.

$$S_{ij} = \sigma_{ij} - \sigma_0 \delta_{ij} \quad (3.110)$$

$$e_{ij} = \varepsilon_{ij} - \varepsilon_0 \delta_{ij} \quad (3.111)$$

$$\sigma_{ij} = \begin{bmatrix} \sigma_{xx} & \sigma_{xy} & \sigma_{xz} \\ \sigma_{yx} & \sigma_{yy} & \sigma_{yz} \\ \sigma_{zx} & \sigma_{zy} & \sigma_{zz} \end{bmatrix} \quad (3.112)$$

$$\varepsilon_{ij} = \begin{bmatrix} \varepsilon_{xx} & \varepsilon_{xy} & \varepsilon_{xz} \\ \varepsilon_{yx} & \varepsilon_{yy} & \varepsilon_{yz} \\ \varepsilon_{zx} & \varepsilon_{zy} & \varepsilon_{zz} \end{bmatrix} \quad (3.113)$$

$$\delta_{ij} = \begin{cases} 1.0, & \text{if } i = j \\ 0.0, & \text{if } i \neq j \end{cases} \quad (3.114)$$

where $h(x_d)$ is a function representing a ratio between cement paste shear strain and concrete shear strain.

$$h(x_d) = Z_d(a_d + b_d) \quad (3.115)$$

$$a_d = g(x_d) \left(\frac{1}{1 - V_{ag}} - 1 \right) + 1 \quad (3.116)$$

$$b_d = \frac{1}{1 - V_{ag}} \quad (3.117)$$

$$Z_d = 0.5 (1 + e^{-10x_d}) \quad \text{if } x_d < 0.1, \text{ then } x_d = 0.1 \quad (3.118)$$

where Z_d is the parameter reflecting the shear strain properties of young cement paste, a_d is the analytical solution obtained when perfect agreement between the aggregate and cement paste is assumed, b_d is the state in which the aggregate particles in the cement matrix are free from rotation and x_d is the intensity index of aggregate dispersion.

3.1.5.3 Solidification of hardened cement paste

Followed by the hydration, this microstructural development model considers that, as hydration proceeds, additional fictitious clusters are included into the original clusters which will provide more stiffness in relation to the thickness of the current clusters. Even though the properties of clusters do not change in relevant to time, the properties of each formed cluster are mutually independent based on the history of age that they formed. Based on this assumption, the hydration of these fictitious clusters are determined by the degree of hydration, which is represented by:

$$\psi_t = \frac{Q_{(t)}}{Q_\infty} \quad (3.119)$$

where ψ_t is the degree of hydration, $Q_{(t)}$ is the amount of heat generated by the hydrated cement and Q_∞ is the total amount of heat generated.

The total stress of the hardened cement paste is expressed by the summation of stress in each cluster, denoted by σ_{ly} . Thus, the state of stress in the cluster is a function of strain at the local time t , strain at the time \dot{t} at which the cluster is formed, and the thermodynamic state.

$$\sigma_{ly} = \sigma_{ly}(t, \dot{t}) \quad (3.120)$$

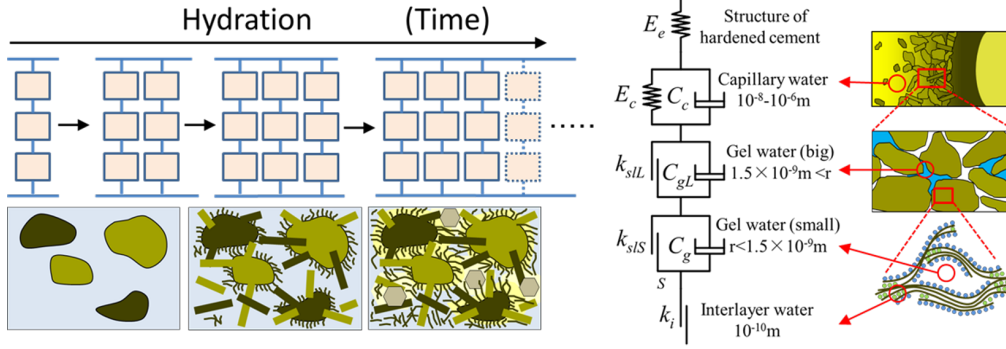


Figure 3.2: Solidifying clusters of cement paste and aging

Refer to Figure 3.2, assumption is made that the strain in each cluster is equivalent to the strain of cement paste and the stress of cement paste is equivalent to the summation of all the cluster stresses regardless of their distinct stress values. Therefore, to express the solidification theory, volumetric and deviatoric stress components are generalized into these integral equations.

$$\dot{\sigma}_{cp}(t) = \int_{i=0}^t \sigma_{ly}(t, \dot{t}) d\psi(\dot{t}) \quad (3.121)$$

$$(S_{ij})_{cp}(t) = \int_{i=0}^t \dot{S}_{ij}(t, \dot{t}) d\psi(\dot{t}) \quad (3.122)$$

where $\dot{\sigma}_{cp}(t)$ is the volumetric stress in the hardened cement paste, $\sigma_{ly}(t, \dot{t})$ is the volumetric stress in the cluster, t is the current time and \dot{t} is the time at which each cluster has been formed, $(S_{ij})_{cp}(t)$ is the deviatoric stress in the hardened cement paste and $\dot{S}_{ij}(t, \dot{t})$ is the deviatoric stress in the cluster. As new clusters formed, their initial stress must be zero despite the concrete strain is not zero since the newly formed cluster cannot be regarded as a component of cement paste yet. Therefore, $\sigma_{ly}(t, \dot{t}) = 0$ and $\dot{S}_{ij}(t, \dot{t}) = 0$.

3.1.5.4 Simplified rheological model for fictitious cluster of cement paste

The existence of water molecules in the pores varies distinctively from interlayer pores to capillary pores with different shapes, sizes, structural connectivity as well as the actual moisture condition in each type of pores. Therefore, the pore structures considered for the fictitious clusters are divided into three categories with their own individual models.

Interlayer pores and interlayer water: In C-S-H gels, which possess a sheet-like layer structure, the pore space between the layers is referred as interlayer pores and contain only one layer of water molecules. Interlayer water is considered to be hardly movable due to applied stress alone, meaning the driving force of water dissipation in interlayer pores is dependent on low relative humidity and high temperature.

Gel pores and gel water: Gel pores (with radius of approximately 10^{-9} to 10^{-8} m) is believed to migrate extremely slow which would exhibit deformation that exists over long period of time. Furthermore, due to the reason that a lot of surface energy exists in gel pore surfaces, deformed gel pores do not recover easily i.e. irreversibility is incorporated for gel pores in the model.

Capillary pores and capillary water: Water in capillary pores that are not filled with gel particles yet (with radius approximately of 10^{-8} to 10^{-6} m), is believed to migrate relatively fast and recoverable under sustained stress. This moisture motion inside capillary pores could be assumed as the greatest component that defines the time-dependent deformation since it governs the short-term creep or early-age creep. Additionally, as hydration proceeds, the capillary pores are gradually filled with hydration products, which will cause a reduction in the pore volume and size. Therefore, the rate of change in creep consequently reduce.

Based on these assumptions, elastic strain, visco-elastic strain, plastic strain and visco-plastic strain are expressed as spring, spring and dashpot, slider and dashpot, and slider, respectively. All of these deformations are connected in series. Therefore, the increment of strain that occurs after normal cluster formation is defined as:

$$\varepsilon_{ly} = \varepsilon_e + \varepsilon_c + \varepsilon_g + \varepsilon_l \quad (3.123)$$

where ε_{ly} is the total strain in each cluster, ε_e is the instantaneous elastic strain in the gel particles and capillary pore structures, ε_c is the visco-elastic strain in the capillary pore structures, ε_g is the visco-elastic strain in the gel particle structures and ε_l is the instantaneous plastic strain related to the interlayer pore structures. As new clusters are originated, their initial strains are equivalent to the total strain at the stage they are included into the parallel system, so as to correspond to zero initial stress. Thus, the volumetric strain, ε_{ly} , in the cluster at time t can be exhibited as the difference between the volumetric strain in cement paste, ε_{cp} , at time t and at time \dot{t} of general cluster formation.

$$\varepsilon_{ly}(t) = \varepsilon_{cp}(t) - \varepsilon_{cp}(\dot{t}) \quad (3.124)$$

where ε_{cp} is the volumetric strain of cement paste obtained from the two-phase composite model depicted above.

3.1.5.4.1 Elastic model of gel particles and capillary pore structures

The spring presented in the Figure [3.2](#) represents the elastic deformation of newly formed gel particles and the larger-scale capillary pore structures composed of these gel

particles and increment of stiffness due to hydration is also incorporated into the formula.

$$\varepsilon_{ly} = E_e \cdot \varepsilon_e \quad (3.125)$$

where ε_{ly} is the volumetric stress in the cluster, E_e is the volumetric stiffness of the elastic spring and ε_e is the instantaneous elastic strain. The volumetric stiffness of the elastic spring represents the stiffness of the newly formed cluster and is expressed as:

$$E_e = \frac{dK_{cp}}{d\psi} \quad (3.126)$$

$$K_{cp} = \frac{E_{cp}}{3(1 - 2\nu_{cp})} \quad (3.127)$$

3.1.5.4.2 Visco-elastic model of capillary pore structures

The reversible deformation in the capillary pore structure formed by gel particles and the motion of water in the capillary pores are expressed by elastic spring and viscous dashpot, respectively, via Kelvin chain as:

$$\sigma_{ly} = E_c \cdot \varepsilon_c + E_c \cdot C_c \frac{d\varepsilon_c}{dt} \quad (3.128)$$

where E_c is the volumetric stiffness of the elastic spring, ε_c is the visco-elastic strain and C_c is the viscous coefficient (1/day) of the dashpot. The volumetric stiffness E_c is used to define the limiting value of deformation of capillary pore structures, which is time-delayed and is expressed as:

$$E_c = a_{ec} E_e f_{ec}(S_{cap}) \quad (3.129)$$

$$a_{ec} = 3.0 \quad (3.130)$$

$$f_{ec}(S_{cap}) = 0.51(1 + S_{cap}^2) \quad (3.131)$$

where a_{ec} is a constant and S_{cap} is the degree of saturation of capillary pores at time t . The constant a_{ec} takes into account the instantaneous elastic deformation and the limiting value of delayed reversible deformation. The function f_{ec} is an index which covers the influence of moisture equilibrium state in capillary pores on the volumetric stiffness E_c . When the saturation in the capillary pores is low, the elastic coefficient will become small due to the reduction in stress from lower amount of water to bear. Consequently, the delay limiting deformation value increases. Additionally, the elastic stiffness of the dried concrete is considered to be small as compared to wet concrete.

Based on the thermodynamic system, the coefficient C_c relates the viscosity of the visco-elastic model due to the state variables of capillary pores (degree of saturation, pore structure, and viscosity of water) which is defined as follows:

$$C_c = a_{cc} \cdot \beta_S^c(S_{cap}) \cdot \beta_T(\eta(T)) \cdot \beta_r^c(B_{cap}) \quad (3.132)$$

$$a_{cc} = 4.3 \times 10^{-3} \quad (3.133)$$

$$\beta_S^c = -3.75(S_{cap})^3 + 5.7(S_{cap})^2 - 1.2(S_{cap}) + 0.075 \quad (3.134)$$

$$\beta_t = 10 + \eta(T) \quad (3.135)$$

$$\beta_r^c = \frac{B_{cap}}{10^6} \quad \text{if } \beta_r^c < 1, \text{ then } \beta_r^c = 1 \quad (3.136)$$

$$\eta = \frac{\eta_i \exp\left(\frac{G_e}{RT}\right)}{\eta_i^{295K}} \quad (3.137)$$

where a_{cc} is a constant (1/day), η is the viscosity of liquid water, η_i is the viscosity of liquid water in non-ideal condition (Pa · s), G_e is the additional Gibbs free energy required for liquid water to flow in non-ideal conditions (J/mol), R is the gas constant (J/mol/K), T is the absolute temperature (K), η_i^{295K} is the viscosity of liquid water in non-ideal condition at temperature of 295K, B_{cap} is a parameter that determine the shape of the capillary pores at the time t (1/m) and $1/B_{cap}$ corresponds to the representative radius of the capillary pores.

As the viscosity of the liquid water in the micro-pores increase, the liquid water's mobility decreases which corresponds to an increment in the viscous coefficient of dashpot. Furthermore, as hydration progresses, the gel volume will increase which cause the capillary pores to become smaller and, hence, an increment in the viscous coefficient will be observed. Additionally, if condensed water completely fill the capillary pores, migration towards adjacent pores might not happen at ease. Therefore, as degree of saturation rises, the coefficient of viscosity also surges.

3.1.5.4.3 Visco-elastic model of gel pore structures

Visco-elastic model represents the delayed and irreversible deformation occurred in the gel pores. Therefore, this deformation is determined by the irreversible dashpot slider as the slider in parallel deforms while water migrates slowly inside the gel pores. In the visco-elastic model, gel voids are divided based on the pore size, which is relatively large even though it is smaller than capillary pores. One portion of gel pores would be those larger-in-size pores that behave like capillary pores, which exhibit short-term behavior and

their saturation could degree under ordinary drying conditions. The other portion would be the smaller-in-size gel pores that exhibit long-term behavior and saturation decreases only under severe drying conditions. Based on our research so far, it is assumed that the boundary between the large gel pore and small gel pore is 1.5 nm. Thus, the visco-elastic deformation is defined as:

For small gel pores: $r \leq 1.5\text{nm}$

$$\frac{d\varepsilon_{gS}}{dt} = \frac{1}{C_{gS}}(\varepsilon_{glimS} - \varepsilon_{g,eq}) \quad (3.138)$$

where ε_{gS} is the visco-plastic strain of gel pores with $r \leq 1.5\text{nm}$, ε_{glimS} is the limiting value of visco-plastic deformation of gel pores with $r \leq 1.5\text{nm}$, C_{gS} is the viscous coefficient of gel pores with $r \leq 1.5\text{nm}$ and $\varepsilon_{g,eq}$ is the equivalent plastic strain.

For large gel pores: $r > 1.5 \text{ nm}$

$$\frac{d\varepsilon_{gL}}{dt} = \frac{1}{C_{gL}}(\varepsilon_{glimL} - \varepsilon_{g,eq}) \quad (3.139)$$

where ε_{gL} is the visco-plastic strain of gel pores with $r > 1.5\text{nm}$, ε_{glimL} is the limiting value of visco-plastic deformation of gel pores with $r > 1.5\text{nm}$, C_{gL} is the viscous coefficient of gel pores with $r > 1.5\text{nm}$ and $\varepsilon_{g,eq}$ is the equivalent plastic strain.

$\varepsilon_{g,eq}$, which is the limiting value of visco-plastic strain, is assumed to be caused by to the stress imposed on the cluster by stress, the degree of saturation and temperature. Furthermore, based on the experiments of creep, they showed that if gel pores are saturated with water, creep deformation is small even under large stresses. Contradictorily, in drying conditions, moisture in gel pores is dissipated which consequently would leave space for additional deformation and this would cause the limiting value of plastic deformation to increase. Also, as temperature elevates, the Gibb's energy of gel water will increase, this increment will improve the motion of water molecules in gel pores, which means increment in plastic deformation.

For small gel pores: $r \leq 1.5 \text{ nm}$

$$\varepsilon_{glimS} = 1.5 \frac{\sigma_{ly}}{E_e} f_{gS}(S_{gel(r \leq 1.5nm)}) \cdot \xi_{TgS}(T) \quad (3.140)$$

$$f_{gS}(S_{gel(r \leq 1.5nm)}) = 1.5 - 0.5S_{gel(r \leq 1.5nm)}^2 \quad (3.141)$$

where σ_{ly} is volumetric stress in hydrated clusters (N/mm^2), E_e is the stiffness of elastic spring (N/mm^2), $S_{gel(r \leq 1.5nm)}$ is the degree of saturation of gel pores with $r \leq 1.5 \text{ nm}$ at time t , T is the absolute temperature (K).

For large gel pores: $r > 1.5$ nm

$$\varepsilon_{glimL} = 1.5 \frac{\sigma_{ly}}{E_e} f_{gL}(S_{gel(r>1.5nm)}) \cdot \xi_{TgL}(T) \quad (3.142)$$

$$f_{gL}(S_{gel(r>1.5nm)}) = 2.5 - 1.5 S_{gel(r>1.5nm)}^2 \quad (3.143)$$

where σ_{ly} is volumetric stress in hydrated clusters(N/mm²), E_e is the stiffness of elastic spring (N/mm²), $S_{gel(r>1.5nm)}$ is the degree of saturation of gel pores with $r > 1.5$ nm at time t , T is the absolute temperature (K).

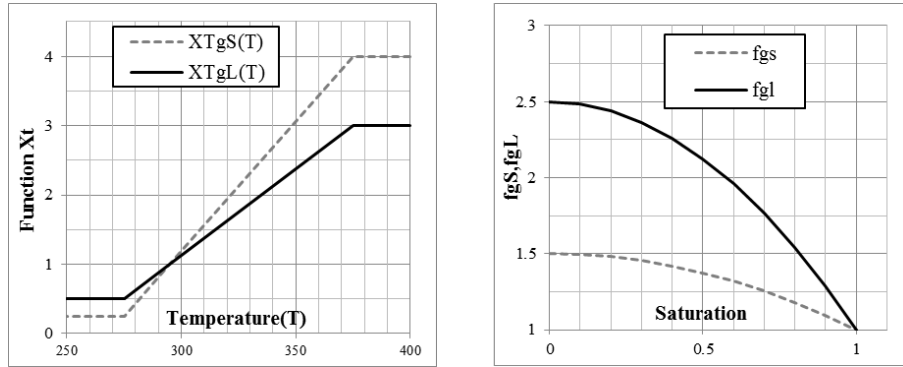


Figure 3.3: Effects of temperature and moisture status in gel pores on visco-plastic strain

The viscous coefficient C_{gS} and C_{gL} is used to define the material properties based on the water motion characteristics, i.e. degree of saturation and viscosity of water, of gel pores as:

For small gel pores: $r \leq 1.5$ nm

$$C_{gS} = a_{cgS} \cdot \beta_S^{gS}(S_{gel(r \leq 1.5nm)}) \cdot \beta_T(\eta(T)) \quad (3.144)$$

$$a_{cgS} = 30 \times a_{cgL} = 30 \times 0.0864 = 5.9(1/day) \quad (3.145)$$

$$\begin{aligned} \beta_S^{gS}(S_{gel(r \leq 1.5nm)}) = & - 3.75(\beta_S^{gS}(S_{gel(r \leq 1.5nm)}))^3 \\ & + 5.7(\beta_S^{gS}(S_{gel(r \leq 1.5nm)}))^2 \\ & - 1.2(\beta_S^{gS}(S_{gel(r \leq 1.5nm)})) + 0.075 \end{aligned} \quad (3.146)$$

$$\beta_T = 10 + \eta(T) \quad (3.147)$$

For large gel pores: $r > 1.5$ nm

$$C_{gL} = a_{cgL} \cdot \beta_S^{gL}(S_{gel(r > 1.5nm)}) \cdot \beta_T(\eta(T)) \quad (3.148)$$

$$a_{cgL} = 0.0864(1/day) \quad (3.149)$$

$$\begin{aligned} \beta_S^{gL}(S_{gel(r>1.5nm)}) &= -3.75(\beta_S^{gL}(S_{gel(r>1.5nm)}))^3 \\ &+ 5.7(\beta_S^{gL}(S_{gel(r>1.5nm)}))^2 \end{aligned} \quad (3.150)$$

$$\begin{aligned} &- 1.2(\beta_S^{gL}(S_{gel(r>1.5nm)})) + 0.075 \\ \beta_T &= 10 + \eta(T) \end{aligned} \quad (3.151)$$

The theoretical consideration concerning the degree of saturation, S_{gel} , and the viscosity of liquid water in the gel pores, ν , is basically the same as that of visco-elastic part in capillary pores as mentioned previously above. When the degree of saturation is higher in gel pores, the water molecules would find it harder to migrate, then C_g will increase. Furthermore, viscosity of liquid water, ν , which is dependent on temperature is also taken into account. Finally, equivalent plastic strain for both small and large gel pores, $\varepsilon_{g,eq}$, could be represented by:

$$\varepsilon_{g,eq} = \begin{cases} \max\left(\frac{W_g}{\sigma_{ly}}, \varepsilon_g\right), & \text{if } \sigma_{ly} \geq 0 \\ h^{n2} + c, \max\left(\frac{W_g}{\sigma_{ly}}, \varepsilon_g\right), & \text{if } \sigma_{ly} < 0 \end{cases} \quad (3.152)$$

$$\varepsilon_g = \varepsilon_{gS} + \varepsilon_{gL} = \int d\varepsilon_{gS} + \int d\varepsilon_{gL} \quad (3.153)$$

where ε_g is the plastic strain, $\varepsilon_{g,eq}$ is the equivalent plastic strain and W_g is the plastic work.

3.1.5.4.4 Plastic model for interlayer pore structures

The interlayer pore plastic deformation model consists of sliders only as it is more related to the motion of water in interlayer pores. It is assumed that applied stress could not bring significant deformation to the interlayer pores as opposed to the thermodynamic variables. Under severe drying condition, as water has been depleted from the interlayer pores, this interlayer pore plastic deformation model contribute significantly to the overall deformation.

$$\frac{d\varepsilon_l}{dt} = E_l \cdot \Phi_{int} \frac{dS_{int}}{dt} \quad (3.154)$$

where ε_l is the plastic strain, Φ_{int} is the interlayer pores' porosity and S_{int} is the degree of saturation in interlayer pores and E_l is the plastic strain in a unit interlayer pore, which is equivalent to $1.22 \times 10^5 \mu$.

3.1.5.5 Model of inherent driving force for shrinkage

As previously explained in Section 3.1.5.3, stress in the hardened cement paste could be calculated by:

$$\sigma_{cp} = \dot{\sigma}_{cp} + \sigma_s \quad (3.155)$$

where σ_{cp} is the volumetric stress generated by hardened cement skeleton and σ_s is the shrinkage stress. This section will cover the calculation of shrinkage stress, σ_s .

Pores exist in various sizes, shapes and forms. In gel and capillary pores, it is assumed that capillary tension acting on condensed liquid is the driving force for shrinkage. On the other hand, for smaller pores, desorption of adsorbed water on the pore surfaces would consequently give rise to disjoining pressure as shrinkage would try to close the small gap in the small pores. This model attempts to divide these mutually interconnected driving forces into two separate identities which relate to shrinkage in condensed water and adsorbed water, respectively.

In the initial stage, the gaseous and liquid phase present in the void are defined by the pore radius r_c where the gas-liquid equilibrium is present. The saturation degree of capillary and gel pores, as the pores are being driven unsaturated, is considered by taking account of the amount of water adsorbed by the BET theory and the amount of moisture present in the inkbottle pores. After that, r_{br} is defined as the limiting radius where the mechanism of shrinkage is separated. If the pore size is larger than r_{br} (L group), shrinkage by capillary tension force is dominant whereby shrinkage by disjoining pressure is dominant in pores with size smaller than r_{br} (S group). Based on various verification, the limiting pore size radius is assumed to be 10 nm. As relative humidity is high, r_{br} becomes larger than the gas-liquid equilibrium interface r_c . Thus, liquid completely fills the pores of S group. Since the liquid water in S group is saturated, disjoining pressure would not contribute to the shrinkage force while only the capillary tension comes into play. However, if the relative humidity is low, which then cause r_{br} to become smaller than the gas-liquid equilibrium interface r_c , the pores in S group become unsaturated and shrinkage due to disjoining pressure will dominate.

3.1.5.5.1 Shrinkage model in high relative humidity state ($r_{br} < r_c$)

Since pores of S group are completely filled with liquid water, the disjoining pressure is very low and will be ignored. So, the capillary tension from pores of L group will account for shrinkage in the system, which is calculated as:

$$\sigma_s = \sigma_{sc} = A \cdot V_L \cdot P_l = A \cdot (V_{cpL} + V_{glL}) \cdot P_l \quad (3.156)$$

where σ_s is the total shrinkage stress applied, σ_{sc} is the shrinkage stress due to capillary tension in pores of L group, A is a coefficient, equivalent to 8.0, V_L is moisture content existing in pores of L group (Φ_L)(volume rate per unit paste (m^3/m^3)), V_{cp-L} is the moisture content existing in capillary pores of L group (pores with radius larger than r_{br})(volume rate per unit paste (m^3/m^3)), V_{gl-L} is the moisture content existing in gel pores of L group (pores with radius larger than r_{br})(volume rate per unit paste (m^3/m^3)) and P_l is the pore water pressure (Pa).

3.1.5.5.2 Shrinkage model in low relative humidity state ($r_{br} \geq r_c$)

On the other hand, as pores in S group become unsaturated, the disjoining pressure decreases as the perpendicular distance between the pore walls increases. As disjoining pressure decreases, contraction force will be exerted on the pore walls and show deformation on the hardened cement paste.

$$\delta F = F_0 - F_t \quad (3.157)$$

The attractive force F_0 provided by the skeletons of hardened cement paste is equal to the disjoining force when pores of S group are saturated. Refer to Derjaguin and Churaev's research, disjoining pressure, which decreases as 2 parallel planes moves apart from each other perpendicularly is defined as:

$$\Pi(h) = K \exp\left(-\frac{h}{\lambda}\right) \quad (3.158)$$

where K is the material specific disjoining pressure (MPa). An estimation done by Maruyama on the disjoining pressure of cement through volume change model, which is based on the measured average adsorption thickness and shrinkage strain, to be 4500 MPa, λ is the length of the disjoining pressure and h is the distance between the two interfaces.

When assuming that all the pores are cylindrical, the disjoining pressure must be averaged in consideration of the fact that pores have various sizes, specific surface area, moisture content, etc. Therefore, the attractive force F_0 received from the solid portion of hardened cement paste is equal to the average of disjoining pressure when pores of S group are saturated over the volume and it is defined by the following equation (the integration interval ranges from r_{min} to r_{br} , since it covers only the saturated portion):

$$F_0 = \Phi_S \cdot \frac{\int_{r_{min}}^{r_{br}} \Pi(2r) dx}{x_0} \quad (3.159)$$

where Φ_S is the porosity of pores of S group, x_0 is the total surface of pores of S group, $\Pi(2r)$ is the disjoining pressure acting on the pores of cylindrical radius r and dx is the increment of the pore surface area at any radius r .

Integration all over surface area would provide the summation of the disjoining pressure when the pores of S group are filled with liquid water. Then, if the pores of group S becomes unsaturated, it is crucial to determine the liquid water stuck in the inkbottle space. Thus, F_t is the pressure which separates the part entirely filled with liquid water below the vapor-liquid equilibrium interface r_c and the part occupied inside the inkbottle space of radius r_c or more.

$$F_t = \Phi_S \cdot \frac{\int_{r_{min}}^{r_c} \Pi(2r)dx + \int_{r_c}^{r_{br}} f_r \Pi(2r)dx}{x_0} \quad (3.160)$$

From the above expression, the shrinkage σ_{sd} caused by decrease in disjoining pressure of pores in group S could be expressed as:

$$\begin{aligned} \sigma_{sd} &= \Delta F = F_0 - F_t \\ &= \Phi_S \cdot \frac{\int_{r_{min}}^{r_{br}} \Pi(2r)dx}{x_0} - \Phi_S \cdot \frac{\int_{r_{min}}^{r_c} \Pi(2r)dx + \int_{r_c}^{r_{br}} f_r \Pi(2r)dx}{x_0} \end{aligned} \quad (3.161)$$

$$\sigma_{sd} = \Phi_S \cdot \frac{\int_{r_c}^{r_{br}} \Pi(2r)dx - \int_{r_c}^{r_{br}} f_r \Pi(2r)dx}{x_0} \quad (3.162)$$

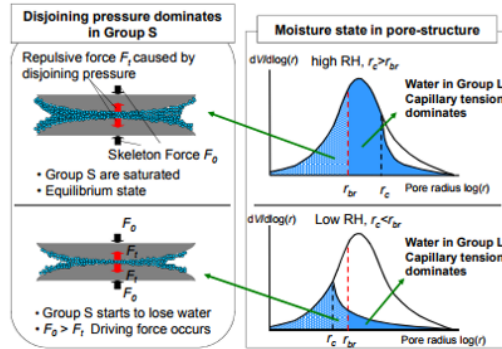


Figure 3.4: Driving force of shrinkage under low and high RH

When the relative humidity due to both capillary tension and disjoining pressure is ultimately high ($r_{br} < r_c$), the driving force for total shrinkage could be expressed as:

$$\begin{aligned} \sigma_s &= \sigma_{sc} + \sigma_{sd} \\ &= A \cdot (V_{cp-L} + V_{gl-L}) \cdot P_l + \Phi_S \cdot \frac{\int_{r_c}^{r_{br}} \Pi(2r)dx - \int_{r_c}^{r_{br}} f_r \Pi(2r)dx}{x_0} \end{aligned} \quad (3.163)$$

3.1.5.5.3 Shrinkage of hardened cement paste and aggregate itself

The volume of resultants produced by the hydration with cement is smaller than the sum of their corresponding reactants before reaction. This is referred as chemical shrinkage, which is the unavoidable shrinkage from hydration itself, which will cause a direct change in volume. On the other hand, after the formation of the clusters of the hardened cement paste from hydration, the formed skeleton constrains the contraction, so that the volume change due to the hydration reaction is considered to be the newly formed pores inside the hardened cement paste.

In addition, cement particles existing in water have different initial arrangement among the particles depending on the water cement ratio. When the water cement ratio decreases, the average distance of the cement particles is small, so some cement particles contacting each other will exist. In some cases, the hydrated products formed are linked to each other. In such a case, the hydration shrinkage seen macroscopically is thought to bring about the volume shrinkage of the whole cement hardened body. Therefore, assuming that the total volume change contributes to the formation of voids and that some parts contribute to macroscopic self-shrinkage, it is assumed that hydration shrinkage contributes differently to self-shrinkage according to the spacing of cement particles. Considering this, the shrinkage strain due to hydration shrinkage is expressed by the following equation:

$$\varepsilon_{sh} = \nu_{ch} f(\delta_m) \quad (3.164)$$

where ε_{sh} is the autogenous shrinkage due to hydration, ν_{ch} is the volume contraction from hydration, δ_m is the maximum thickness of outer deposit layer of cement particles as calculated from the pore structure formation model and is determined from the average particle size and Blaine value of the used binder and $f(\delta_m)$ is the contribution of hydration shrinkage to autogenous shrinkage with average distance of particles as a parameter.

The hydration shrinkage is the shrinkage amount which is obtained as the concrete mixture decreases its volume before and after hydration reaction and is calculated as:

$$\nu_{ch} = \frac{W_{ch}}{\frac{1}{\rho_l} - \frac{1}{\rho_{ch}}} \quad (3.165)$$

where W_{ch} is the bound water (mass per unit concrete), ρ_l is the density of liquid water and ρ_{ch} is the density of bound water ($1.25 \times 10^3 \text{ kg/m}^3$)

Due to the difficulty in obtaining $f(\delta_m)$ directly from experiments, the following formula would approximate the value through various sensitivity analysis referring to their

macroscopic self-shrinkage behavior.

$$f(\delta_m) = 0.0045 \exp(-a\delta_m^b)$$

$$a = 1.2 \times 10^{-4}$$

$$b = 6.0$$
(3.166)

For concrete with water-to-cement ratio of approximately 50%, $f(\delta_m)$ decreases and autogenous shrinkage almost provide no contribution to hydration shrinkage. However, regarding low water-to-cement ratio, the spacing of cement particles and effect of autogenous shrinkage on total hydration shrinkage increases.

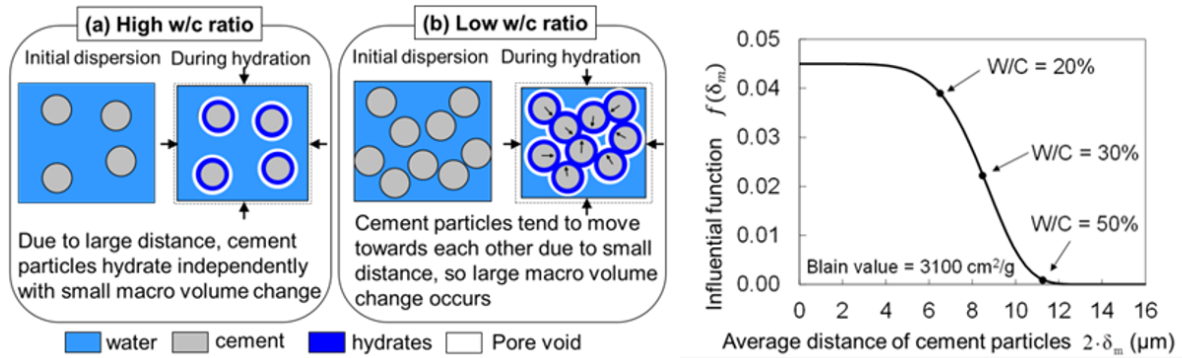


Figure 3.5: Effect of cement particle distribution by w/c and its contribution to hydration shrinkage

3.1.5.5.4 Shrinkage of aggregates

Volumetric change in aggregate affects total shrinkage in concrete in the same manner as hardened cement paste. In the model, shrinkage due to capillary tension and surface energy in aggregate is also considered. However, comparing to the aggregate shrinkage itself, the two aforementioned influences deem a rather lower shrinkage value. Based on experimental results, the aggregate shrinkage model is regarded as a relation between saturation degree in the pores of aggregates and the shrinkage amount of the aggregates.

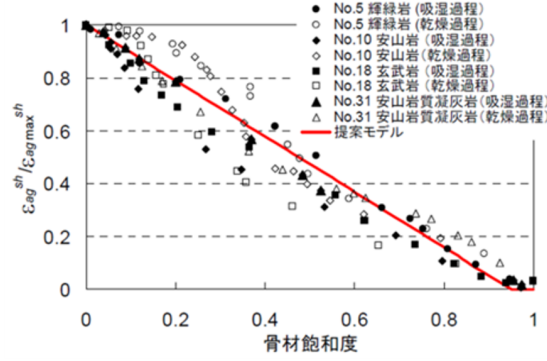


Figure 3.6: Relationship between aggregate shrinkage and aggregate saturation

$$\varepsilon_{ag}^{sh} = \begin{cases} \varepsilon_{ag}^{sh} \left(1.0 - \frac{S_{ag}}{0.95}\right), & \text{if } S_{ag} \leq 0.95 \\ 0.0, & \text{if } S_{ag} > 0.95 \end{cases} \quad (3.167)$$

3.1.5.6 Concrete strength model

3.1.5.6.1 Compressive strength model

There have been many reports which explained the applicability of concrete porosity to express the strength development. However, Otabe[28] are concerned with the fact that porosity theory has its limitation in obtaining the strength of concrete. Therefore, the strength development model in this thermodynamic system will be based upon the hydration products which are responsible for the hardened cement matrix, bulk density, volume of hydrates, etc. First and foremost, explanation on the range of applicability of porosity theory on the strength development of concrete would be done. At a constant void volume, P_{cr} , when the strength is zero, the formula proposed by Schiller[29] shows:

$$f_c = C \ln \left(\frac{P_{cr}}{P} \right) \quad (3.168)$$

$$C = 81.5$$

$$P_{cr} = 0.31$$

where f_c is the compressive strength of cement paste (N/mm^2), P_{cr} is the void volume at zero strength (ml/ml) and P is the void volume (ml/ml)

P_{cr} is assumed to be constant irrespective of the water-to-cement ratio. However, realistically, as water-to-cement ratio decreases, the void volume when the strength is

zero also decreases. For the mean time, P_{cr} is defined as the initial void volume, $V_{cap-ini}$.

$$P_{cr} = \frac{\frac{W}{C} \cdot \rho_c}{\frac{W}{C} \cdot \rho_c + 1} \quad (3.169)$$

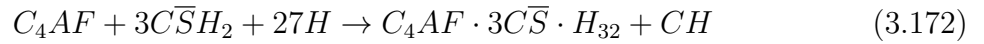
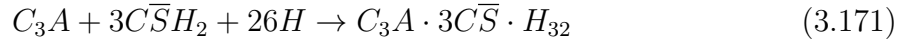
where $\frac{W}{C}$ is the water-to-cement ratio (dimensionless) and ρ_c is the density of cement (kg/cm^3)

The bulk volume of total hydration products, $V_{hyd,total}$ was also considered as the strength increases with the volume of hydrated products. Hence, the void volume is computed by the subtraction of $V_{hyd,total}$ from unit paste volume.

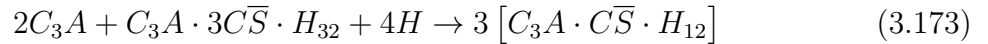
$$P = 1 - V_{hyd,total} \quad (3.170)$$

On the other hand, $V_{hyd,total}$ was obtained from the volumetric change rate of hydration products. The volumetric change rate of hydration products is obtained from the chemical reaction of each mineral and its corresponding reaction rate.

Stoichiometric equations for Aft formation:



Stoichiometric equations for Afm formation:



Stoichiometric equations for C-S-H and other minor hydrates formation:

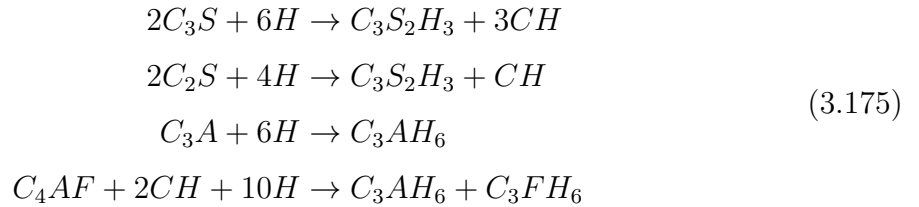


Table 3.1: Summary of the calculated solid phase volume change

Pr_{C_3S}	Pr_{C_2S}	Pr_{C_3Sm}	Pr_{C_4AFm}	Pr_{C_3A}	Pr_{C_4AF}
1.55	1.51	1.20	1.53	1.74	1.75

On the other hand, the fraction of reacted volume R_i of each mineral that participate in the hydration process can be obtained from the rate of hydration obtained from the heat of hydration model as follows:

$$R_i = V_c \cdot p_i \cdot \frac{Q_i}{Q_{i,\infty}} = \frac{1}{\frac{W}{C} \cdot \rho_c + 1} \cdot \rho_i \cdot \frac{Q_i}{Q_{i,\infty}} \quad (3.176)$$

$$V_c = \frac{1}{\frac{W}{C} \cdot \rho_c + 1} \quad (3.177)$$

$$V_w = \frac{\frac{W}{C} \cdot \rho_c}{\frac{W}{C} \cdot \rho_c + 1} \quad (3.178)$$

where ρ_c is the density of cement, V_c is the initial cement volume occupied in the cement paste per unit volume, V_w is the volume of water filled in cement paste per unit volume, ρ_i is the composition ratio of each mineral i , $Q_{i,\infty}$ is the ultimate heat generated by mineral compound i and Q_i is the accumulated heat generated by mineral compound i in the cement.

The volume of hydration products can be obtained through the multiplication of the volume R_i of the reacted mineral i with the solid volume change rate of its corresponding mineral Pr_i . It should be noted that the bulk volume of hydration products is larger than the absolute volume as they contain fine pores (gel and interlayer pores) whereby no more hydration products can deposit. In the hydration heat model, the specific porosity of the hydration products at room temperature is assumed to be 0.28 with respect to the volume of the hydrated products. Model proposed by Otabe [28] assumes that entrapped water in the hydrated cement matrix also contributes to strength development. Therefore, the total bulk volume of hydration products existing in capillary pores could be obtained by the following equation:

$$V_{hyd_total} = \sum (Pr_i \cdot R_i + 0.15\rho_i \cdot R_i) \quad (3.179)$$

The hydration product volume fraction D_{hyd_out} occupied in capillary voids is calcu-

lated as:

$$D_{hyd.out} = \frac{V_{hyd.total} - V_{hyd.ini}}{V_{cap.ini}} \quad (3.180)$$

Therefore, the strength development function based on $D_{hyd.out}$ which is a value between 0 and 1 is calculated as:

$$f_c = f_\infty \left\{ 1 - \exp\left(-\alpha D_{hyd.out}^\beta\right) \right\} \quad (3.181)$$

where f_∞ is the ultimate strength (N/mm²) and α, β are coefficients.

However, based on the equation above, it could not provide the difference between early-age strength and long-term strength. Since $D_{hyd.out}$ is assumed to be the same in the function, the indifference is expected to be from the value. Also, in reality, as the compressive stresses apply to the hardened cement paste, the distance between the particles would get closer. This simply means that the compressive strength increases as water-to-cement ratio decreases. Therefore, the strength development model also includes the effect of voids between the cement particles.

$$\theta = \left(V_{cap.ini}^{\frac{1}{3}} \right) = \left(\frac{\frac{W}{C} \cdot \rho_c}{\frac{W}{C} \cdot \rho_c + 1} \right)^{\frac{1}{3}} \quad (3.182)$$

Then, the compressive strength formula is defined as

$$f_c = f_\infty \left[1 - \exp\left\{-\dot{\alpha} \left(\frac{D_{hyd.out}}{\theta} \right)^\beta\right\} \right] \quad (3.183)$$

$$f_\infty = \left(A \frac{P_{C3S}}{P_{C3S} + P_{C2S}} + B \frac{P_{C2S}}{P_{C3S} + P_{C2S}} \right) \quad (3.184)$$

Then, the model was extended for the application of blast furnace slag cement as well through this model.

$$f_c = f_\infty \left[1 - \exp\left\{-\dot{\alpha} \left(k \cdot \frac{D_{hyd.out}}{\theta} \right)^\beta\right\} \right] \quad (3.185)$$

$$f_\infty = \left(A \frac{P_{C3S}}{P_{C3S} + P_{C2S}} + B \frac{P_{C2S}}{P_{C3S} + P_{C2S}} \right) \cdot P_c + C \cdot P_{sg} \quad (3.186)$$

where k is the coefficient indicating the distance of hydration particle distribution, P_{C3S} is the composition ratio of alite in Portland cement, P_{C2S} is the composition ratio of belite in Portland cement, P_c is the composition ratio of Portland cement, P_{sg} is the composition

ratio of slag and A, B, C is the coefficients contribute to the final ultimate strength of alite, belite and slag, respectively.

3.1.5.6.2 Tensile strength model

The tensile strength of concrete could be obtained by the following equation based on the compressive strength.

$$f_t = 0.58f_c^{2/3} \quad (3.187)$$

3.2 Nonlinear mechanics of reinforced concrete computational system (COM3)

Microscopically progressive micro-cracks in interfacial transition zones between the cement paste matrix and aggregates, which macroscopically cause the whole concrete composite to undergo softening processes, would eventually form a geometrical discontinuity that divide the material, in other words, crack. Realistically, such phenomenon which involves a geometrical discontinuity should be model through the mean of geometry separation. This crack concept is referred as discrete crack model. However, such treatment would mean the nodal connectivity has to be frequently changed to fit with the crack geometry, which entirely misfit the whole concept of finite element method which requires a continuum space for numerical integration. Its counterpart is the smeared crack model, which assumes the whole concrete, cracked or uncracked, to be a continuum whereby the notion of crack is describable in terms of stress-strain relations.

COM3 is a nonlinear structural mechanics of reinforce concrete currently being developed at Concrete Laboratory of the University of Tokyo which implements the smeared crack model. The outline of this model would be discussed below.

3.2.1 Overall composition of the model including cracks

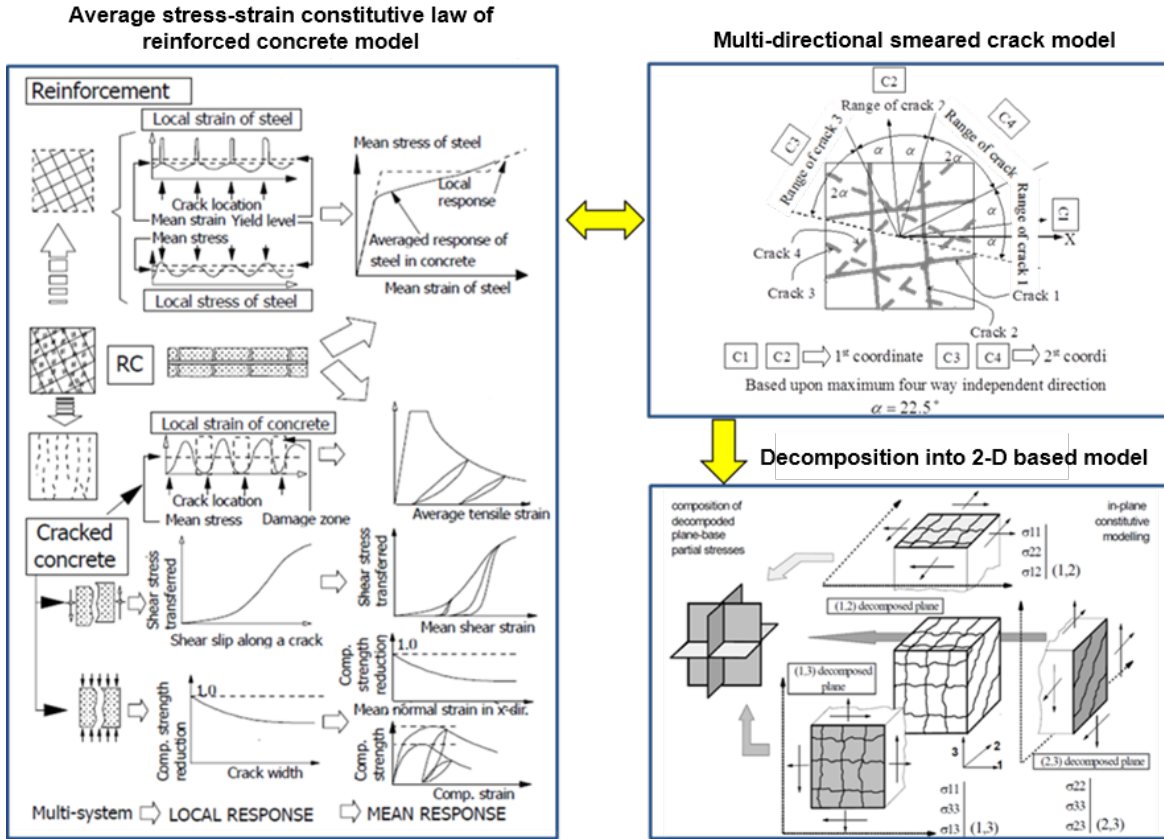


Figure 3.7: Conceptual diagram of cracks in RC from the constitutive modeling

The model of reinforced concrete is expressed by the superimposition of the constitutive law of concrete and reinforcing bars. The moment that maximum principal stress of the concrete reaches the tensile strength of concrete, a three-dimensional orthogonal coordinate system with the vertical direction of the crack plane as the principal axis is assumed as shown in Figure 3.7. Through the use of fixed multi-directional non-orthogonal smeared crack, expressing independent cracks could be possible based on the state of principal stress on the three planes: Plane (1,2), Plane (1,3) and Plane (2,3). Through combining the one-dimensional compression, tension and shear force in a crack plane, a fixed multi-directional non-orthogonal crack model spatially average in two-dimensional plane could be obtained. Individual constitutive laws of compression, tension and shear transfer, which are time-dependent and expressed in term of repetitive accumulation of strain, are added as a fracture parameter to the constitutive law of the average stress-strain relationship verified under short-term load as shown in Figure 3.7 (Left). Although this model does not consider the micro-scale defects as DuCOM does, it still takes into consideration the progress of microscopic damage such as fatigue and creep rupture at high

stress. In the integrated multi-scale computational system, DuCOM-COM3, the progress of stress would be stopped at COM3 once crack occurs and the stress progress is computed from DuCOM through various thermodynamic processes ranging from hydration, pore-structure development, vapor-moisture equilibrium and migration, cluster expansion, etc. Therefore, the coalescence of the system will decide the whole behavior.

Chapter 4

Experimental Investigation on Expansive Additives

Contents

4.1 Introduction	53
4.2 Experimental Programme	54
4.2.1 Materials	54
4.2.2 X-ray Diffraction and Thermogravimetric Experiment	54
4.2.3 Isothermal conduction calorimetry	59
4.2.4 Unrestrained expansion of expansive cement paste	65
4.3 Conclusion	67

4.1 Introduction

In order to realize this expansive additive model, experimental investigations into the phenomena that leads to expansion in the first place shall be done. As already mentioned in Section 2.3, hydration, volume fraction of the expansive crystals, and local crystallization pressure are the precursors in volumetric expansion of expansive additive system. Therefore, the experimental studies, which will be presented in the following sections comprise of hydration studies and unrestrained expansion of expansive additive cement paste with these parent phases: f-Lime (f- CaO), Hauyne ($C_4A_3\bar{S}$) and Anhydrite ($C\bar{S}$).

4.2 Experimental Programme

4.2.1 Materials

The chemical and mineral composition of various raw materials utilized in this study are listed in Table 4.1 and Table 4.2. As shown in Table 4.2, three types of expansive additives with different amount of f-Lime, Hauyne and Anhydrite were used, which would enable us to view the correlation between the amount of CH and ettringite crystals that are formed and expansion intensity.

Table 4.1: Chemical composition in - (1) Power-CSA (pcsa) & (2) #20

Expansive mat.	Density	Blaine fineness	Chemical composition (Weight %)						
	g/cm ³	cm ² /g	LOI	SiO ₂	Al ₂ O ₃	Fe ₂ O ₃	CaO	MgO	SO ₃
Denka-pcsa	3.10	-	3	1.2	5.0	1.2	69.5	0.9	19.5
Denka-#20	3.10	-	3	1.5	9.0	0.6	51.8	1.4	29
Taiheiyo-HyperExpan	3.16	-	1.2	4.2	1.1	1.2	74.0	0.51	16.5
OPC	3.16	3490	0.6	21.8	4.5	2.9	64	1.84	2.26

Table 4.2: Mineral composition in - (1) Power-CSA (pcsa) & (2) #20 & (3) OPC

Materials	Phases (Weight %)						
	C ₃ A	C ₂ S	C ₃ S	C ₄ AF	f-CaO	C ₄ A ₃ S	C \bar{S}
Denka-pcsa	-	-	-	-	44.0	12.2	31.0
Denka-#20	-	-	-	-	17.0	27.0	46.0
Taiheiyo-HyperExpan	-	-	20.4	-	43.0	-	30.9
OPC(bogue)	5.6	18.3	62.2	5.6	-	-	-

4.2.2 X-ray Diffraction and Thermogravimetric Experiment

4.2.2.1 Sample Preparation

Two types of expansive additives were used in the study: Denka-PCSA (free-lime content is higher than Hauyne content) and Denka-#20 (free-lime content is lower than Hauyne content). The water-to-binder ratio was 0.4. Only 100% and 50% replacement ratio with ordinary Portland cement were used in this study as the 100% replacement case would be used to derive a simple reference heat rate and 50% replacement ratio would be used to validate the results after installing the simple heat rate. To ensure the consistency of the

pastes, samples were prepared by following procedures according to ASTM C305-20 [30] and practical guidance proposed by Scrivener et al. [31]. In the future, a more intensive hydration study will be done. In order to minimize bleeding, the pastes were stored in cylinder bottles whereby the bottles were rotated horizontally for approximately 6 h or more until the pastes set.

4.2.2.2 Methods

As hydrated expansive crystals is one of the factors that govern the expansion characteristics, it is extremely crucial to keep track of the amount of Hauyne, Anhydrite and Free-Lime consumed and the amount of ettringites and CH produced. In this study, solvent exchange method utilizing isopropanol was conducted since it does not harmfully influence the microstructure [31]. At these designated ages (0.0625, 0.125, 0.1875, 0.25, 0.3125, 0.375, 0.5, 1, 3, 7 and 14 days), the sample was crushed into pieces of below 1 cm and gently ground into powder by hand. Any type of machine grinding was not used in this test because it has significant effect on phase assemblage and then the microstructural analysis of cement paste [31]. After that, the ground powder was immediately immersed in isopropanol for about 10 minutes, after which the powder sample was separated from isopropanol through suction and retained on filtered paper. The collected powder sample was again immersed in isopropanol for an additional 2 days whereby isopropanol would be replaced for the third time and kept for a total of 1 week [32]. After this hydration stoppage process, all samples were dried in a desiccator with silica gels for 1 week. The specimens are all stored in vacuum condition to avoid carbonation and environmental control room at 20°C. After drying, all samples would be sieved through 100 μm and used for XRD and TG analyses.

Internal standard method was used to determine the amount of amorphous inside the powders. Ten percent corundum (Al_2O_3), relative to the weight of cement, was blended with the sieved hydrated powder. The dry mixed powder was then placed in the sample holder for X-ray diffraction analysis via backloading approach. Measurement of powder X-ray diffraction was conducted via a D2 Phaser X-ray diffractometer (Bruker) under the following conditions: Cu-K α X-ray source, 30 kV tube voltage, $2\theta=5^\circ$ to 70° scanning range, 0.02° step width and $0.05^\circ/\text{min}$ scanning speed. For Rietveld analysis, TOPAS software (Bruker) was utilized. The phases that were considered include: alite, belite, aluminate, ferrite, periclase, gypsum, bassanite, portlandite, ettringite, calcium monosulfoaluminate, and calcite. The refined parameters consist of phase scale factors, background coefficients, peak shape parameters, and preferred orientation, as needed to obtain a goodness of fit less than 3. The amorphous content was calculated by using the

following equation [33]:

$$W_{amor} = \frac{100 \times W_{rva} - W_{add}}{W_{rva} (100 - W_{add})} \times 100 \quad (4.1)$$

where W_{amor} is the amorphous material mass percentage, W_{rva} is the mass percentage of the internal standard based on Rietveld analysis and W_{add} is the mass percentage of the internal standard added.

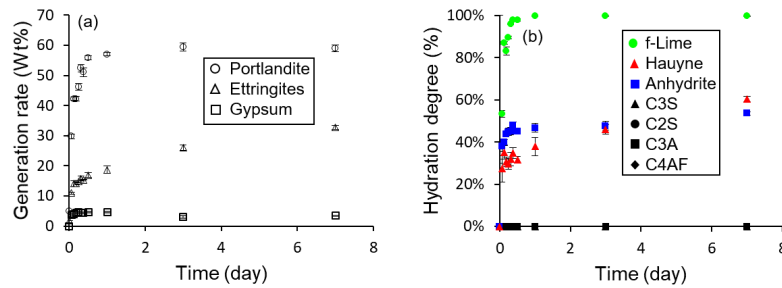
To calculate the chemically combined water from XRD analyses, the water inside each hydrated chemical compound is extracted, i.e. portlandite (1 H from CH), ettringite (32 H from $C_6A\bar{S}_4H_{32}$), gypsum (2 H from $C\bar{S}H_2$), and bassanite (1/2 H from $C\bar{S}H_{1/2}$). Furthermore, it was assumed that the amorphous content in the OPC-expansive additive blend is mainly C-S-H. The water that would be bound to C-S-H (4 H from $C_{1.7}SH_4$) is determined from the amorphous content and the chemical formula based on the stoichiometric equations:



TGA for the calcium hydroxide and loss on ignition(LOI) was conducted at a heating rate of 2°C/min upto 1000°C under a nitrogen atmosphere. The weight percentage of calcium hydroxide was calculated between the temperature of 415 °C and 515 °C [34].

The degree of hydration of phases was determined by initially adjusting the phase at the designated time relative to the original unhydrated phases by removing LOI factor.

4.2.2.3 Results from X-ray diffraction and Thermogravimetric analysis



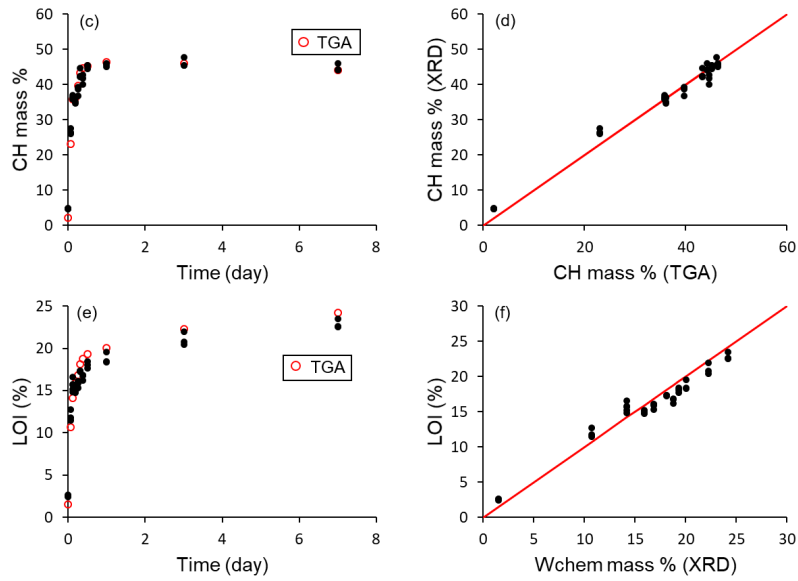


Figure 4.1: Experimental results for expansive additives: PCSA with replacement ratio of 100%

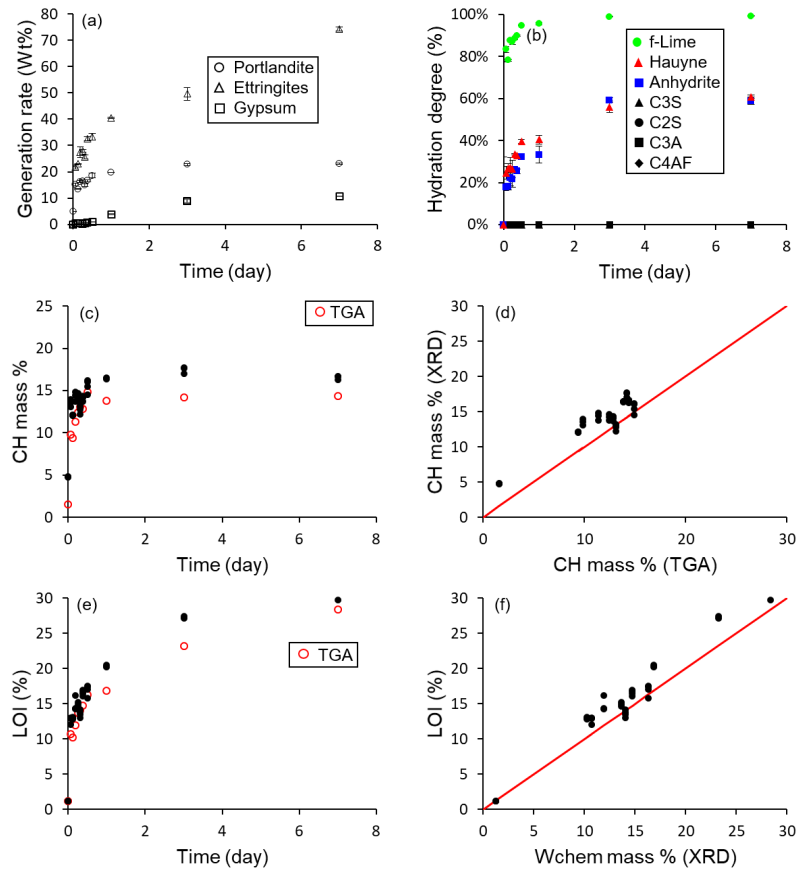


Figure 4.2: Experimental results for expansive additives: #20 with replacement ratio of 100%

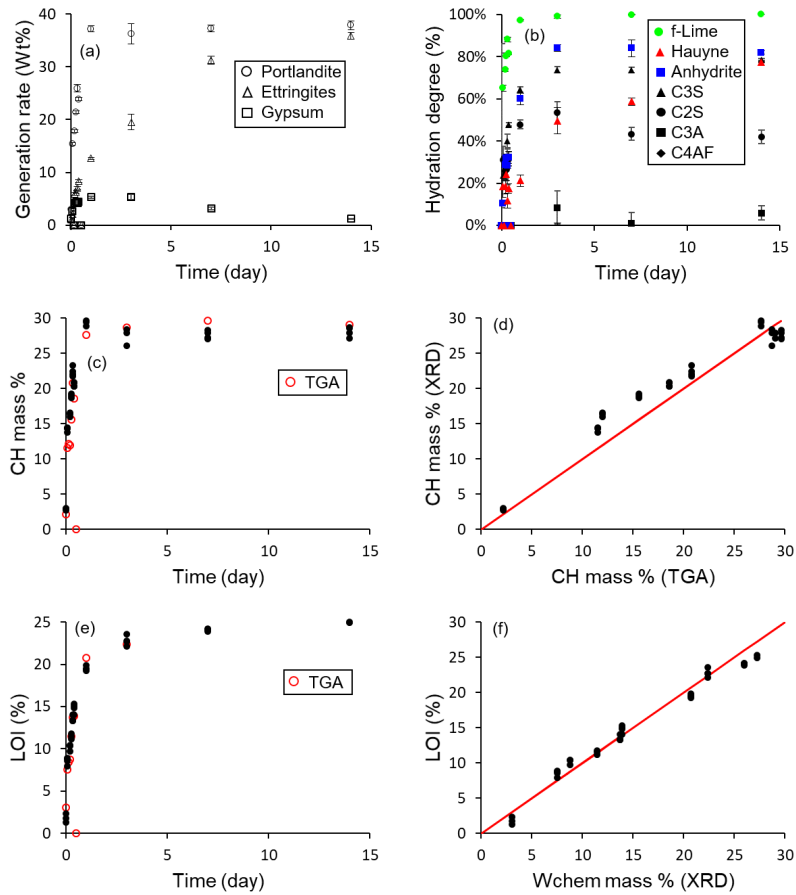
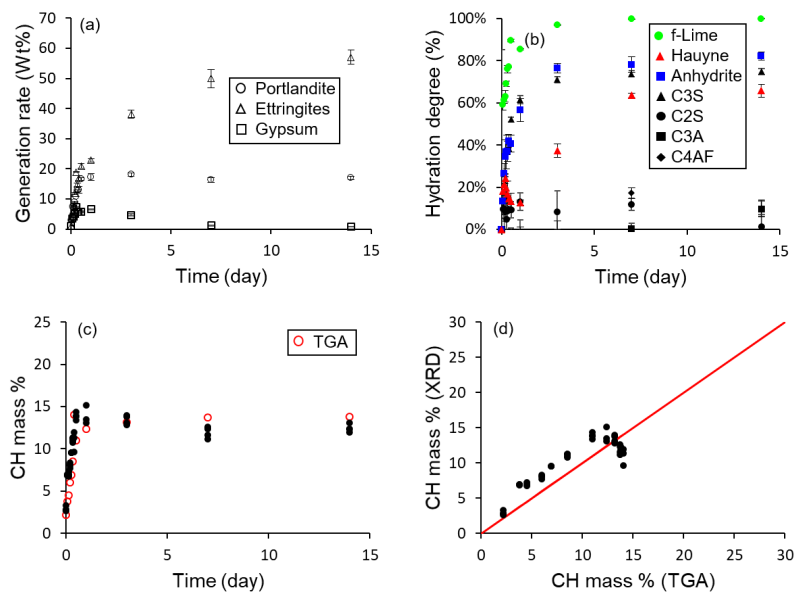


Figure 4.3: Experimental results for expansive additives: PCSA-OPC system with replacement ratio of 50%



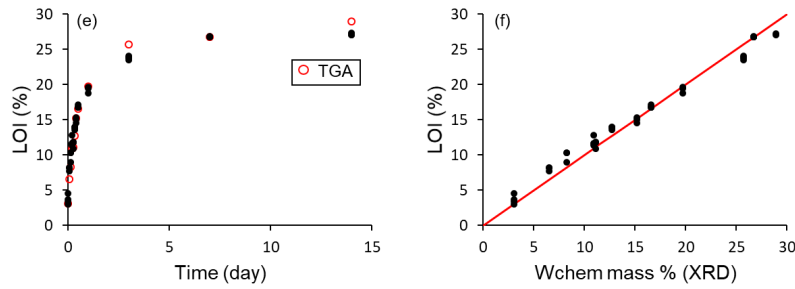


Figure 4.4: Experimental results for expansive additives: #20-OPC system with replacement ratio of 50%

Based on the results, which are shown here from Figure 4.1 to 4.4, qualitatively, it could be concluded that hydration of free-lime is the fastest among the three type of expansive additive phases. This result of free-lime hydration aligns with the evidence mentioned [35]. It also suggest a hypothesis that, if the content of free-lime is high in the expansive additive and ordinary Portland cement system, the particle would start to contact and attain a rigidly deformable microstructure in faster manner. As free-lime hydration consumes abundant amount of water, we could see the stagnation in the hydration of Hauayne and Anhydrite since, presumably, the free-water for hydration has been almost consumed. Additionally, the hydration of Anhydrite and Hauayne is rather complicated inside the cement and expansive additive systems as they both have a lot of interaction with other co-existing clinker phases. Therefore, further studies shall be needed to conduct regarding the effect of low water supplies (low water-to-binder ratio) and lower replacement ratios of expansive additives.

4.2.3 Isothermal conduction calorimetry

4.2.3.1 Sample Preparation

Cement paste samples were prepared at water-to-binder ratio of 0.40. 0%, 10%, 20%, 50% and 100% replacement ratio of OPC were used for the corresponding expansive additives. All three types of expansive additives from Table 4.2 were used at their respective replacement ratio. Three samples were conducted for each replacement ratio of the respective expansive additives.

4.2.3.2 Method

An isothermal conduction calorimeter was used to monitor the evolution of heat of hydration in #20-OPC, pcsa-OPC and HyperExpan-OPC system. An isothermal calorimeter with four sample ampoules was used to determine heat evolution. The paste samples

were mixed manually in the ampules for a period of 2 minutes before inserting them in the respective channels. It shall be noted that the data for the first 30 minutes was not considered for analysis to avoid the heat associated with mixing and placing the externally prepared samples, and to allow the samples to stabilize at the set temperature of 20°C. The samples were monitored continuously for 72 hours.

4.2.3.3 Calculation of degree of hydration based on Isothermal Calorimetry data

The degree of hydration could be defined as the ratio between the amount of heat liberated through exothermic reaction and the maximum accumulated heat liberated by the present mineral phases.

$$\alpha_{(t)} = \frac{Q_{(t)}}{Q_{max}} = \frac{\sum Q_{(t)}^i}{\sum Q_{max}^i}$$

The maximum heat liberated by the total binder (OPC and XP) could be determined by the summation of fractional contribution of maximum heat release from each mineral phases as listed in Table 4.3.

$$Q_{max} = \rho_{C_3A} \cdot Q_{C_3A} + \rho_{C_3S} \cdot Q_{C_3S} + \rho_{C_4AF} \cdot Q_{C_4AF} + \rho_{C_2S} \cdot Q_{C_2S} + \rho_{C_4A_3\bar{S}} \cdot Q_{C_4A_3\bar{S}} + \rho_{f-CaO} \cdot Q_{f-CaO} + \rho_{C\bar{S}} \cdot Q_{C\bar{S}} \quad (4.4)$$

Thus, based on the mineral composition determined through XRD-Rietveld analysis from Table 4.2, the maximum heat liberated by different mixtures could be determined. Then, the degree of hydration could also be determined from isothermal calorimetry test by dividing the experimental accumulated heat with the theoretical maximum heat as explained above.

Table 4.3: Standard enthalpies of formation of clinker phases (J/g)

Authors	C ₃ A	C ₃ S	C ₄ AF	C ₂ S	f-CaO	C ₄ A ₃ \bar{S}	C \bar{S}
Arai et al. [36]	870	504	420	260	-	-	-
Bentz [37]	1144	517	725	262	-	-	-
Bogue [38]	866	500	125	260	-	-	-
Catharin [39]	1340	500	420	251	1172	-	-
Lerch [40]	866	500	420	260	1166	-	-
Newman et al. [41]	-	-	-	-	-	-	145
Skalamprinos et al. [42]	-	-	-	-	-	555	-
Taylor [43]	1144	517	418	262	-	-	-
Woods et al. [44]	840	570	125	260	-	-	-

In the thermodynamic numerical framework, DuCOM-COM3, standard enthalpies of formation of clinker phases for OPC cement from Arai et al. [36] has been adopted. As for expansive additives, three more phases ($f\text{-CaO}$, $C_4A_3\bar{S}$ and $C\bar{S}$) will be added since their presence in terms of weight ratio are quite prominent.

4.2.3.4 Results from isothermal calorimetry

Based on the isothermal calorimetry tests, following observations could be made. Using the weight fraction from Table 4.2 and standard enthalpies from Table 4.3, we could determine the maximum amounts of heat of hydration. Then, by using the amounts of heat liberated from hydration in isothermal calorimetry test, we would be able to determine the degree of hydration of the system.

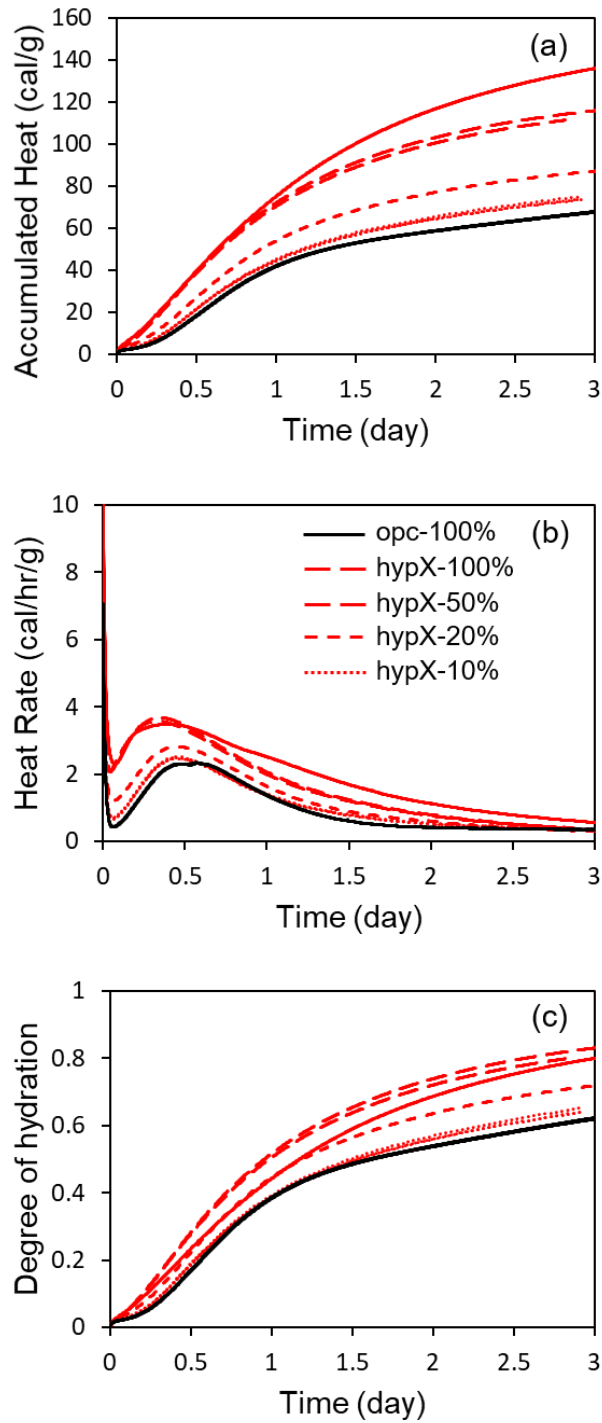


Figure 4.5: Isothermal calorimetry results after 30 minutes from the specimens inserting moment; (a) Heat rate & (b) Accumulated heat & (c) Degree of hydration by diving with the theoretical maximum heat release of HyperExpan-blended binders

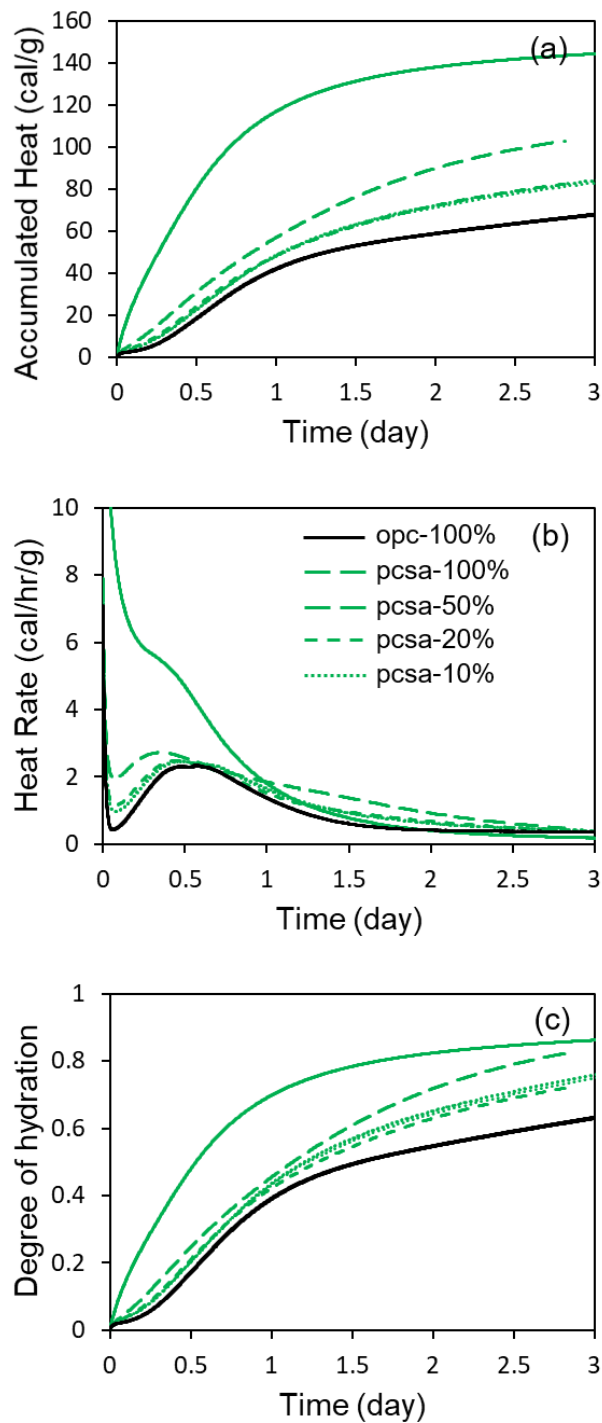


Figure 4.6: Isothermal calorimetry results after 30 minutes from the specimens inserting moment; (a) Heat rate & (b) Accumulated heat & (c) Degree of hydration by dividing with the theoretical maximum heat release of pcsa-blended binders

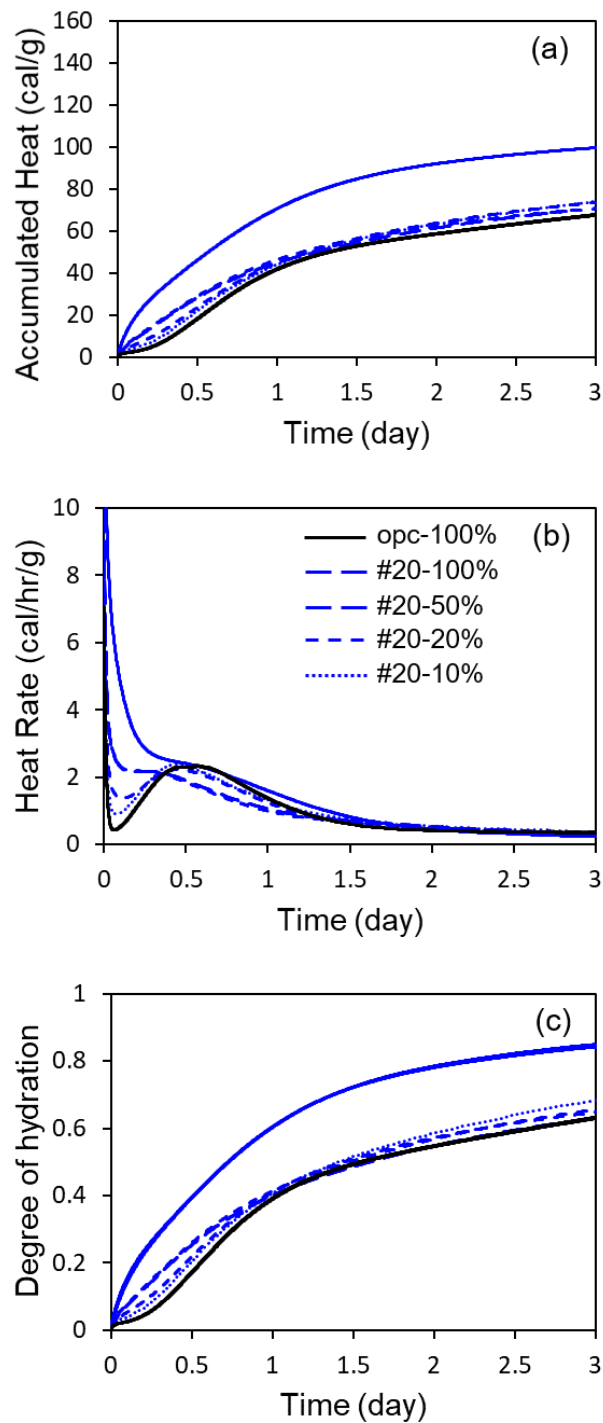


Figure 4.7: Isothermal calorimetry results after 30 minutes from the specimens inserting moment; (a) Heat rate & (b) Accumulated heat & (c) Degree of hydration by diving with the theoretical maximum heat release of #20-blended binders

According to the results from Figure 4.5 to Figure 4.7, all three expansive additives exhibit different hydration behaviors at 100% replacement ratio. Hydration of Denka-

PCSA (Figure 4.6 (b)) exhibits the highest heat rate, which could be explained by the high content of free-lime as free-lime relatively has a high enthalpy of formation coupled with its high solubility when in contact with water. On the other hand, if we turn our attention to hydration of Denka-#20, we could observe that the higher content of hauyne and lower content of free-lime cause the total heat release to reduce while also retard the total hydration degree before 1.5 day period. Interestingly, based on the hypothesis that free-lime hydrates extremely fast, behavior of Taiheiyo-HyperExpan was quite unexpected with its low hydration rate at the early stage of hydration. As Taiheiyo-HyperExpan's phases comprise of quite an abundant amount of alite, it is speculated that there could be some interaction between free-lime and alite phases. However, for this preliminary study, intensive interaction between the other phases in the ordinary Portland cement and expansive additive system would not be cover since these interactive effects seem rather low in the case of replacement ratio below 10%. However, future study shall be conducted to cover the cases where very high replacement ratio is needed (more than 10% replacement ratio with OPC).

4.2.4 Unrestrained expansion of expansive cement paste

4.2.4.1 Sample Preparation

Cement paste samples were prepared at water-to-binder ratio of 0.40. 0%, 3%, 6% and 10% replacement ratio of OPC were used for Taiheiyo-HyperExpan and Denka-#20 expansive additives. Three samples were prepared for each batch to check the consistency of the data.

4.2.4.2 Method

Various tests were conducted to determine the method for strain measurement such as contact gages, surface strain gages and mold strain gage. Contact gage has the advantage of low cost, however, the disadvantage is the possibility of missing the early deformation. As mentioned by Wyrzykowski et al. [45], deciding the reference point is extremely crucial for absolute value of expansion. Immediately after demolding, the expansion would become unrestrained that leads to a sudden change in volume. Thus, manual length measure could lead to a significant scatter in data between the sample series. Furthermore, surface strain gage has the disadvantage of defect possibility if the attached surface is not properly smoothed and glued. Thus, through numerous trial tests, embedded mold gage was decided to be utilized for this experiment. The molds that were used have the size of $4 \times 4 \times 16$ cm³. To reduce the effect of friction by the steel mold, teflon sheets were

placed at the bottom of the mold where paste would have contacted. To ensure the consistency of the pastes, samples were prepared by following procedures according to ASTM C305-20 [30] and practical guidance proposed by Scrivener et al. [31]. The pastes were cast at room temperature of $20 \pm 20^\circ\text{C}$. To minimize bleeding, each paste was gently re-scooped at 30 min, 1 h, 2 h, 3 h and 4 h again inside the $4 \times 4 \times 16 \text{ cm}^3$ steel mold. After that, the mold gage, Tokyo Sokki PMFL-50T, was embedded in the center of the paste. Every mold gage was test to check whether it functions normally or not before placing them inside the pastes. Then, each specimen were sealed with plastic wrap for sealed curing in an environmental control chamber with temperature of $20 \pm 20^\circ\text{C}$. Then, after around 9 hours, each specimen was gently removed from the mold, carefully wrapped with plastic sheet and placed on the racks without any load on the top. The measurement of the strain starts around 30 mins after the paste has been placed inside the mold.

4.2.4.3 Results from unrestrained expansion of expansive cement pastes

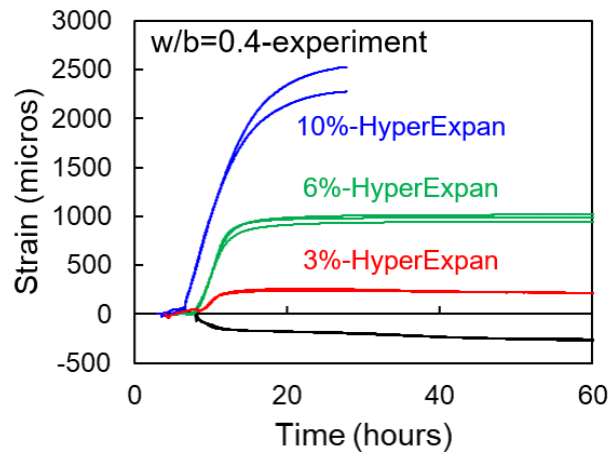


Figure 4.8: Unrestrained $4 \times 4 \times 16 \text{ cm}^3$ cement paste of ordinary Portland cement and Taiheyo HyperExpan expansive additive system

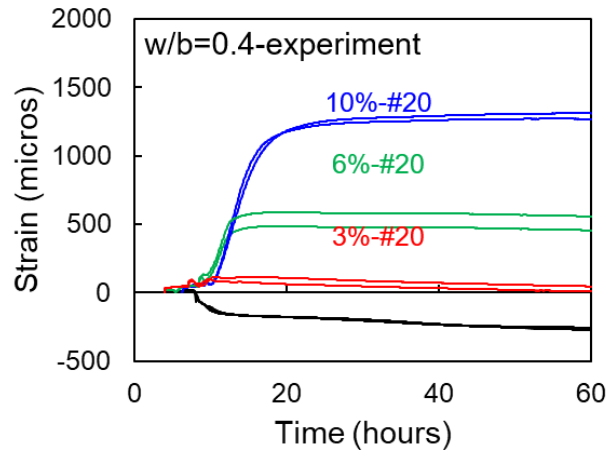


Figure 4.9: Unrestrained $4 \times 4 \times 16$ cm³ cement paste of ordinary Portland cement and Denka #20 expansive additive system

With increase in the amount of expansive additive, there was an obvious increase in the expansion whereby most of the expansion of the ordinary Portland cement and expansive additive pastes was completed in the first 20 hours of hydration. The more the addition of expansive additives, the later the time when the final expansion would be reached. This could probably be explained from the fact that the microstructure became denser, which in turns disrupt the supply of water to further aids in hydration mechanism of the expansive additive phases. This claim has already been observed in ordinary Portland cement clinker phases [1].

4.3 Conclusion

This chapter described the experiments conducted regarding expansive additive, which focus on hydration and expansion of the cement pastes. Initially, the hydration study that involved determining degree of hydration of phases through XRD-Rietveld and TGA as well as isothermal conduction calorimetry, for verification purposes, was conducted. Then, unrestrained expansion test of cement paste bars were conducted to observe the expansion behavior as well as model verification. The followings could be concluded from this chapter:

- Hydration of free-lime based expansive additive produce the highest amount of heat due to the enthalpy of formation of free-lime phase.
- Hydration degree of free-lime is the highest among the expansive additive phases, whereby it finishes at roughly 1 day in the case of 100% replacement ratio.

- Hydration degree of hauyne and anhydrite in the case of 100% replacement ratio stagnate after due to the reason that water might be fully consumed in the very early stage.
- Free-lime based expansive additive shows higher expansion strain than that of CSA-based given the same amount of addition. It could be postulated that the expansive force given by portlandite of free-lime is higher than that of ettringites given by Hauyne.

Chapter 5

Thermodynamic Modeling of Expansive Additives

Contents

5.1 Introduction	69
5.2 Overview of expansive additive modeling framework	70
5.3 Hydration of expansive phases	70
5.3.1 Thermal activity of expansive additive phases	71
5.3.2 Reference heat rate of expansive additive phases	71
5.3.3 Results based on the newly installed hydration model for expansive additives	75
5.4 Micro-structure formation of expansive addtitives and OPC system	77
5.5 Local crystallization pressure	78
5.5.1 Determination of Saturation Index (SI)	79
5.6 Upscaling of local crystallization pressure to macroscopic crystallization stress	81
5.7 Analyses of macroscopic expansion based on crystallization pressure	82
5.8 Limitation of the current linear isotropic model of crystallization pressure	84
5.9 Conclusion	85

5.1 Introduction

As many researchers [46, 47, 48, 49, 50, 51] have discussed regarding how pressure could be built up in a system comprised of crystals, supersaturation is one of the major factors which controls the expansion. Thus, this chapter aims to estimate the macroscopic crystallization stress from the local crystallization pressure, which is derived from the state of supersaturation in the pore solution and fraction of expansive phases of cement and expansive additive system. Various models, incorporating with the original DuCOM models, were used to calculate the crystallization stress, coupled with shrinkage behavior to estimate the strains from cement paste to concrete.

5.2 Overview of expansive additive modeling framework

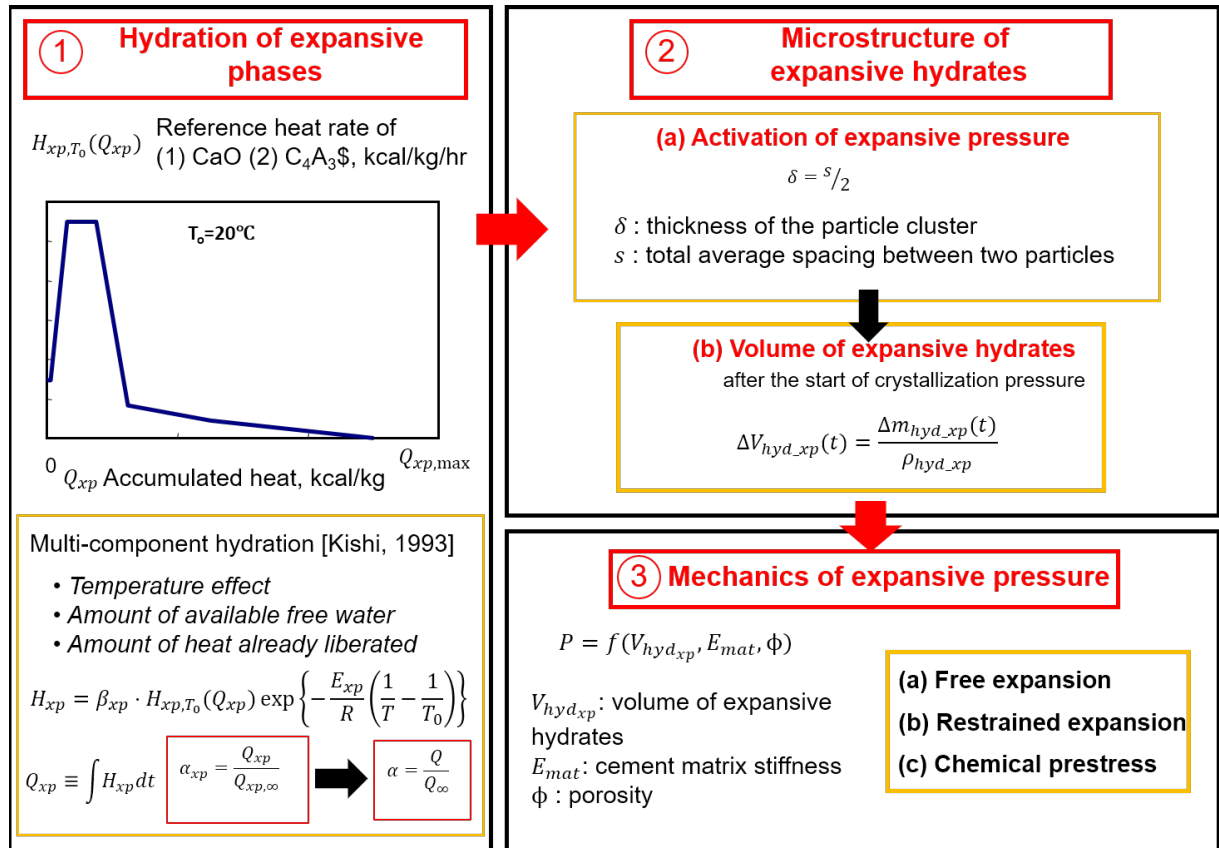


Figure 5.1: Proposed expansive additive modeling framework

The modeling flow consists of these three main focuses: 1) Hydration of expansive phases, which is an extension on the current multi-component heat of hydration model presented in Section 3.1.2.1 2) Microstructure of expansive hydrates, which is an extension on the current pore-structure development model presented in Section 3.1.3.2 and 3) Macroscopic expansive stress, which is an extension on the current solidification model of hydrated cement cluster presented in Section 3.1.5.3.

5.3 Hydration of expansive phases

As mentioned previously in Section 3.1.2.1, the current DuCOM model for hydration contains all of the clinker phases already. However, for the expansive additive phases, namely Hauyne, Anhydrite and free-Lime, they are still absent. Therefore, following the same approach to determine the degree of hydration of each clinker phase (refer to Section 3.1.2.1), the reference heat rate and thermal activities for each expansive additive phase shall be investigated.

$$H_C = \beta_i H_{i,T_0} (Q_i) \exp \left[-\frac{E_i}{R} \left(\frac{1}{T} - \frac{1}{T_0} \right) \right] \quad (5.1)$$

where β_i is the reduction factor due to availability of free water of i phase, $-\frac{E_i}{R}$ is the thermal activity of i phase and H_{i,T_0} is the reference heat rate of i phase (Reference temperature is $T_0 = 20^\circ\text{C}$).

5.3.1 Thermal activity of expansive additive phases

The thermal activity, $-\frac{E_i}{R}$, could be obtained from literature from experimental activation energy of the expansive additive phases.

- Hauyne[52]: $E_{Hauyne} = 231000 \text{ J/mol} \rightarrow -\frac{E_{Hauyne}}{R} = -27780 \text{ WK/kg}$
- Anhydrite[53]: $E_{Anhydrite} = 62700 \text{ J/mol} \rightarrow -\frac{E_{Anhydrite}}{R} = -7541 \text{ WK/kg}$
- Free-Lime[54]: $E_{Free-Lime} = 58200 \text{ J/mol} \rightarrow -\frac{E_{Free-Lime}}{R} = -7000 \text{ WK/kg}$

5.3.2 Reference heat rate of expansive additive phases

The accumulated heat of cement system is calculated via the equation:

$$Q_c = \int H_c dt = \int \sum \rho_i H_i dt$$

Therefore, the accumulated heat of cement and expansive additive system could be followed as:

$$Q_{c+xp} = \int (\sum \rho_i H_i dt + \sum \rho_{xp,i} H_{xp,i}) dt$$

where i : cement minerals (C_3A, C_4AF, C_2S, C_3S , Slag, Silica fumes and Fly ash) and xp, i : expansive additive minerals (f-Lime, Anhydrite and Hauayne ($C_4A_3\bar{S}$) from #20 (Denka[AFts based]) and P-CSA (Denka[f-Lime based])).

The steps to determine the reference heat rate of the expansive additive phases are listed in the steps below. As an example, Free-Lime hydration in the case of 100 % replacement ratio of Denka PCSA was used.

5.3.2.1 STEP 1:

Through a combined QXRD/TG method, $\alpha_{xp,i}$ would be determined.

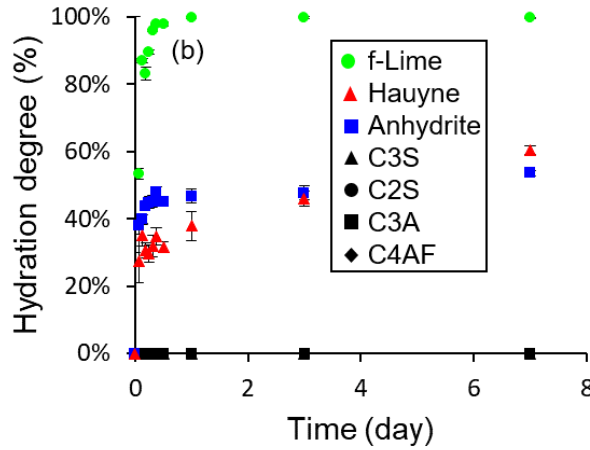


Figure 5.2: Hydration degree of expansive additive phases in 100% replacement ratio of Denka PCSA

5.3.2.2 STEP 2:

Using the experimental $\alpha_{xp,i}$, $Q(t)$ (the heat liberated at time t) and $H(t)$ (heat rate of the mineral component) could be determined based on the equation:

$$\alpha(t)_{xp,i} \approx \alpha(Q(t))_{xp,i} = \frac{Q(t)_{xp,i}}{Q_{xp,i}^{max}} \quad (5.2)$$

$$Q(t)_{xp,i} = \alpha(Q(t))_{xp,i} \times Q_{xp,i}^{max} \quad (5.3)$$

$$H(t)_{xp,i} = \frac{dQ(t)_{xp,i}}{dt} \quad (5.4)$$

t that would be considered in QXRD/TG method consists of 1d, 3d and 7d. Therefore, at each t , corresponding $H(t)_{xp,i}$ could be determined and empirically set at heat rate of each expansive additive mineral phase. Note that $Q_{xp,i}^{max}$ is the theoretical standard enthalpy of formation from Table 4.3.

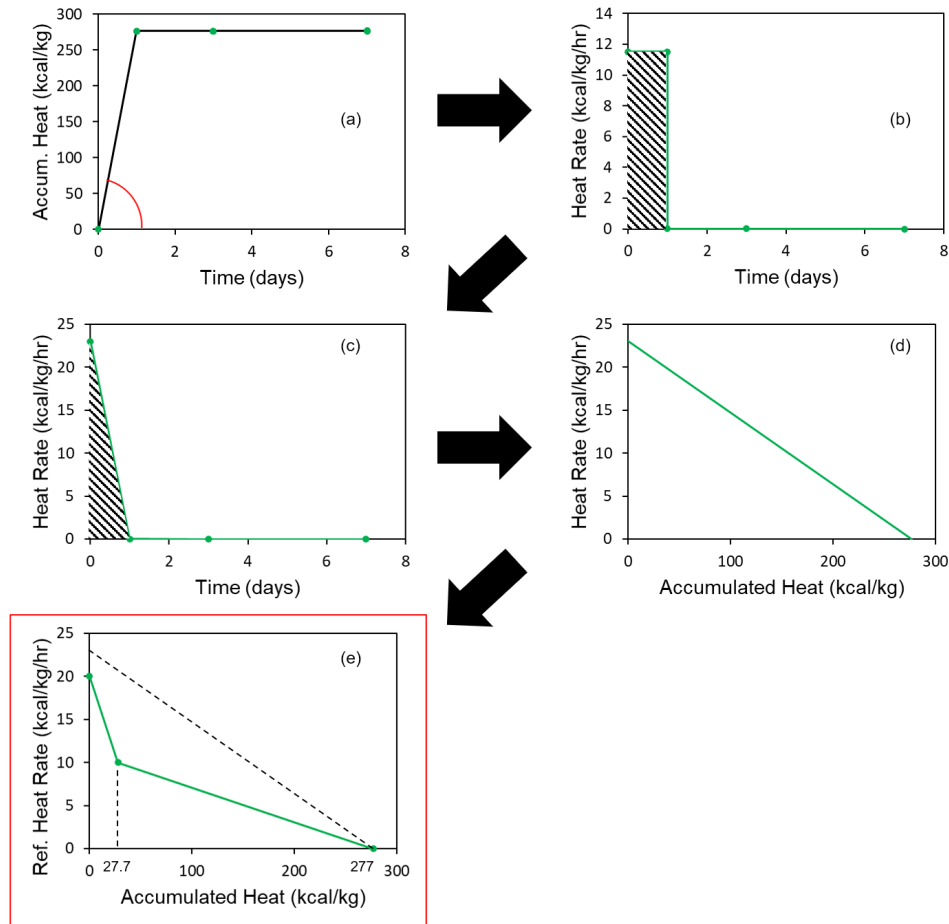


Figure 5.3: Process of determining reference heat rate for expansive additive phases

In Figure 5.3(a), the accumulated heat was able to obtained according to Equation 5.3. Then, based on the slope from Figure 5.3(a), the heat rate in Figure 5.3(b) is consequently determined. However, it does not seem logical to assume such a step function for hydration process as hydration tends to stagnate due to denser micropore structure at time goes by. Thus, a linear heat rate as shown in Figure 5.3(c) was adopted by keeping the same accumulated heat (hatched area under the curve of Figure 5.3(b) and Figure 5.3(c)). After that, plotting the heat rate against the accumulated heat, we would be able to obtain the linear heat rate against accumulated heat curve for free-lime based on the experiment

conducted (Figure 5.3(d)). As for the model, a bi-linear curve was adopted as shown in Figure 5.3(e) after consideration of the fact that hydration in the very early stage when unreacted phases are immediately in contact with water should be much more rapid than that of later stage. Thus, the slope of the heat rate in the first 10% of accumulated heat was assumed as shown in Figure 5.3(e).

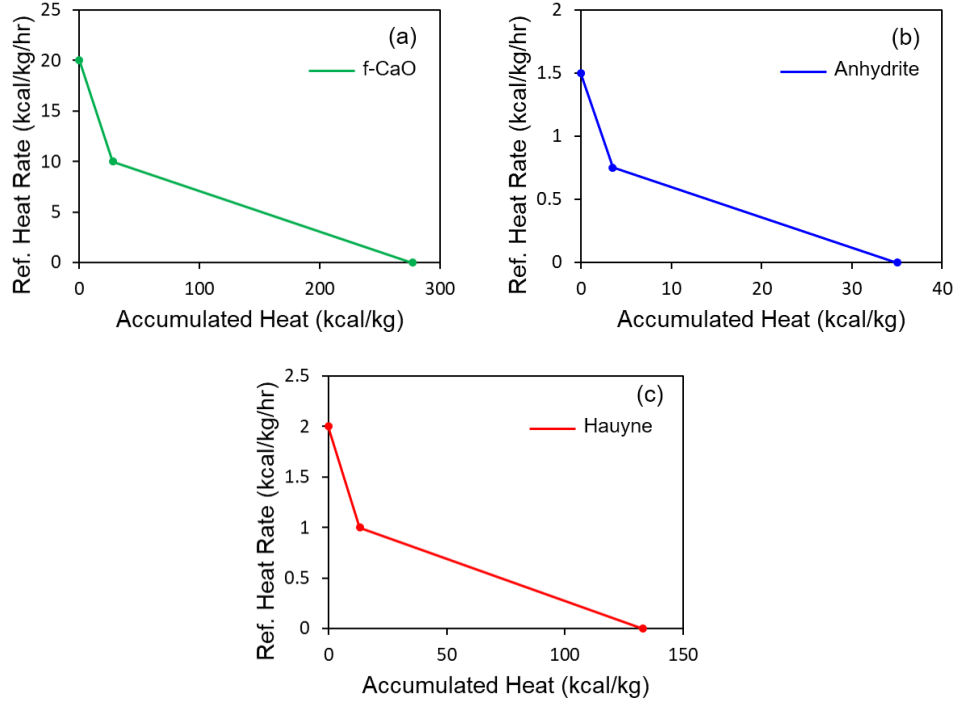


Figure 5.4: Reference heat rate of expansive additive phases installed in the multi-component hydration heat model

5.3.2.3 STEP 3:

Through isothermal calorimetry, H_{c+xp} would be determined. However, at first, to re-verify and ensure the validity of DuCOM's OPC heat model, OPC at $w/c=0.4$ calorimetry test were conducted and compared with DuCOM's analyses as will be shown below.

5.3.2.4 STEP 4:

After the verification, suppose a mixture of OPC90%+Hyperexp10% at $w/c=0.4$. $Q_{xp,i}^{DuCOM}$ will be used to compare with $Q_{xp,i}^{isothrml.cal}$.

IF $Q_{xp,i}^{DuCOM} \approx Q_{xp,i}^{isothrml.cal}$, then $H(t)_{xp,i}$ consideration is acceptable.

IF $Q_{xp,i}^{DuCOM} \neq Q_{xp,i}^{isothrml.cal}$, then further phenomena need to be considered and used as modification factors $H(t)_{xp,i}$.

5.3.2.5 Reduction factor due to availability of free water of expansive additive phases

The reference heat rate set in the proposed model is based on the assumption water supply is always sufficient for hydration to proceed. However, the actual hydration rate is lower than the reference heat rate when the water supply is reduced from chemically-bound water, evolving denser micro-pore structure and limited channel of water source, since it is impossible to assume that sufficient free water exists around the powder particles. In the current DuCOM model, the reduction in the heat rate is assumed due to a shortage of free water resulting from the reduced probability of contact between the reacting surface of the particles and the free water[1]. Hence, the proposed hydration heat model of expansive additives also use the following equation to express the decline in the heat-generation rate:

$$\beta_{xp} = 1 - exp \left\{ -r \left\{ \frac{\omega_{free}}{100 \cdot \eta_{xp}} \right\}^s \frac{1}{s_{xp}^{1/2}} \right\} \quad (5.5)$$

where η_{xp} is the normalized cluster thickness of inner product, defined by: $\eta_{xp} = 1 - \left(\frac{Q_{xp}}{Q_{xp,\infty}} \right)^{\frac{1}{3}}$, ω_{free} : the free water percentage i.e. physical water existing in micro-pores allows hydration to sustain and serves as precipitation space for hydrates, s_{xp} : the normalized Blaine value of the phase and r and s : material constants.

5.3.3 Results based on the newly installed hydration model for expansive additives

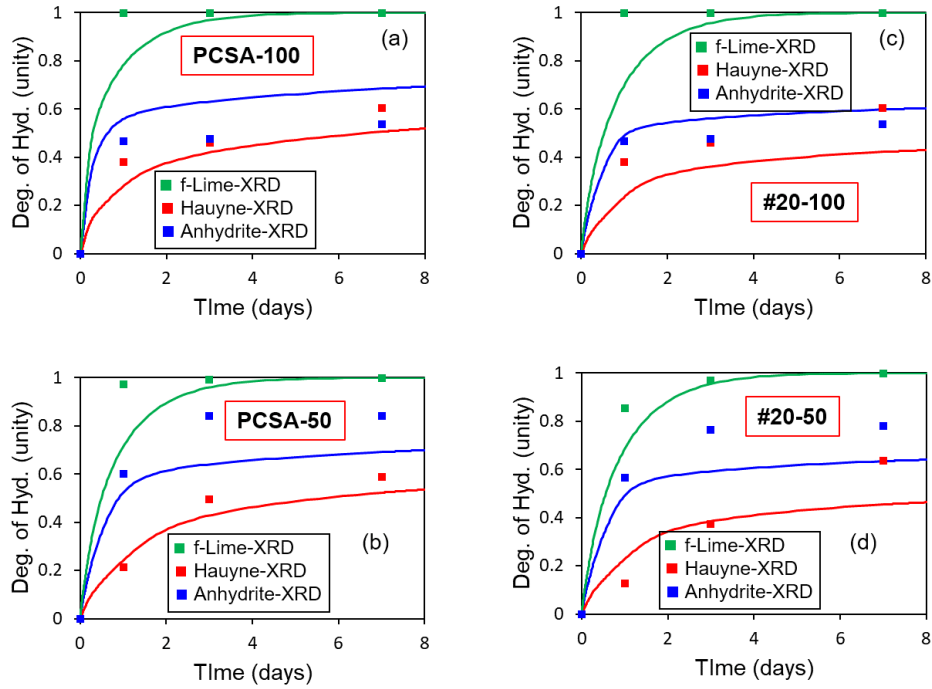


Figure 5.5: Verification of XRD results versus the analytical results from DuCOM

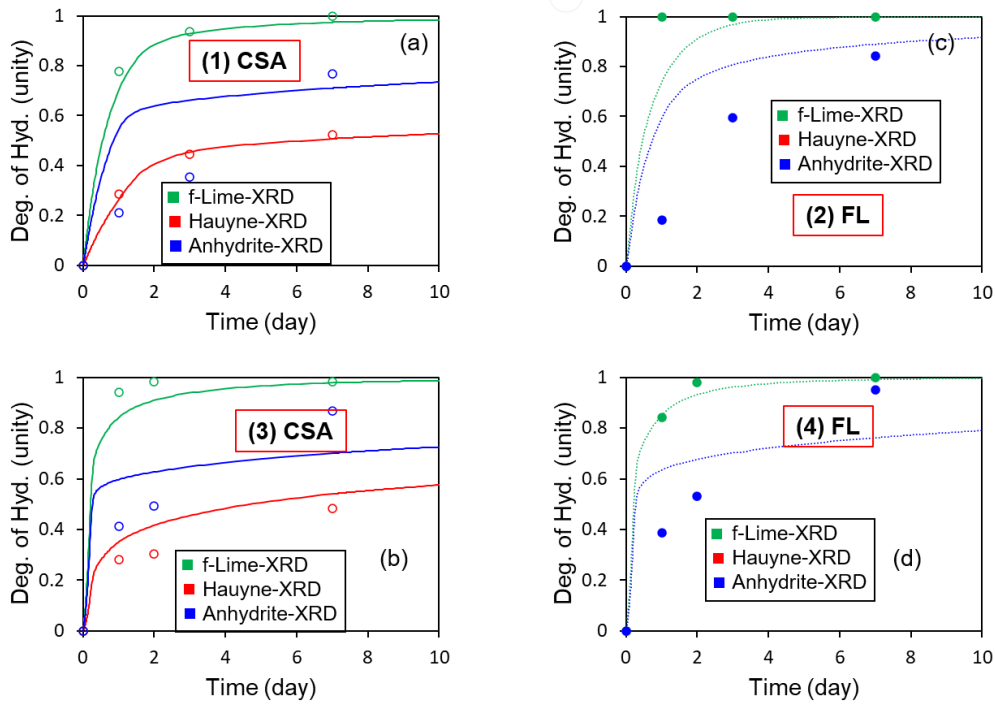


Figure 5.6: Verification of XRD results [(1) and (2) from Morioka [21]; (3) and (4) from Denka internal report] versus the analytical results from DuCOM

Figure ?? is the degree of hydration of 50% and 100% replacement ratio. The dots represents the XRD results whereby the line represents the analytical results. Quantitatively, it is not matching, but this seems to be pretty reasonable. Figure ?? are further comparison between XRD experimental results from Morioka and Denka Company. Please be noted that: the main parent expansive phases, which are responsible for causing the expansion would be f-lime and hauayne. Therefore, it even though anhydrite hydration degree is not matching well, but it is not of great concern. It is undeniable that the study of hydration should also be considered at lower replacement ratio in addition to the interaction between different cement phases to ensure the validity of the model. However, as a preliminary step towards making expansive additive model a realization, such sophisticated considerations are not made for the time being.

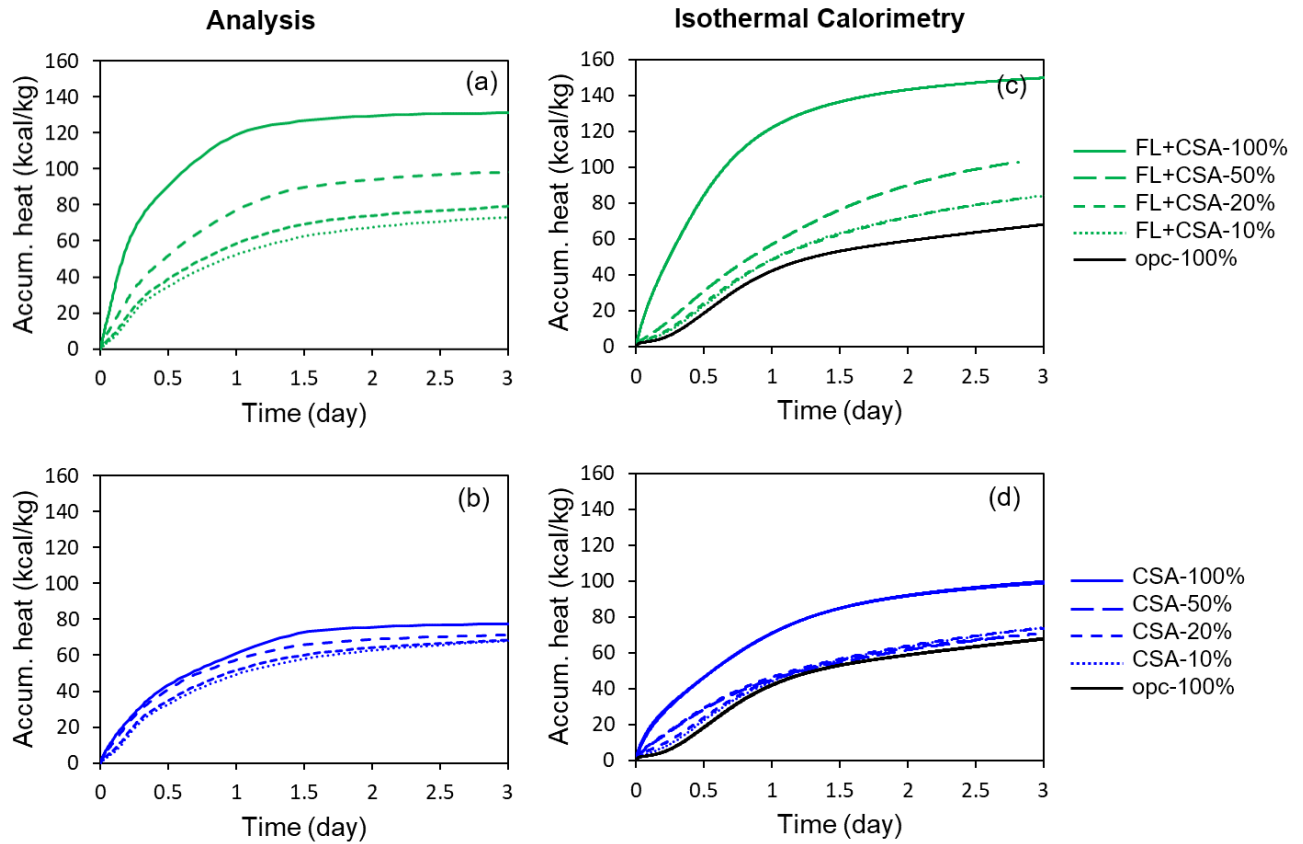


Figure 5.7: Verification of isothermal calorimetric results versus the analytical results from DuCOM

Nonetheless, based on the accumulated heat from isothermal calorimetric experiment and the results given by the model as shown in Figure [??], they seem to have some fairly good agreement as a starter. Thus, as stated previously, preliminarily, this model is taken for computing various parameters such as hydration degree and the amount of expansive hydrates for subsequent models.

5.4 Micro-structure formation of expansive additives and OPC system

A system of ordinary Portland cement and expansive additives comprises of various hydrates. It is crucial that the information of the fraction of expansive hydrates, namely ettringites and calcium hydroxides, could be obtained. In the current DuCOM system, the hydrates from ordinary Portland cement contain only C-S-H gels and CH crystals, whereby ettringites are somehow intrinsically covered in the volume of C-S-H gels formed

(Refer to Section 3.1.3.2). Thus, to keep the extension to the model in a simple manner, an assumption was made that only the ettringites from expansive additives could cause expansion and would be superimposed to the current system based on the stoichiometric balance. Similarly, only CH crystals from f-CaO could cause expansion and these expansive CH crystals would be superimposed to the current system in the same fashion as that of ettringites. However, not all of expansive hydrates would be able to cause expansion. In the early stage of hydration, the dispersed particles most likely have abundant amount of free room for precipitation to occur without introducing the built-up of stresses. As expansive pressure is a form of compressive stress between the adjacent particles, it is logical to assume that the expansion only arise once the particles around the vicinity can exert stress on each other through the form of contacting.

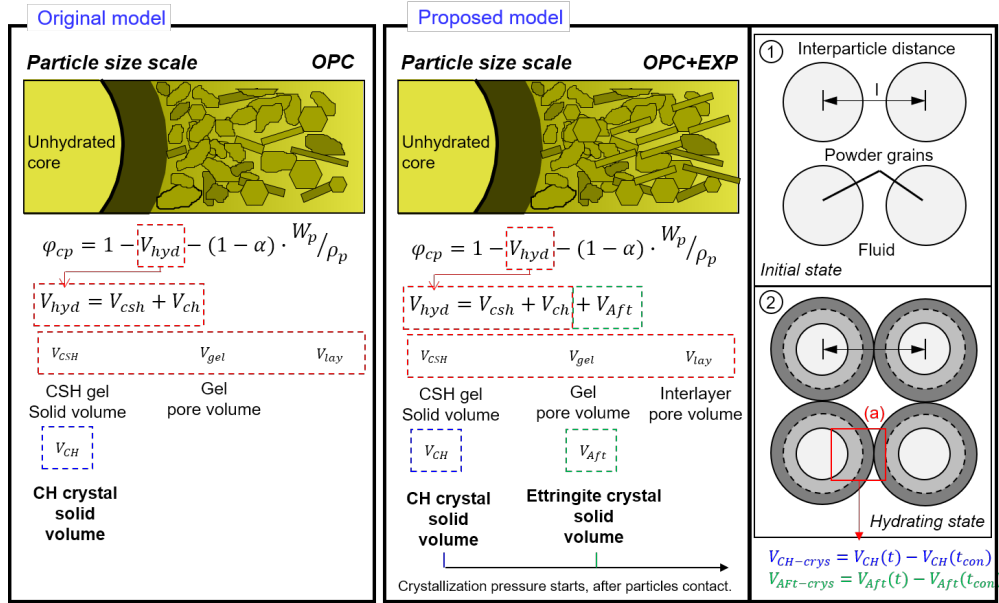


Figure 5.8: Original and proposed microstructure model of ordinary Portland cement and expansive additive system

5.5 Local crystallization pressure

As supersaturation is one of the major factors which controls the expansion [46, 47, 48, 49, 50, 51], from a thermodynamic point of view, Correns [55] proposed the following equation to calculate the local crystallization pressure as:

$$p_c = \frac{RT}{v} \ln \left(\frac{K}{K_{sp}} \right) \quad (5.6)$$

where R is the gas constant (8.314 J/K/mol), T is the absolute temperature, v is the

molar volume of the crystals ($v_{Aft} = 735 \text{ cm}^3/\text{mol}$ and $v_{CH} = 33 \text{ cm}^3/\text{mol}$), K is the ionic activity and K_{sp} is the solubility products of the ions that will form the crystal hydrates in the pore solution. Alternately, $\ln\left(\frac{K}{K_{sp}}\right)$ could also be referred as Saturation Index or Saturation Factor.

5.5.1 Determination of Saturation Index (SI)

As in the aforementioned Equation 5.6, the most influenced variable or factor in causing the local crystallization pressure is $\ln\left(\frac{K}{K_{sp}}\right)$ as the other parameters are more or less constant. Typically, Saturation Index could be determined from the concentration of the ions in the pore solutions that would make up the crystal products. Refer to Figure 5.9, dissolution process in (1) would give rise in the ionic concentration of relevant ions whereby these ions would determine whether the pore solution has reached supersaturated state or not. Then, once the supersaturated state is achieved, precipitation of coresponding products based on the interaction between the ions in the pore solutions would occur. One limitation lies here in the case where the multi-component heat of hydration model (refer to Section 3.1.2.1) is used. The calculation from this model allows us to obtain the hydration products immediately based on the amount of heat that is release by each clinker and expansive additive phase, without the need to consider the equilibrium between the solid phases and aqueous solution. In other words, step (2) in Figure 5.9 was disregarded. Therefore, to obtain the Saturation Index directly from DuCOM via pore solution is practically impossible as of now.

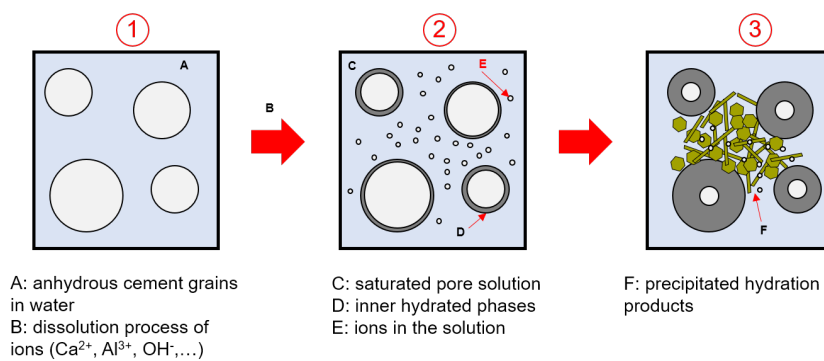


Figure 5.9: Dissolution and precipitation process of cement clinker and expansive additive phases

However, a rather simple treatment could be proposed to imitate the Saturation Index through a function of unreacted parent phases instead of ionic concentration. It may be plausible if it is somehow boldly assumed that the unhydrated particles are like particles which are ready to dissolve in the pore solution and ready to precipitate to form hydration

products. Chaunsali and Mondal [56] determined the Saturation Index of ettringite in a Calcium Sulfo Aluminate and ordinary Portland cement system through pore solution extraction. Concurrently, the aforementioned author also conducted X-Ray diffraction to determine the mass of the phases in the system. Based on the result of Chaunsali [57], it shows that by 1 day of hydration process, the amount of Hauyene reacted was approximately 40% whereby there is no trace of Hauyene by the age of 7 days.

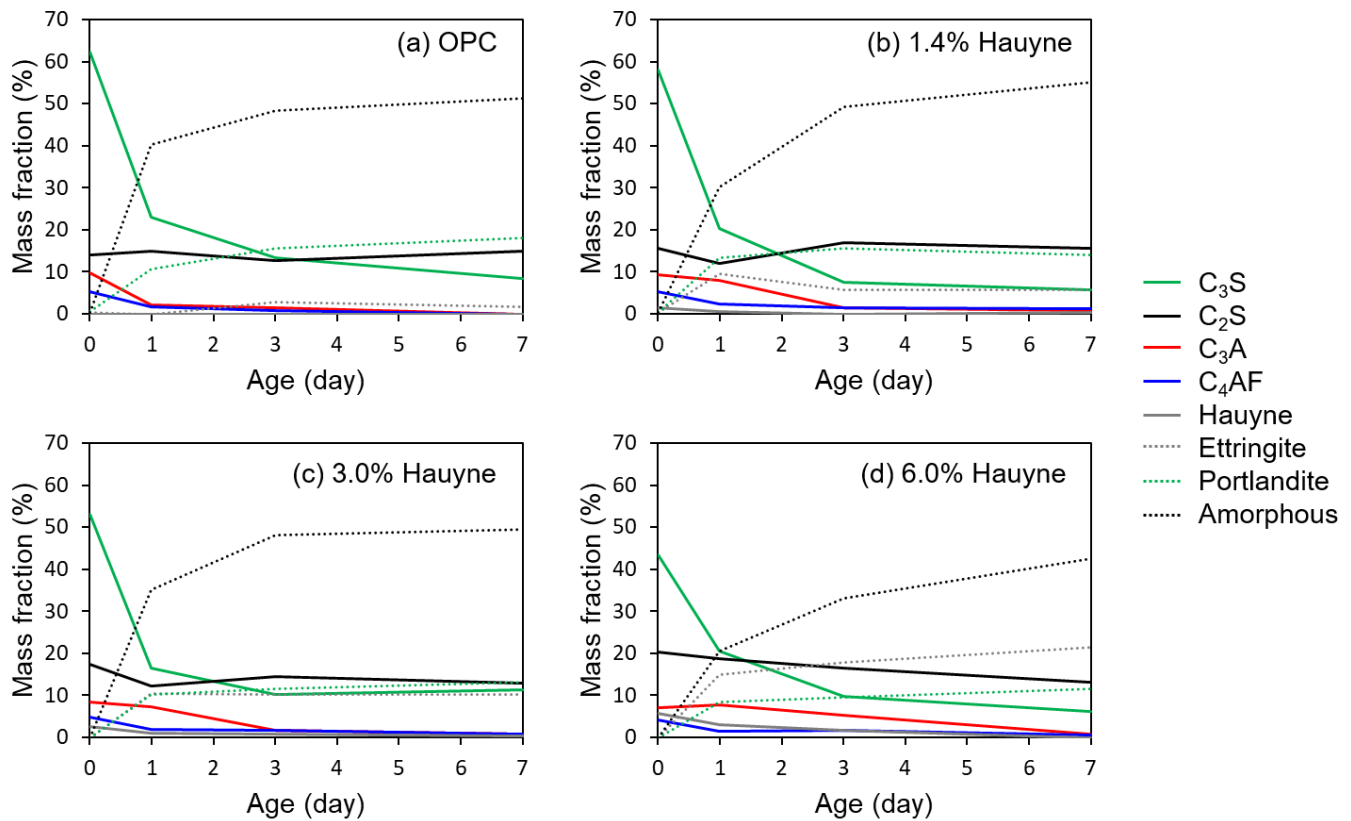


Figure 5.10: Mass of unhydrated and hydrated phase in OPC-CSA system with: a) 0% CSA (0% Hauyene) b) 7% CSA (1.4% Hauyene) c) 15% CSA (3% Hauyene) and d) 30% CSA (6% Hauyene) [from Chaunsali and Mondal [56]]

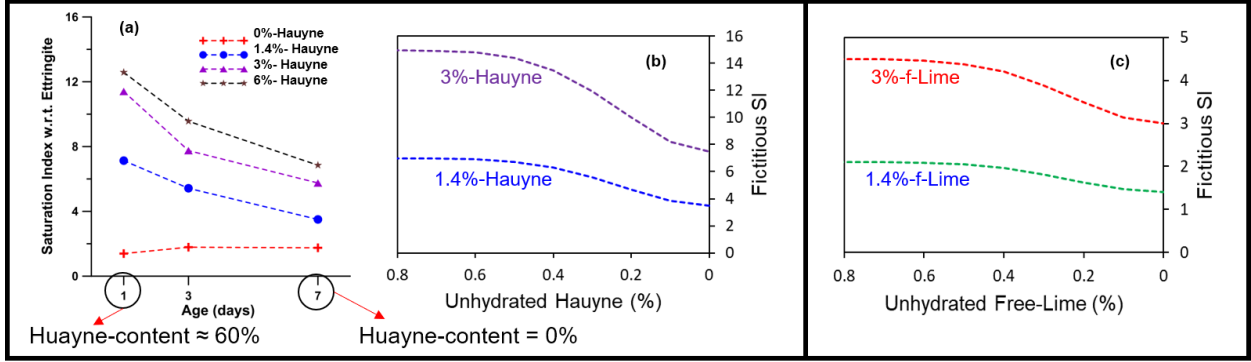


Figure 5.11: (a) Saturation Index of ettringites based on different contents of Hauyne [from Chaunsali and Mondal [56]] (b) Fictitious Saturation Index of Ettringites (c) Fictitious Saturation Index of CH

Hence, a fictitious Saturation Index for ettringite based on unhydrated Hauyne is proposed through the equation shown below:

$$SI_{ett} = \left\{ 5 - 2.5 \cdot \exp \left(-10 \cdot \frac{Q_{hauyne}}{Q_{max,hauyne}} \right) \right\} \cdot \rho_{hauyne} \quad (5.7)$$

where Q_{hauyne} is the amount of heat released by hauyne hydration, $Q_{max,hauyne}$ is the maximum amount of heat that could be released from hauyne (complete hydration) and ρ_{hauyne} is the mass fraction of hauyne in the cement used.

As for free-lime, based on a study by Gartner et al. [58] on Saturation Index for CH in Portland cement paste, with free-lime content around 1%, the saturation index was approximately 1. Thus, the following equation is assumed for the Saturation Index of CH in a similar approach as that of ettringites.

$$SI_{ch} = \left\{ 1.5 - 0.5 \cdot \exp \left(-10 \cdot \frac{Q_{free-lime}}{Q_{max,free-lime}} \right) \right\} \cdot \rho_{free-lime} \quad (5.8)$$

5.6 Upscaling of local crystallization pressure to macroscopic crystallization stress

Based on poromechanics, under the effect of pore pressure and heat, Coussy [47] introduced a relationship between the mean stress and strain in a linear isotropic body as:

$$\sigma_{exp} = b(S_c p_c + S_L p_L) + 3\alpha K \Delta T \quad (5.9)$$

where σ is the mean stress, ε is the mean strain, K is the bulk modulus and α is the thermal expansion coefficient, b is the Biot coefficient, ΔT is the difference in temperature,

S_c and S_L are the saturation level of the crystal and liquid, respectively and p_c and p_L are the local crystallization pressure of the crystal and pressure of liquid, respectively.

As DuCOM have already considered the effect of liquid pressure and thermal dilation, Equation 5.9 reduces to:

$$\sigma_{exp} = b(S_c p_c) \quad (5.10)$$

Tentatively, the biot coefficient is assumed to be 0.61 as investigated by Ulm et al. 59. S_c could be obtained as a fraction of the expansive hydrates in the total volume of cement paste.

Then, in coherent with shrinkage model, the linear isotropic expansive stress is added to the system by superimposing the macroscopic crystallization stress with the current model as mentioned in Section 3.1.5.5 as:

$$\sigma_{cp} = \dot{\sigma}_{cp} + \sigma_s + \sigma_{exp} \quad (5.11)$$

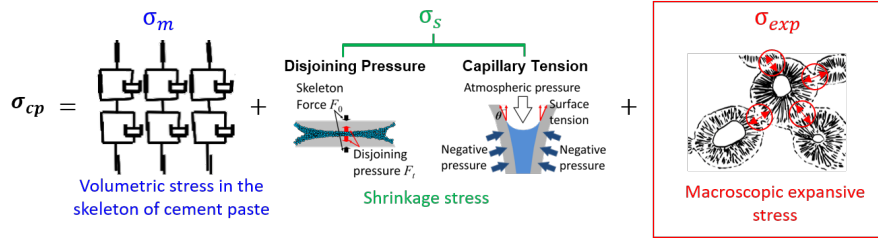


Figure 5.12: Superimposition of crystallization stress on the expansive cement matrix

Thus, this model has the capability in assessing the mechanical behavior of expansive cement paste, mortar and concrete from its expansion in early hydration period to its shrinkage in the later stage of hydration.

5.7 Analyses of macroscopic expansion based on crystallization pressure

Based on the experimental results, which have been shown in Section 4.2.4.3, analyses was conducted and compared based on the coupling of the aforementioned models.

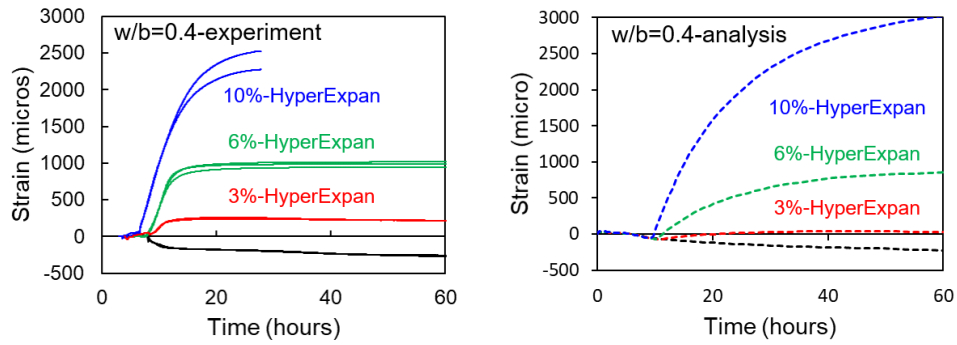


Figure 5.13: Analytical and experimental results on unrestrained $4 \times 4 \times 16$ cm³ cement paste of ordinary Portland cement and Taiheyo HyperExpan expansive additive system

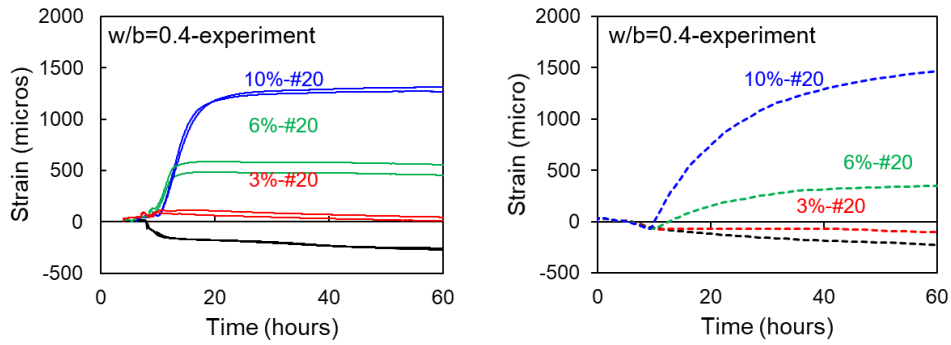


Figure 5.14: Analytical and experimental results on unrestrained $4 \times 4 \times 16$ cm³ cement paste of ordinary Portland cement and Denka #20 expansive additive system

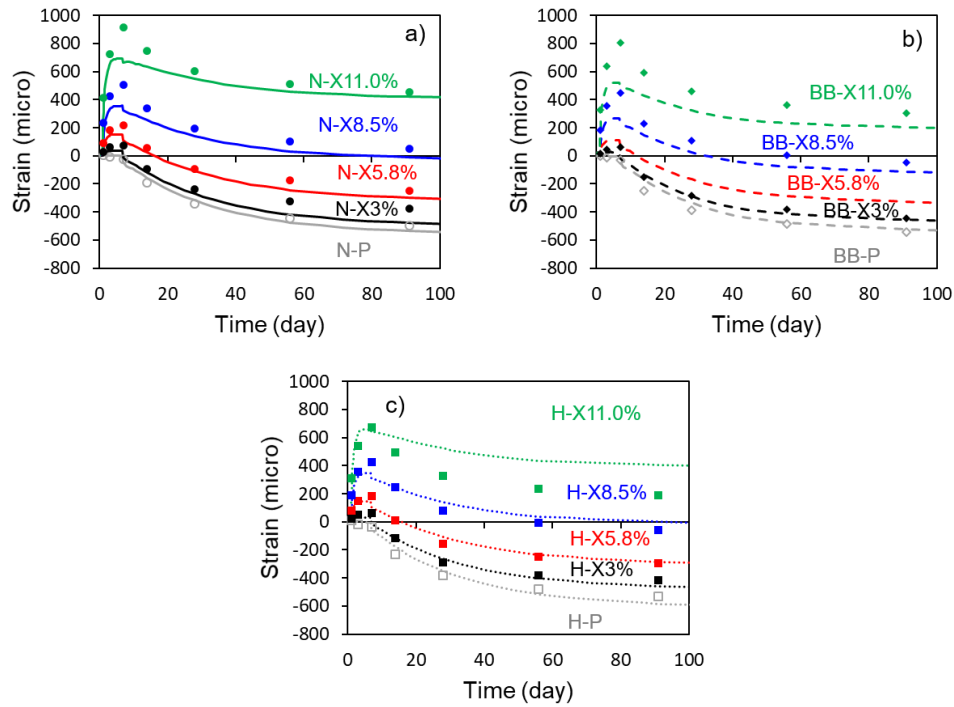


Figure 5.15: Analytical and experimental results on concrete under JIS-A-6202 Standard ($10 \times 10 \times 40 \text{ cm}^3$ with 0.97% of reinforcement ratio)

For reference to Figure [6.8](#), the specimens were cured in water for 7 days before exposing to an environmental condition with relative humidity of 60% at 20°C. *N*, *BB*, *H* and *X* represent ordinary Portland cement, Blast-furnace slag cement (40% Slag), High early-strength cement and Denka-PCSA expansive additive, respectively. It could be seen that the current model could capture the behavior of both expansion and shrinkage of concrete at various mix design quite considerably at typical replacement ratio for shrinkage compensating effect whereby, for higher replacement ratio in the case of ordinary Portland cement and Blast-furnace slag cement, the discrepancy might be linked to the decrease in modulus of elasticity of the cement matrix.

5.8 Limitation of the current linear isotropic model of crystallization pressure

However, in the case of restrained expansion at higher reinforcement ratio, the linear isotropic analytical model could not capture the restraining effect well as shown in Figure [5.16](#). Therefore, investigation into utilization the approach of ASR poromechanical model based on 2-phase biot theorem was done.

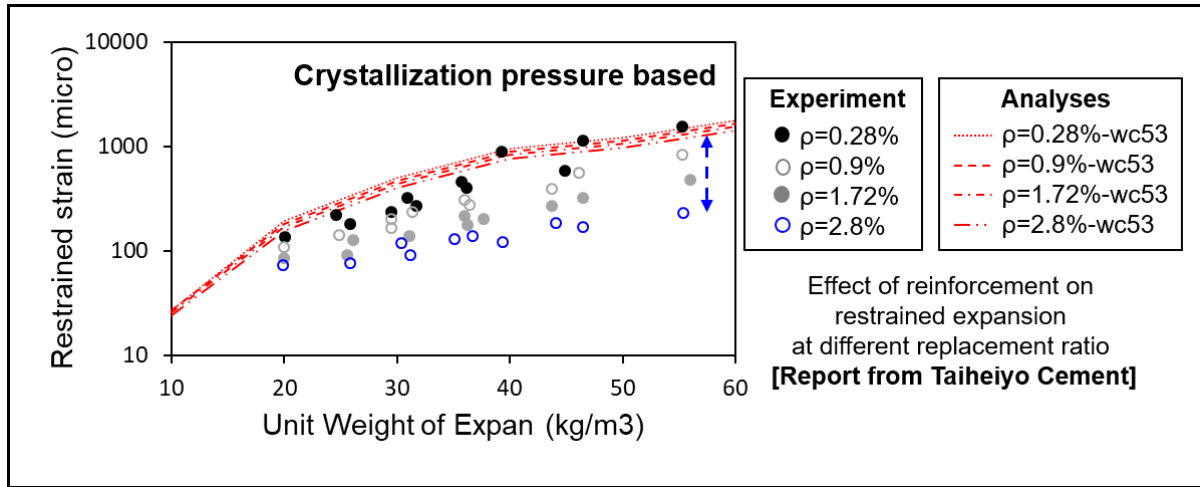


Figure 5.16: Effect of reinforcement on restrained expansion at different replacement ratio based on Expan expansive additive [60]

5.9 Conclusion

This chapter described the development of expansive additive models, which based on multi-component heat of hydration model, micropore structure model and crystallization pressure model. On the basis of Arrhenius' law of reactions, reference heat rate and thermal activity of expansive additive phases were determined for the purpose of hydration degree calculation. The reference heat rate was derived based on 100% replacement ratio with ordinary Portland cement. It is undeniable that the study of hydration should also be considered at lower replacement ratio in addition to the interaction between different cement phases to ensure the validity of the model. However, as a preliminary step towards making expansive additive model a realization, such sophisticated considerations are not made for the time being. Nonetheless, based on the accumulated heat from isothermal calorimetric experiment and the results given by the model, they seem to have some fairly good agreement as a starter. Thus, as stated previously, preliminarily, this model is taken for computing various parameters such as hydration degree and the amount of expansive hydrates for subsequent models. Then, the volume of expansive hydrates would be computed in the microstructure after balancing with other unhydrated and hydrated phases. However, not all of the phases would contribute to expansion. As the particles, which are initially dispersed in equivalent distance, hydrate, thickness of their clusters increases. Once the cluster thickness of a particle reaches half of the interparticle distance, particle contact would occur. Only after that, the volume of formed expansive hydrates would contribute to expansion. Then, the local crystallization pressure of the expansive hydrate crystals are calculated based on fictitious Saturation Index. Following

that, upscaling from local crystallization pressure to macroscopic stress in the cement matrix through poromechanics was introduced. Coupling with the solidification model, which covers both shrinkage and creep of the cement matrix, the model could properly capture the behavior of cement paste and concrete under JIS-A-6202 standard. The followings could be concluded from this chapter:

- Based on multi-component heat of hydration model[3], hydration of Hauyne, Anhydrite and f-Lime were added to the system.
- Based on the reaction degree and mass percentage of Hauyne and f-Lime, the volumetric change of the expansive hydrates were added into the microstructure of the current system.
- After particle contacts have been made, the expansive hydrates produced afterwards would contribute in volumetric expansion by upscaling from local crystallization pressure to macroscopic stress.
- However, the isotropic model based on upscaling from local crystallization pressure to macroscopic stress could not capture the behavior of concrete under different restrained conditions well. Thus, investigation into the possibility of using ASR poromechanical model was conducted and will be presented in the next chapter.

Chapter 6

Poromechanical model to express anisotropic behavior

Contents

6.1 Introduction	87
6.2 Expansion from Alkali-silica reaction versus Expansive additive	88
6.3 Current model in DuCOM regarding Alkali-silica reaction .	88
6.4 Adaptation of Alkali-silica reaction poromechanical model for Expansive additive expansion model	90
6.4.1 A factor expressing the free precipitation space of expansive hydrates under external restraint, β	90
6.4.2 Analytical results	93
6.5 Conclusion	98

6.1 Introduction

The previous linear isotropic model based on fictitious Saturation Index as mentioned in Chapter 5 has the capability to predict the expansion under low restrained conditions at low replacement ratio conditions. However, in the case where high restrained conditions are present, the model could not express the effect of restraining stress on expansive cement or concrete matrix properly. On the other hand, to predict the expansion of Alkali-silica reaction in concrete, Maekawa and Fujiyama [61], Takahashi et al. [62] has developed a poromechanical model based on 2-phase biot theorem that takes into account

the micro-chemical reactions between species and interaction between multi-directional cracks. Therefore, this chapter would present the feasibility of using the aforementioned poromechanical model approach and its application on expansive additive to express the anisotropic behavior of expansive cement or concrete under the effect of external restraints.

6.2 Expansion from Alkali-silica reaction versus Expansive additive

Alkali-silica reaction is one of the most concerned concrete defects in which aggregates possessing particular forms of silica would react with alkali hydroxide in concrete to generate a form of gel, commonly referred as ASR gels. These gels could adsorb water from the paste or environment to induce expansive pressure that is high enough to cause substantial damages to concrete structures [63]. These ASR gels, which are most frequently seen on the reactive aggregates, are reacted and formed through a couple steps in the pore solution of dissolution, ion exchange and alkali recycling [64]. Going through these aforementioned process cyclically, nano-colloidal alkali-silica particles agglomerate to form gel clusters of 2 or 3 dimension larger [65, 66], which are ASR gels itself. Furthermore, according to Vayghan et al. [67], these viscous ASR gels could express a viscous characteristic that allows them to possess yield strength of up to 85 kPa. This claim shows a high probability that the gels must have been in very close contact with each other.

Similarly, as mentioned in various literatures [11, 12, 13, 14, 22], reactions of expansive haayne and free-lime phases also take place in the pore solutions where its precipitation back on the particles lead to the build up of expansive stress. Thus, it is reasonable to believe that the (1) the scale of reactions of expansion-inducing phases of both ASR and expansive additives are of approximate magnitude and (2) only when the particle are in close contact with each other that expansive pressure could be created from the volume increase of the ASR gels or expansive crystals. Therefore, it is explainable that ASR poromechanical model could be adopted for modeling of expansion in the system of expansive hydrates.

6.3 Current model in DuCOM regarding Alkali-silica reaction

To explain the complex anisotropic expansion of ASR, a chemo-mechanical model of ASR extended upon a multi-scale chemo-hygral computational system, DuCOM-COM3 was

developed by Takahashi et al. [62]. Many sub-models exist within this ASR model to explain micro to macro-scale mechanism relating to expansion phenomena. However, the most related case to expansive additive on the anisotropic behavior under restraint would be a parameter, β , which is determined as a liquid-solid ratio with 0 being fully liquid and 1 being fully solid [68, 69, 70, 71]. The solid part would exert anisotropic pressure whereby the liquid part would exert the isotropic pressure. In other words, the physical meaning of β parameter would be intrinsic viscosity of the gel whereby if the β parameter is 0, liquid state of gel would be able to flow and cause hydrostatic pressure in every direction as opposed to its counterpart when β parameter is 1 (Figure 6.1 for reference). Overview of the model could be referred to in Figure 6.2. After obtaining the pressure, both component would be combined with cement matrix stress to create the total stress through [61, 72]:

$$\sigma_t = \sigma_{cp} + p_{ai} + \delta_{ij}p_i \quad (6.1)$$

where σ_t is the total stress, σ_{cp} is the cement matrix stress, p_{ai} is the anisotropic pressure, p_i is the isotropic pressure and δ_{ij} is the Kronecker delta 1 if $i = j$; 0 if $i \neq j$.

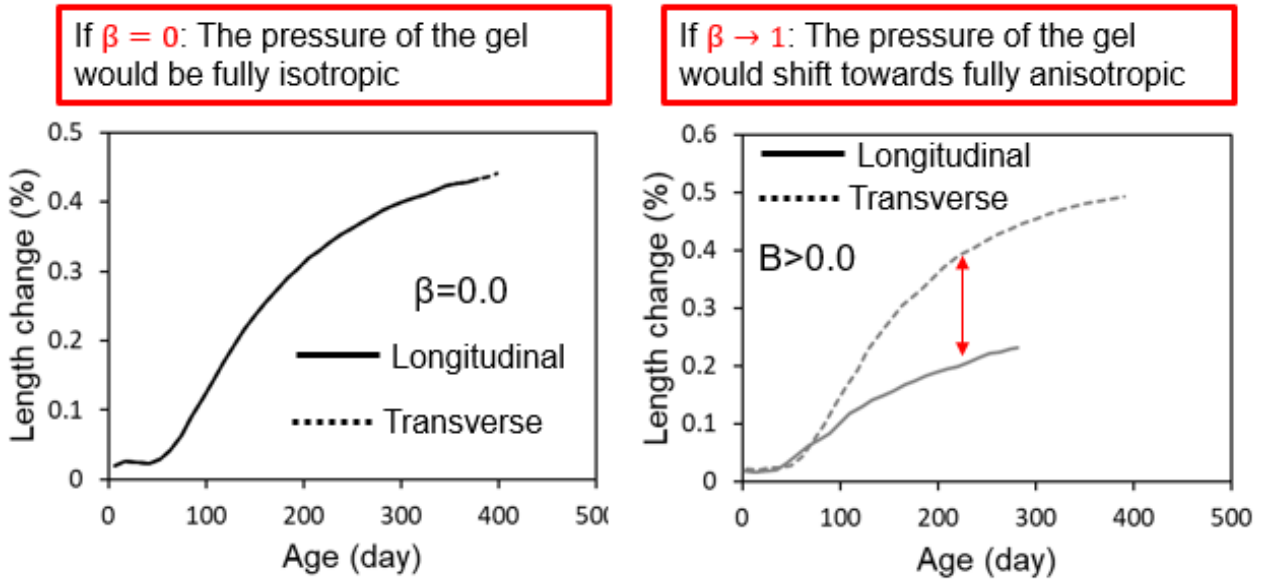


Figure 6.1: Analytical results to display the effect of β parameter, redrawn from Takahashi et al. [69]

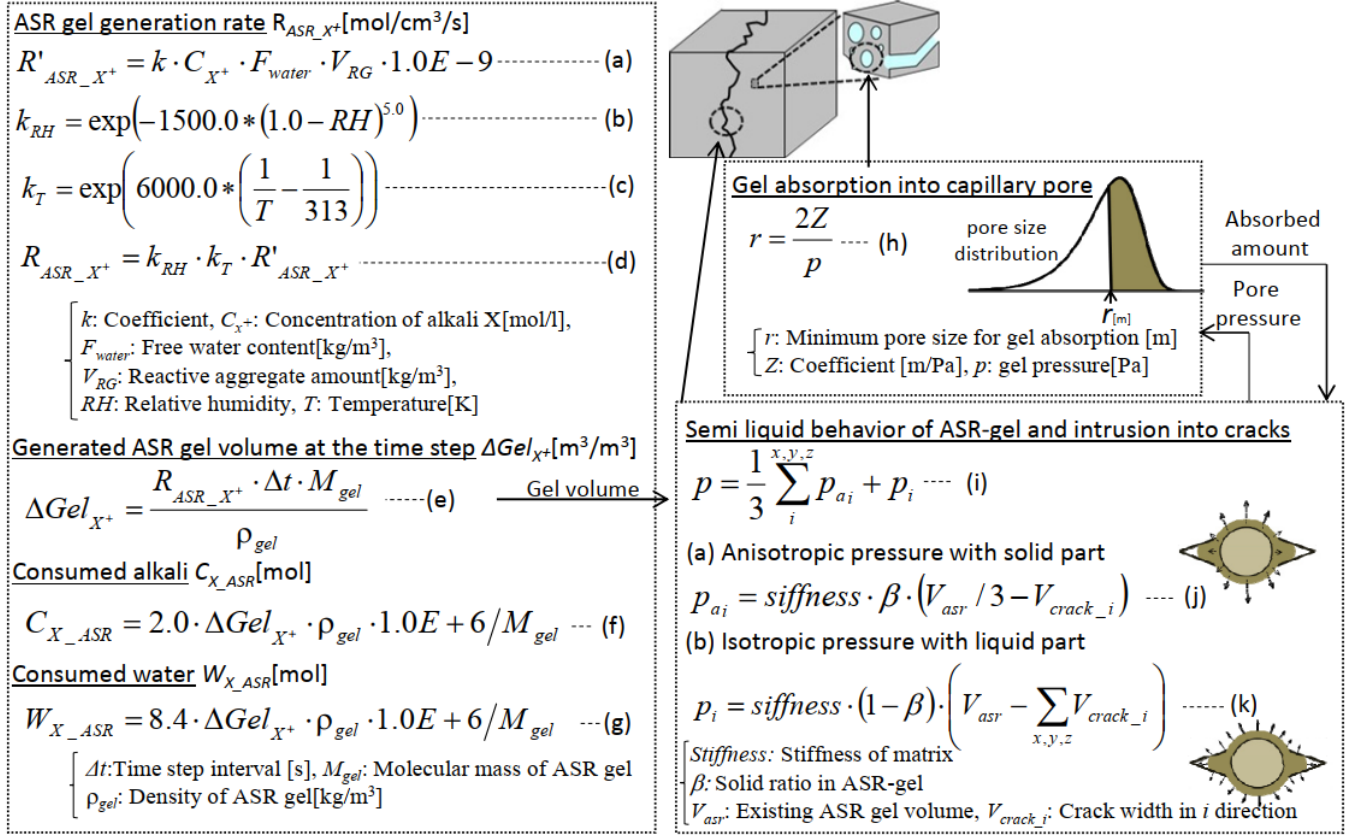


Figure 6.2: Overview calculation scheme of ASR gel generations and stress formations [68, 69, 70, 71]

6.4 Adaptation of Alkali-silica reaction poromechanical model for Expansive additive expansion model

6.4.1 A factor expressing the free precipitation space of expansive hydrates under external restraint, β

To simulate the effect of anisotropy in the system of expansive hydrates, adoption of the β parameter was done. However, the mechanism which cause the anisotropy in the system of ASR and expansive hydrates are different. Unlike ASR gels, the expansive hydrates, ettringites and portlandites, that are formed from the reaction of their parent particles, hauyne and free-lime, respectively, are in the form of precipitated crystals. Thus, β parameter does not represent the solid-liquid state of hydrates as shown in the aforementioned Section [6.3].

In the case where there is no external restraint, the expansive pressure are more or less equal in magnitude. However, when expansion happens with restraint conditions, a

hypothesis could be raised that the anisotropy in the system exists on the basis that the growth and precipitation of expansive hydrates is more favor towards regions where lower restraining forces are acting. This would lead to anisotropy in the system [73].

So, an adaptation of β parameter to reflect the anisotropy due to precipitation space was introduced. If there is no restraint, β is equal to 0, the space will be free for precipitation. Hence, the expansive pressures would be equal in all directions. If there is restraint in a direction, the expansive pressure in that direction would decrease whereby the other direction would increase instead.

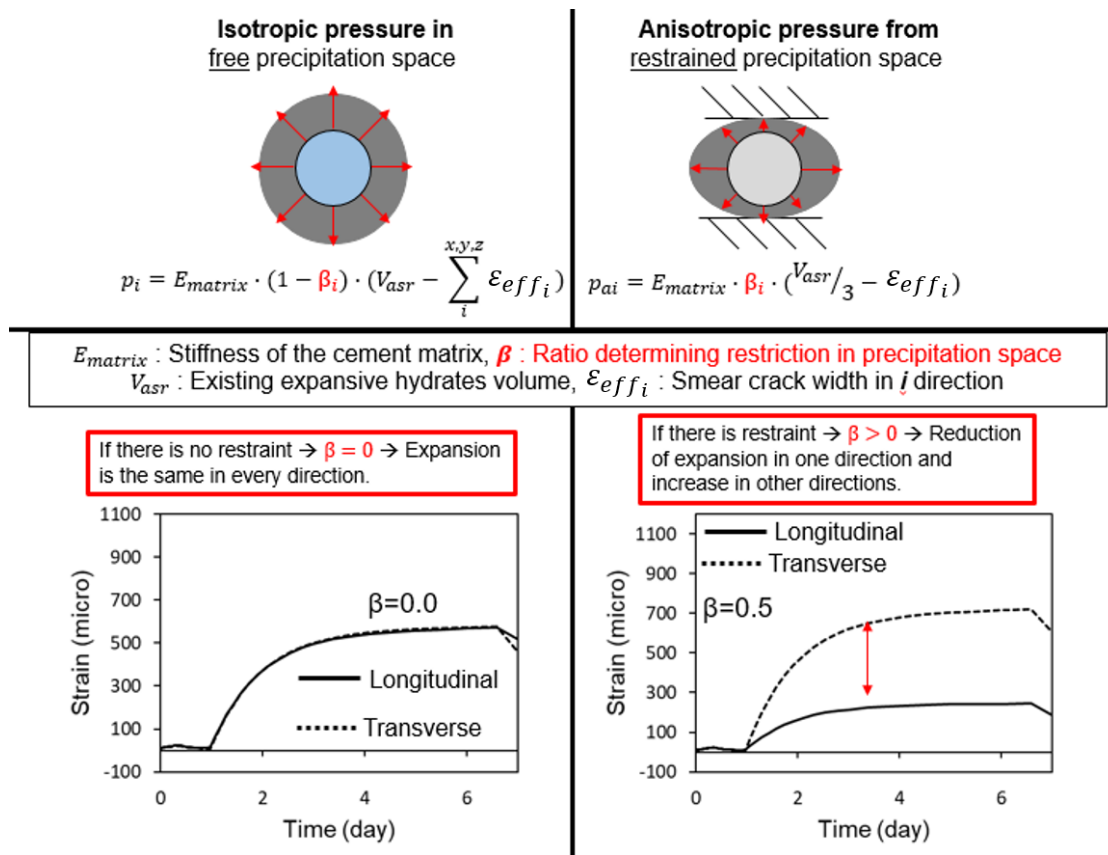


Figure 6.3: Anisotropy model expression for expansive additive system

It is important to keep in mind that E_{matrix} is not simply the bulk modulus of the cement paste. Given that $s.g_{CH} = 2.24$ and $s.g_{Et} = 1.73$, production of ettringite with the same amount would in turn cause more expansion. However, that is clearly not the case as can be seen from Figure 5.13 and 5.14 in which haunyne-based expansive additive shows a lesser expansion characteristic as compared to that of free-lime based expansive additive. Thus, the bulk stiffness should somehow consider the state of effect of crystallization pressure mentioned in Section 5.5. Refer to Figure 5.11, 1% mass of free-lime, the saturation index is roughly 1.5 whereby for 1% mass of haunyne, the saturation index is

about 5. Then, assuming the same temperature during reaction, based on Equation 5.6, the crystallization pressure of ettringite and portlandite are:

$$\begin{aligned} \frac{p_{C_{ett}}}{p_{C_{ch}}} &= \frac{\frac{RT}{v_{ett}} \times SI}{\frac{RT}{v_{ch}} \times SI} \\ &= \frac{5}{\frac{735}{1.5}} \\ &= \frac{5}{33} \\ p_{C_{ett}} &= 0.15 \times p_{C_{ch}} \end{aligned} \quad (6.2)$$

Then, the bulk modulus of for expansive concrete with free-lime expansive additive portion is: $E_{matrix,CH} = b \times E_{matrix}$ where b is the biot coefficient and $E_{matrix,Ett} = b \times 0.15 \times E_{matrix}$ where 0.15 is based on the assumption above. Then, the bulk modulus considered inside the matrix for calculation of pressure is determined by averaging $E_{matrix,CH}$ and $E_{matrix,Ett}$ based on the volume fraction. Further studies shall be done by calculating this pressure generation based on the state of supersaturation instead to express the thermodynamic state more properly. It is also worth mentioning that ε_{eff_i} is the smear crack width in a direction, which corresponds to the apparent strain (strain disregarding the thermal strain) of the concrete or cement paste.

As for tentative consideration, β parameter is considered as a function of reinforcement ratio. In the near future, β parameter would be considered in terms of pressure imposed on the system instead to take into account the effect of external pressure as well as reinforcement conditions.

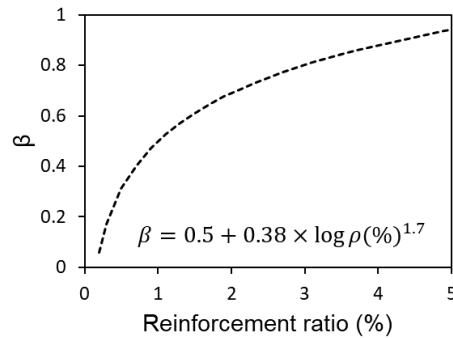


Figure 6.4: Tentative β parameter to express the anisotropic behavior

6.4.2 Analytical results

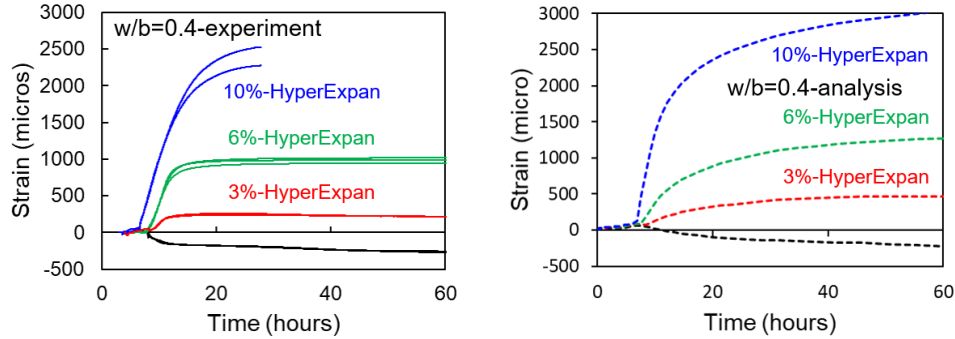


Figure 6.5: Analytical and experimental results on unrestrained $4 \times 4 \times 16 \text{ cm}^3$ cement paste of ordinary Portland cement and Taiheyo HyperExpan expansive additive system (Poromechanical Model)

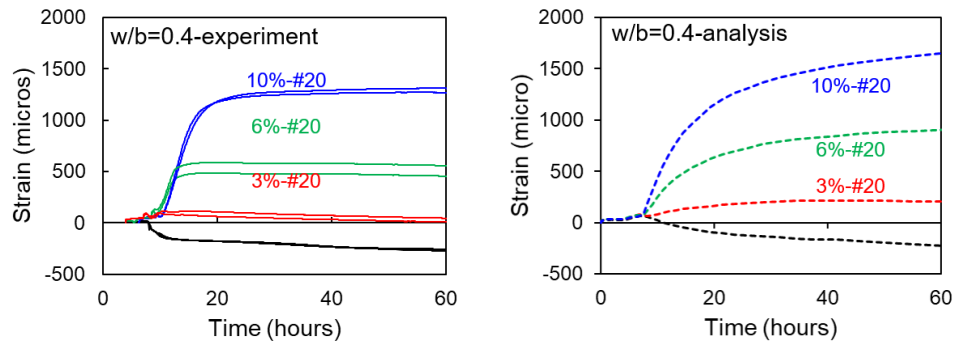


Figure 6.6: Analytical and experimental results on unrestrained $4 \times 4 \times 16 \text{ cm}^3$ cement paste of ordinary Portland cement and Denka #20 expansive additive system (Poromechanical Model)

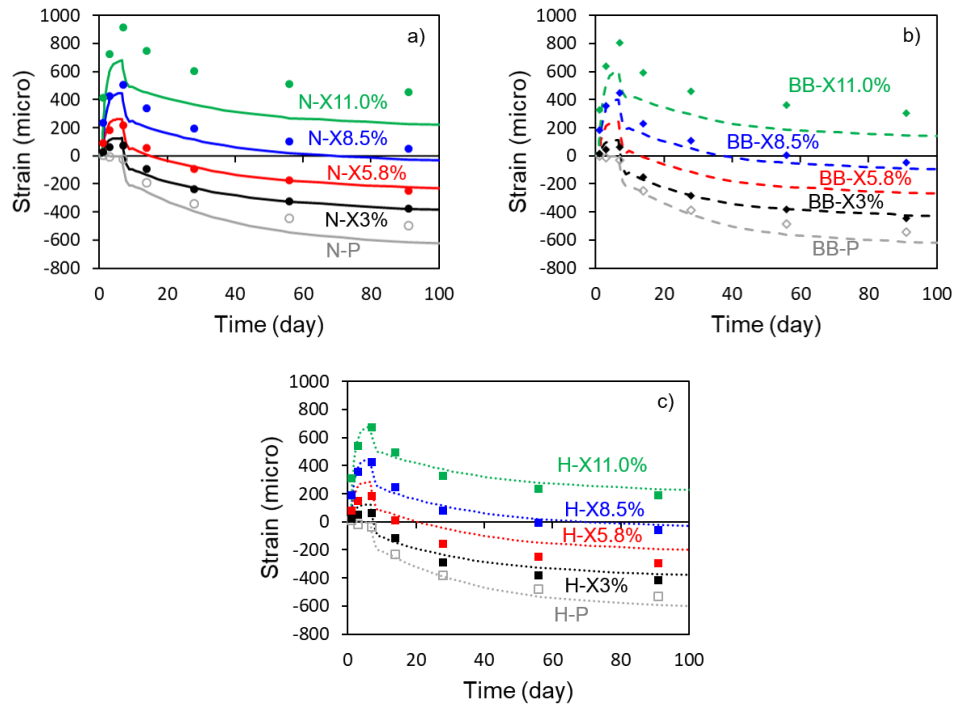


Figure 6.7: Analytical and experimental results on concrete under JIS-A-6202 Standard ($10 \times 10 \times 40 \text{ cm}^3$ with 0.97% of reinforcement ratio (Poromechanical))

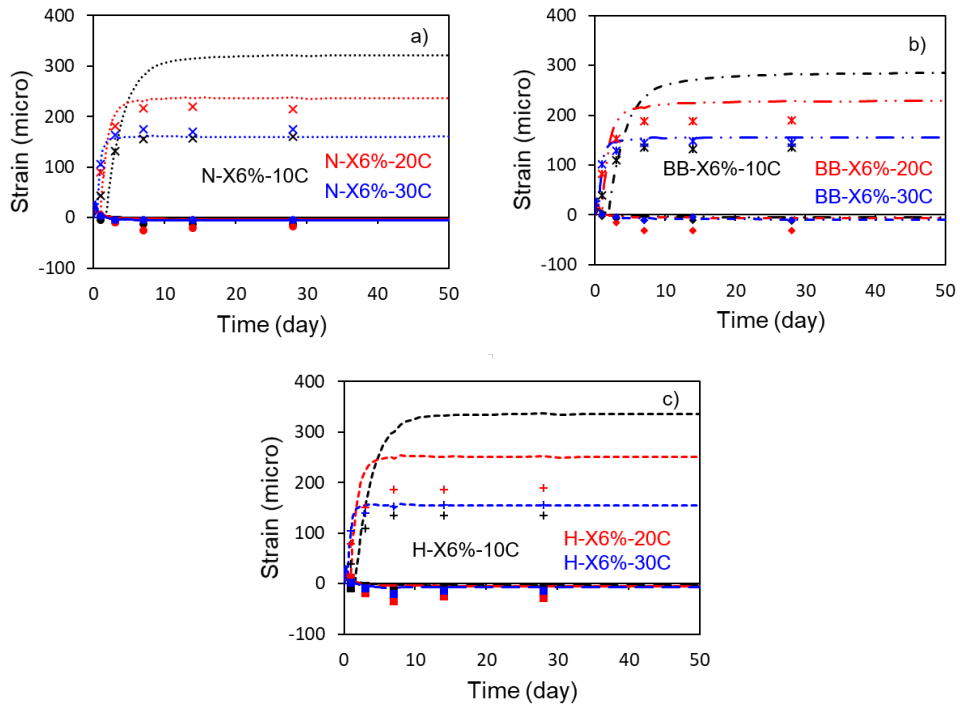


Figure 6.8: Analytical and experimental results on concrete under JIS-A-6202 Standard ($10 \times 10 \times 40 \text{ cm}^3$ with 0.97% of reinforcement ratio with water curing condition at different temperatures (Poromechanical))

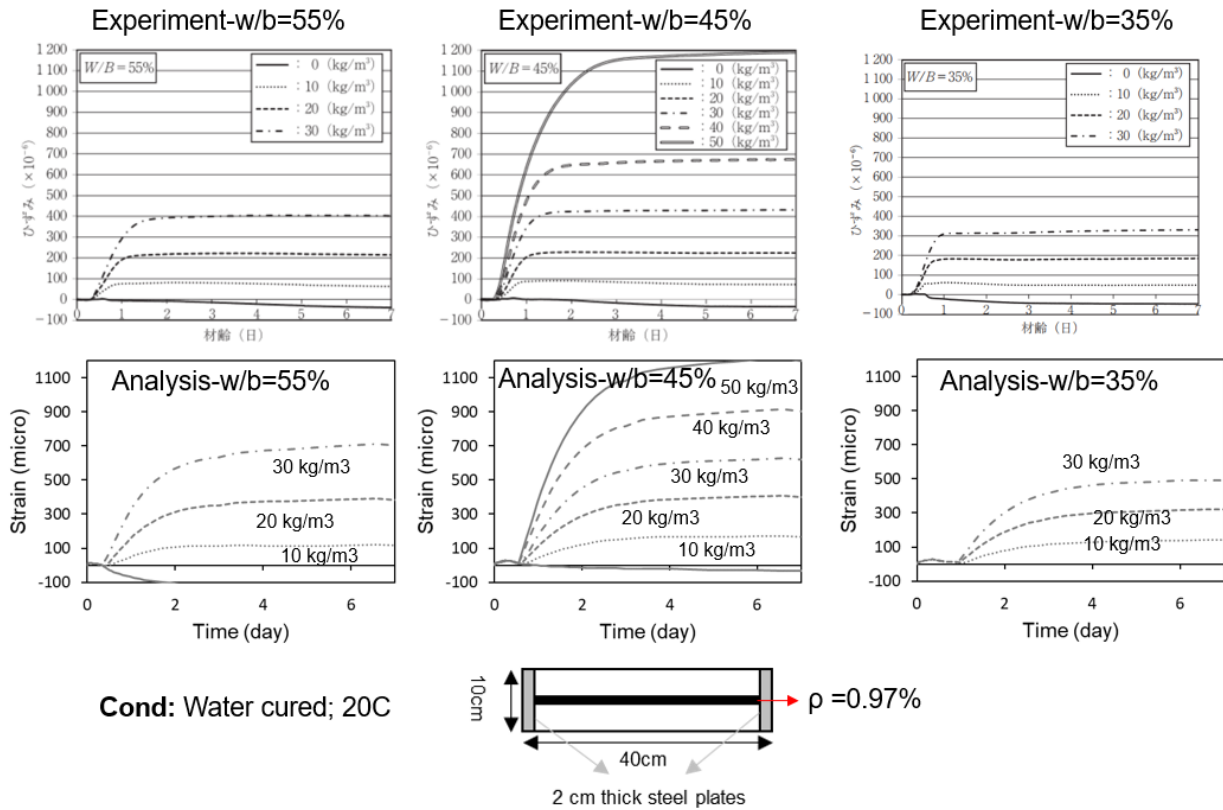


Figure 6.9: Analytical and experimental results on lime-based expansive additive by Tsujino et al. [74] (Poromechanical Model)

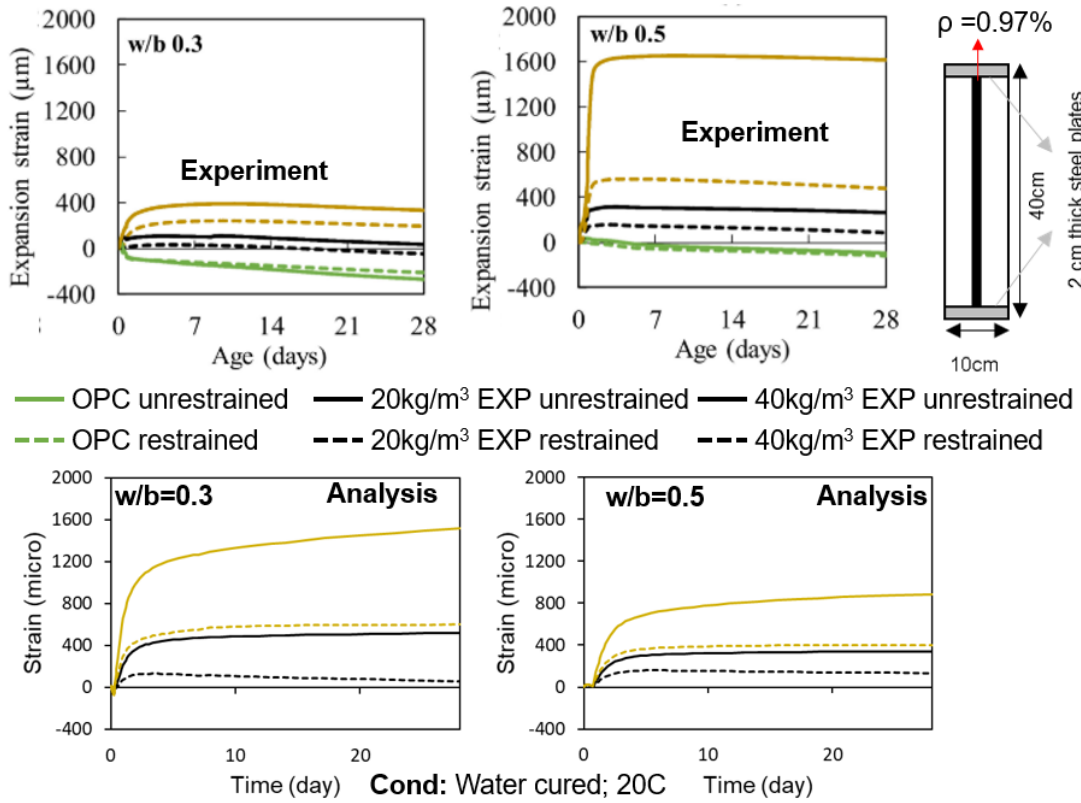


Figure 6.10: Analytical and experimental results on Denka#20 expansive additive by NGUYEN et al. [75] (Poromechanical Model)

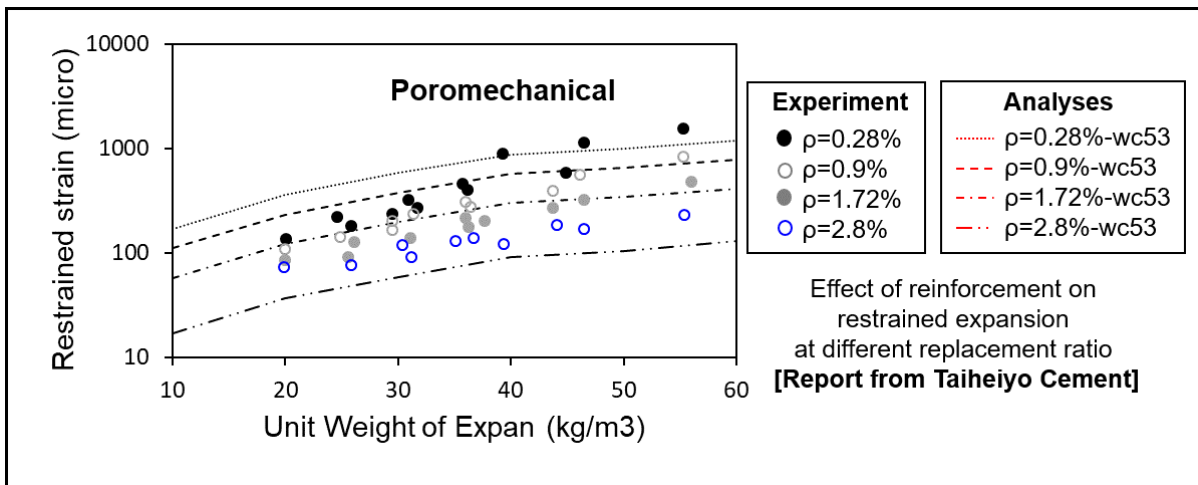


Figure 6.11: Effect of reinforcement on restrained expansion at different replacement ratio based on Expan expansive additive [60] (Poromechanical Model)

6.5 Conclusion

This chapter illustrated how ASR poromechanical model was used to reflect the anisotropic behavior of expansion based on Biot two-phase theorem. In the ASR model, to reflect the anisotropic behavior, a β parameter was introduced to reflect the isotropic portion, contributed by liquid part of ASR gel, and anisotropic portion, contributed by solid part of ASR gel. Then, in the case of expansive additive, a similar approach was done by setting the β parameter to reflect the precipitation space of expansive additives. Based on this modification, the effect of restraints could be captured more properly under the application of ASR poromechanical model using the modified β parameter. The followings could be concluded from this chapter:

- ASR poromechanical model concept was adopted for expansive additive mechanical stress generation to reflect the anisotropic behavior under restrained conditions.
- β parameter based on to reinforcement ratio and direction of restraint was proposed, which shows the the restrained behavior of reinforcement bars could be captured more properly.
- There are still some discrepancy in the analytical results which are at higher replacement ratio, lower w/b ratio and different curing temperatures other than 20°C.

Chapter 7

Conclusion

Growing interest in durability of building structures has marked the crack controlling technology that plays significant role on the durability of concrete structures. Cracking mechanisms have been quantitatively studied on the basis of the largely accumulated research results and some countermeasures have been proposed from the viewpoints of material science, construction technology and structural engineering. One of which is the use of ‘expansive additive’, which would offset the shrinkage strain from reaching the cracking strain. As the name of the material suggests, expansive additives would literally expand the concrete via the existence of expansive hydrates, that could be ettringites (Aft or trisulfoaluminate phase) or portlandites (calcium hydroxide) or magnesium oxide.

Two major applications of expansive additive are: (1) To compensate the shrinkage of concrete due to thermal contraction when mass concrete lowers its temperature from high hydration heat; huge autogenous shrinkage, especially those high-performance concretes and self-compacting concrete that incorporate the use of low w/c and mineral admixtures like silica fume, fly ash and blast furnace slag; drying shrinkage from concrete which are exposed to dry and arid climate (2) To induce chemical pre-stress on pre-cast concrete elements such as pipes, tunnel linings and box culverts. Introduction of chemical pre-stress is achieved by restraining the expansive force of expansive concrete with reinforcing bars to obtain the reaction force. Although a wide range of applications could be done with expansive concrete, there is still a lack of ‘quantitative’ research to estimate the amount of expansion produced by expansive additives. Usually, it depends on the conducted trial tests on different mix proportion and experience of engineers who have dealt with expansive concrete to estimate and judge whether the mix design and amount of expansive additive would be applicable for the concrete structures or not.

On the other hand, the Concrete Laboratory of the University of Tokyo, has been developing a multi-scale thermodynamic analytical platform, coded as DuCOM-COM3,

with the ultimate goal of achieving a ‘lifespan simulator’ of concrete structures. This computational platform incorporates the hydration of cement particles, micro-pore structure development, transports of multi-species and non-linear structural analysis which deals with macroscopic response of structures. Verification of the analytical models to real structures have been performed throughout the years. Therefore, the main goal of this study is to increase the multi-scale chemo-physics model’s capability by adopting an ‘expansive agent’ model, which is based on chemical kinetics and microstructural formation. As a part of this main goal, this study aims to initialize the framework for modeling of expansive additive on the basis of DuCOM-COM3 system as following: (1) Hydration model for the phases in expansive additives based on multi-mineral hydration concept (2) Microstructural formation with expansive additives and (3) Macroscopic expansive pressure that enable the expansive cement paste, mortar and concrete to increase its volume.

In the current DuCOM’s multi-component hydration heat model, main mineral phases, namely hauyne, free-lime and anhydrite, which exist in expansive additives are not present. Therefore, XRD-TGA analyses on various mixtures to determine the reference heat rate of those minerals was executed at 20°C. After obtaining the approximate heat rate of those minerals, the reference heat rate was installed into the multi-component heat model and analytical results were compared with isothermal calorimetric results. However, the installed reference heat rates was considered without the effect of interaction with other mineral phases. Thus, further studies on the effect of temperature and interaction between other species shall be done in the future to enhance the model

Then, based on the amount of expansive hydrates formed as calculated from the heat of hydration model, its volume fraction was added into the microstructure system, which in turns would influence and reflect the compressive strength, modulus of elasticity and moisture transport of the concrete mixing with expansive additive.

As a first approach, linear isotropic crystallization pressure based model was used to model the macroscopic expansive stress. The macroscopic expansive stress is based on poromechanical model approach as a function of Biot coefficient, saturation of crystals and local crystallization pressure. Theoretically speaking, local crystallization pressure should be calculated based on the ionic activity of expansive hydrates. Due to some limitation of DuCOM system to produce the Saturation Index based on the ion concentration in the thermodynamic aqueous-solid system, a fictitious Saturation Index based on unhydrated expansive phases was proposed. With the model, under JIS-A-6202 standard, it could predict the behavior of expansive concrete properly. However, in the case of different restrained conditions, it could not reflect the anisotropic behavior of the concrete correctly. Thus, further investigation into ASR poromechanical model based on two-phase biot

theorem was conducted.

Due to the similar nature of expansion between ASR and expansive additive, as the scale of reaction and mechanism of expansion is closely related, it could be reasonably feasible to apply the ASR poromechanical model for expansive additives. By adapting the ASR poromechanical model to reflect the anisotropic behavior due to precipitation space, the model could capture the restrained effect in a more appropriate manner in uniaxial condition.

As shown in this work, this infant model of expansive additives still needs more improvement to realize the goal of expansive additive model for predicting the expansion capability and assessing possible damage from expansion in the case where high amount of usage is preferable. Thus, in the future, study on the effect of temperature and interaction with cement phase should be the initial priority to further ensure the validity of the heat model, following by the effect of restraints considering stress field. The study at higher replacement ratios, different restraint conditions and crack assessment for chemical prestress usage shall be completed in the next stage before it could be confidently used to assess the any type of expansive additives to be used for both shrinkage compensating and chemical prestressing.

The generalized overview of the expansive agent model could be explained from Figure [7.1](#):

- a** In the initial stage, the omniscient Unhydrated powder particles are dispersed in an ordered state with average interparticle distance, l .
- b** As hydration progresses, inner and outer products are formed, which mainly contain CSHs, CHs and AFts. Once contact points between the adjacent particles have established, expansion would initiate.
- c** The expansive stress would be dependent on the amount of expansive hydrates, namely CHs from Free-Lime and AFts from Hauyne.

The detailed overview into the framework of modeling could be interpreted from Figure [7.1](#):

- A** Based on the composition of the clinker, the hydration degree would be calculated based on Multi-component heat of hydration model proposed by Kishi and Maekawa [\[3\]](#), which is based on the amount of heat release by each component.
- B** Based on the hydration degree, the microstructure of cement matrix is formed whereby fractional volume of expansive hydrates, CHs and AFts, could be determined.

- C** However, not all of the volume of the expansive hydrates are accounted for expansion. In fact, only the volume of expansive hydrates after contact points have been made would contribute in expansion. Then, the macroscopic expansive stress could be expressed through a summation of anisotropic and isotropic pressure.
- D** Superimposing with the current solidification model, which determines the creep and shrinkage of both cement paste and aggregates, this system of calculation could capture the behavior of both expansion and shrinkage of cement matrix based on the initial chemical composition of the binder.
- E** Expansive high-early strength concrete with Denka PCSA at different replacement ratio under JIS-A-6202 Standard

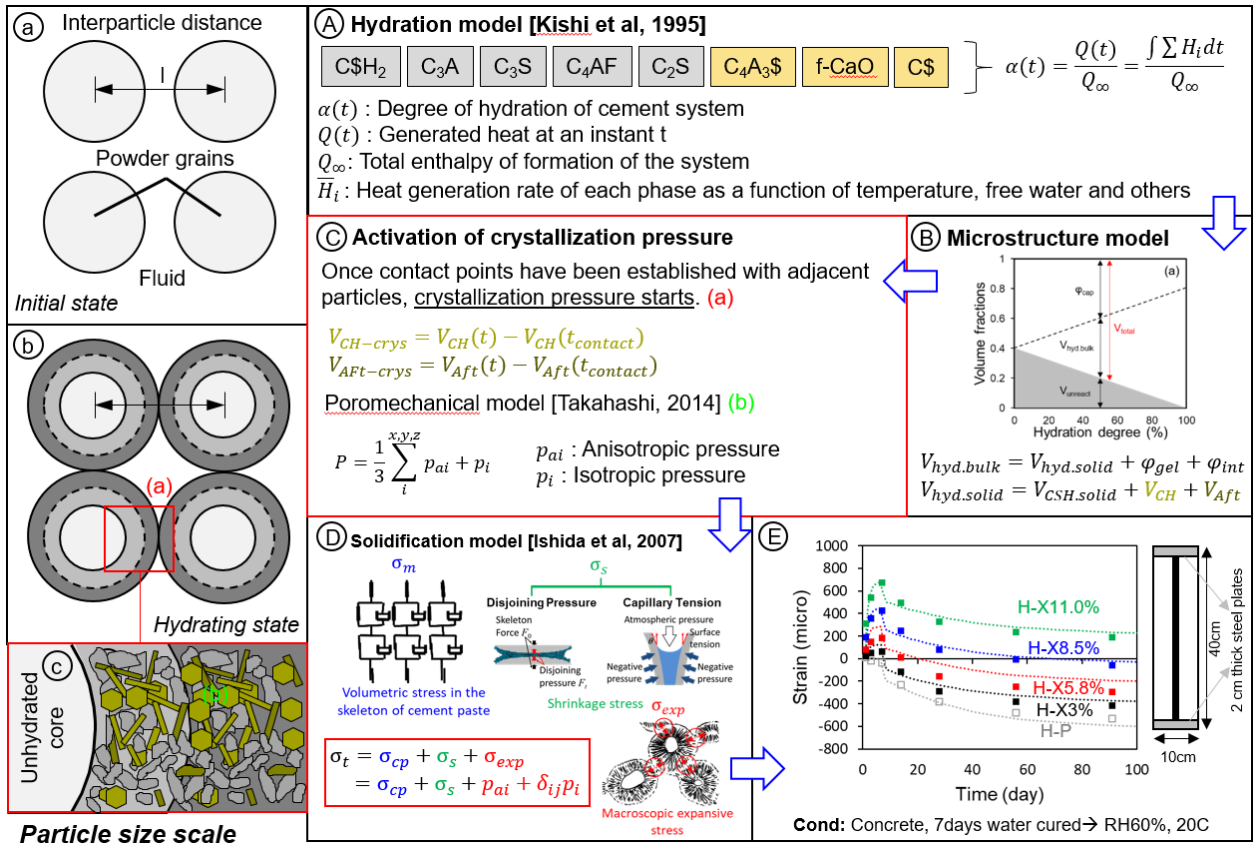


Figure 7.1: Overall modeling framework of expansive additives

Chapter 8

Appendix

8.1 Effect of temperature

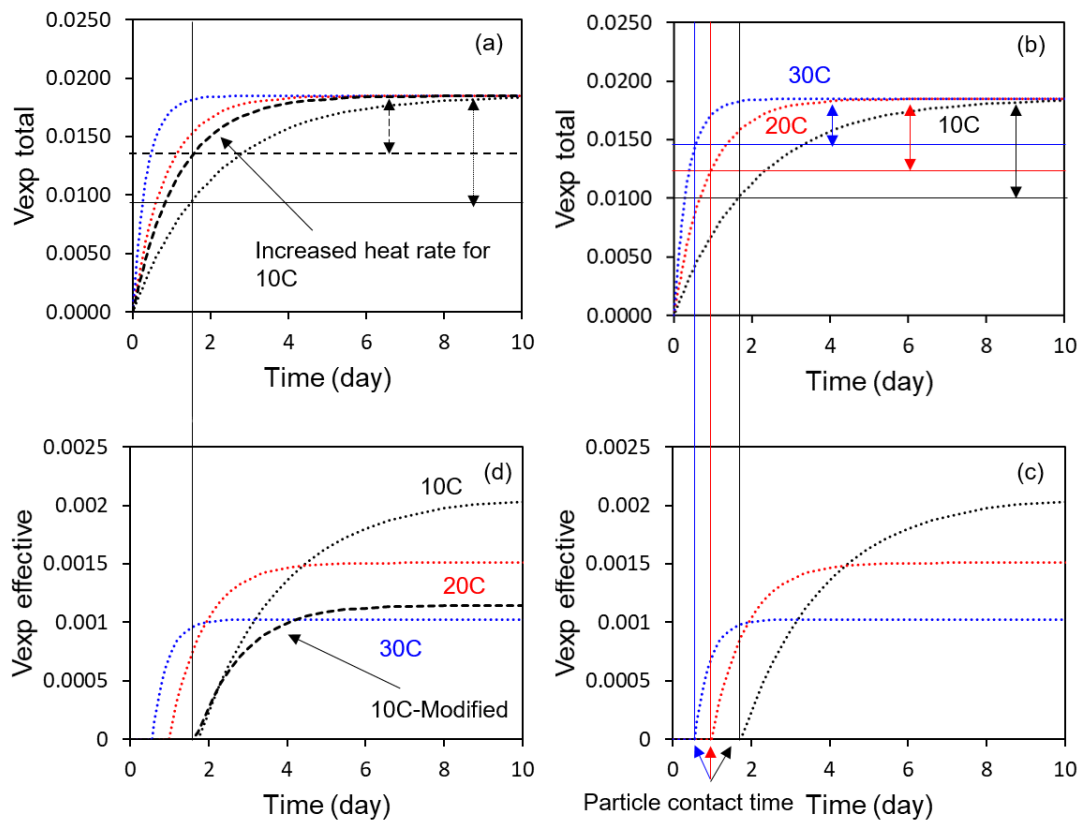


Figure 8.1: (a) Total volume of expansive hydrates focusing on modified heat rate for 10°C; (b) Total volume of expansive additive at 10, 20 and 30°C; (c) Effective expansive hydrates i.e. expansive hydrates after particle contact; (d) Effective expansive hydrates i.e. expansive hydrates after particle contact with the modified heat rate increment for 10°C

Based on the current analytical results regarding the effect of temperature, which was presented in Chapter 6, the behavior at 10 °C could not be properly captured. It was believed that, the rapid the hydration of expansive additive, the early the expansion as well as the intensity of the ultimate expansion as the rigid structure, that could accomodate expansive stress to deform, is established earlier. However, based on the experimental results, it did not appear so as 10 °C showed a delay in expansion while also exhibiting low ultimate expansion. As a matter of fact, Polivka [76] found the same experimental pattern regarding the effect of temperature as there seems to be a peak in ultimate expansion at 20 °C while both 38 °C and 7 °C both showed lower ultimate expansion. Based on the report by Ogawa and Roy [12], expansion occurs on when the concrete gains enough stiffness, then the expansive hydrates which are produced after could contribute to expansion. Thus, one possible reason for the discrepancy in simulation of 10 °C case is that, the current degree hydration of expansive additive phases in 10 °C could be underestimated. And this is reflected in Figure 8.1(a). As an example of free-lime based expansive additive at roughly 6% replacement ratio, the value right here, around 0.018, in Figure 8.1(b) represents the max volume of expansive hydrates i.e. degree of hydration is max. It seems logical as lower temperature reflects lower rate of formation. However, in Figure 8.1(c), if we consider in terms of effective expansive hydrates, 10 °C show the highest amount, leading to the highest expansion in simulation. Now, in Figure 8.1(a), if we assume that the heat rate for 10C is increased to the dashed line, higher than the current simulated result, dot line. Under such modification, the effect of temperature of expansive additive could be reflected to show the peak behavior under different temperature. This maybe is the possible way to modify the model; however, more experimental data is needed, especially hydration degree of expansive additive phases under different temperature to validate the modified model.

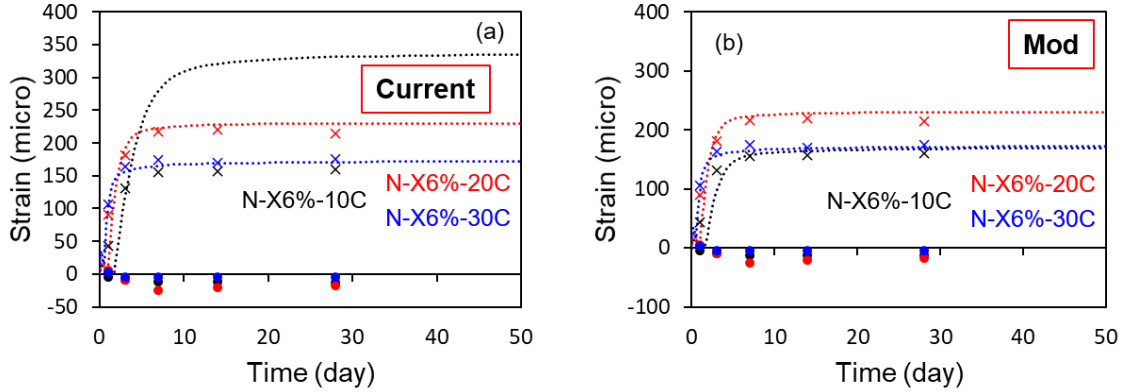


Figure 8.2: (a) Current simulated results due to the effect of temperature based on current expansive additive model (b) Modified simulated results due to the effect of temperature based on current expansive additive model (by increasing the heat rate of expansive additive hydration at lower temperature)

8.2 Chemical prestress

The work of Tsuji [77] was proposed in order to predict the amount of chemical prestress for practical purposes. The idea behind his method was that the tensile strain in restraining bars would be induced by the expansive forces of concrete and the work induced on the bars is the same as that of expansive concrete. Generally speaking, as the degree of restraint increases, the strain of restrained steel reduces, yet the amount of chemical prestress increases as time goes by. The idea of work U produced in the restrained member by the chemical prestress per unit volume of concrete is proposed as follows:

$$U = \frac{1}{2}\sigma_{cp}\varepsilon = \frac{1}{2}\rho E_s \varepsilon^2 \quad (8.1)$$

where σ_{cp} is the chemical prestress, ε is the elongation of restrained steel, ρ is the reinforcement ratio and E_s is the Young's modulus of restrained steel. Thus, the following equation was adopted as a preliminary calculation of prestress induced by expansive additive model in DuCOM.

The experiment that were used to check with the model was from Oshio et al. [78], which were high-strength expansive cement with free-lime type expansive additives and high early-strength cement at water-to-binder ratio of 0.3. The specimens were cured in water until the twenty-eighth day at 20 °C. Different reinforcement ratios were used for the test. The simulated results are shown in comparison with experimental results as follows:

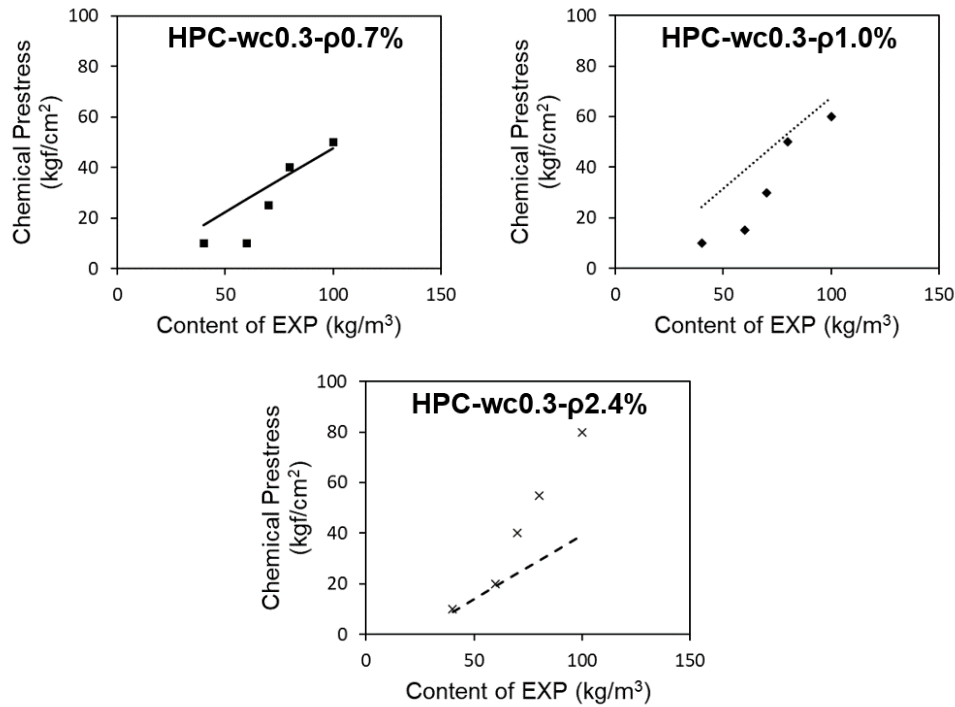


Figure 8.3: Simulated versus experimental chemical prestress based on experiment conducted by Oshio et al. [78]

Preliminarily, by embedding this chemical prestress formula as a function to predict the chemical prestress in DuCOM-COM3, the qualitative trend could be captured. However, as previously shown in Chapter 6, the prediction for strain at high replacement ratio and low water-to-binder is still not quantitatively correct. Therefore, only after those issues have been investigated and fixed, this embedded model of chemical prestress could be used confidently to predict chemical prestress in real structures.

8.3 Interaction between expansive additive and cement phases

It is understood that one of the limitations in the current heat of hydration model is the interaction between expansive additive and cement phases. Morioka [21] conducted a study to find the interaction between alite and aluminate phase on two types of expansive additives. XRD-Rietveld analyses were conducted on different mix proportion as expressed in Table 8.1. According to that study, it was found that interaction between expansive additive and cement phases exists as presented in Figure 8.4(a) and Figure 8.4(b). However, quantitatively, it could not be used to invoke a model. Nonetheless, simulations

based on the expansive additive heat of hydration model were conducted based on the mix proportions as stated in Morioka [21].

Table 8.1: Mineral composition in - (1) CSA & (2) FL Expansive additive

Materials	Phases (Weight %)						
	C_3A	C_2S	C_3S	C_4AF	f-CaO	$C_4A_3\bar{S}$	$C\bar{S}$
CSA	-	-	-	-	17.0	27.0	46.0
FL	-	-	20.4	-	43.0	-	30.9

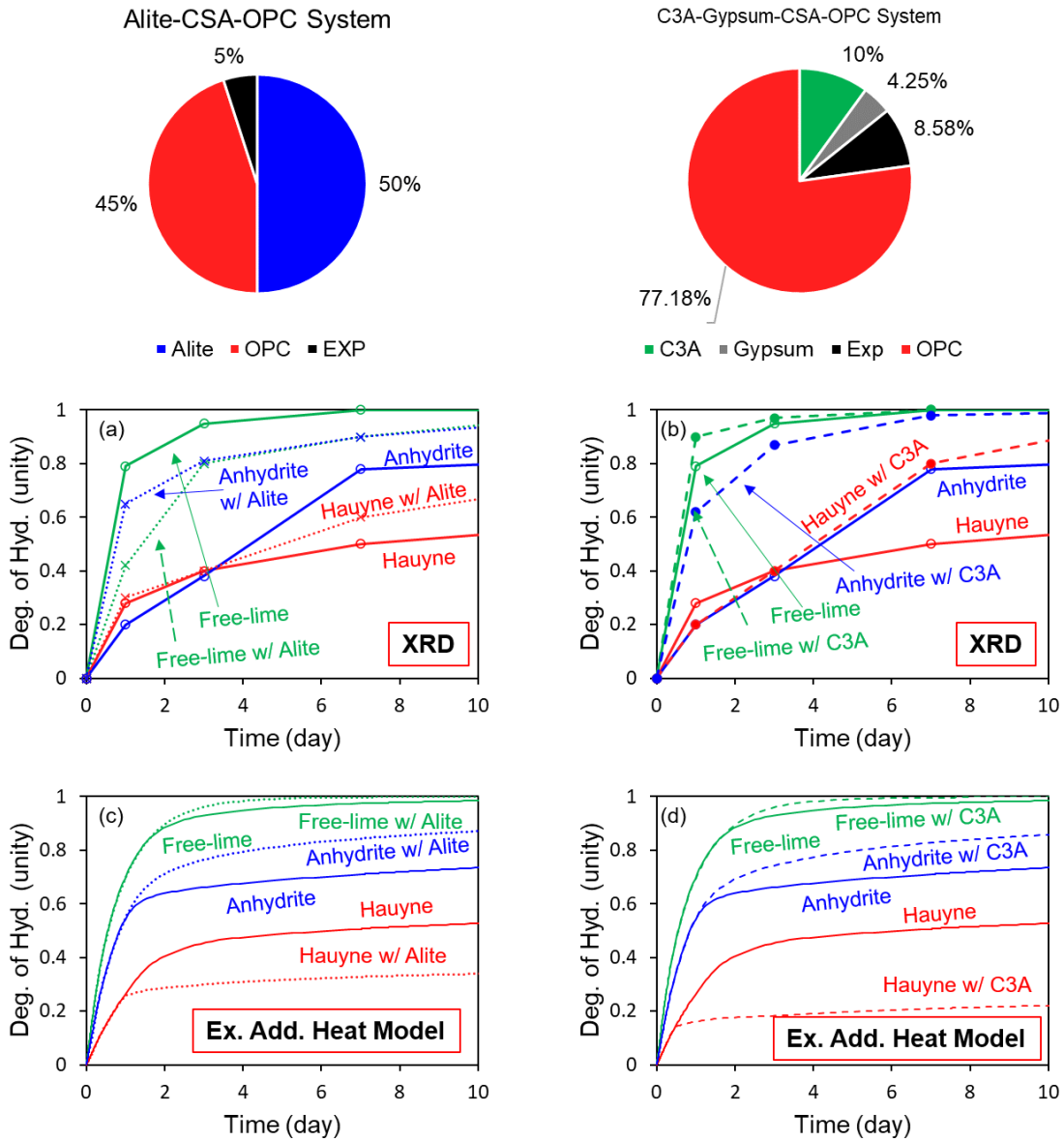


Figure 8.4: Interaction between cement and expansive additive phases. (a) and (b) are experimental results redrawn from Morioka [21]; (c) and (d) are analytical results from DuCOM’s simulations

In the current simulated results, no interaction between the phases is considered in the model. However, based on the mineral compositions, hydration degree of the phases would change due to the fact that the heat release between different amount of phases would affect the temperature, consequently affect the heat rate. However, further investigations are still needed to quantitatively determine parameters that show the interactions between the phases especially in case of system of C_3A and Hauayne as the reactions of these two phases both require sulfates to react in forming ettringites that cause the expansion.

Bibliography

- [1] K. Maekawa et al. *Multi-scale Modeling of Structural Concrete*. Taylor & Francis, 2007. ISBN 9783540773405.
- [2] K. Maekawa et al. *Non-Linear Mechanics of Reinforced Concrete*. Spon Press: London, 2003. ISBN 9780415271264.
- [3] T. Kishi and K. Maekawa. Multi-component model for hydration heat of portland cement. *Doboku Gakkai Ronbunshu*, 1995(526):97–109, 1995. doi: 10.2208/jscej.1995.526_97.
- [4] Bryant Mather. Expansive cements. Technical report, ARMY ENGINEER WATERWAYS EXPERIMENT STATION VICKSBURG MS, 1970.
- [5] Henry Lossier and A Caguol. Expanding cements and their application—self-stressed concrete. *Le Genie Civil (Paris)*, 121(8):61–65, 1944.
- [6] H Lafuma. Expansive cement. In *Proc. of the 3rd Inter. Symp. on the Chem. of Cement*, pages 581–597, 1952.
- [7] A Klein and GE Troxell. Studies of calcium sulfoaluminate admixtures for expansive cements. pros. 1958.
- [8] S. Nagataki and H. Gomi. Expansive admixtures (mainly ettringite). *Cement and Concrete Composites*, 20(2-3):163–170, 1998. ISSN 09589465. doi: 10.1016/S0958-9465(97)00064-4.
- [9] Min Deng, Dongwen Hong, Xianghui Lan, and Mingshu Tang. Mechanism of expansion in hardened cement pastes with hard-burnt free lime. *Cement and concrete research*, 25(2):440–448, 1995.
- [10] W Kurdowski and A Thiel. On the role of free calcium oxide in expansive cements. *Cement and Concrete Research*, 11(1):29–40, 1981.

-
- [11] Craig W Hargis, Ana Paula Kirchheim, Paulo JM Monteiro, and Ellis M Gartner. Early age hydration of calcium sulfoaluminate (synthetic ye'elinite, c4a3s) in the presence of gypsum and varying amounts of calcium hydroxide. *Cement and Concrete Research*, 48:105–115, 2013.
- [12] K t Ogawa and DM Roy. C4a3s hydration, ettringite formation, and its expansion mechanism: Ii. microstructural observation of expansion. *Cement and Concrete Research*, 12(1):101–109, 1982.
- [13] P. K. Mehta. Effect of Lime on Hydration of Pastes Containing Gypsum and Calcium Aluminates or Calcium Sulfoaluminate. *Journal of the American Ceramic Society*, 56(6):315–319, 1973. ISSN 15512916. doi: 10.1111/j.1151-2916.1973.tb12503.x.
- [14] V Alunno Rossetti, G Chiochio, and AE Paolini. Expansive properties of the mixture c4ash12-2cs i. an hypothesis on the expansion mechanism. *Cement and Concrete Research*, 12(5):577–585, 1982.
- [15] HFW Taylor, C Famy, and KL Scrivener. Delayed ettringite formation. *Cement and concrete research*, 31(5):683–693, 2001.
- [16] Ryuichi Komatsu, Norihiro Mizukoshi, Koji Makida, and Katsuo Tsukamoto. In-situ observation of ettringite crystals. *Journal of crystal growth*, 311(3):1005–1008, 2009.
- [17] Vagn Johansen, Niels Thaulow, and Jan Skalny. Simultaneous presence of alkali—silica gel and ettringite in concrete. *Advances in Cement Research*, 5(17):23–29, 1993.
- [18] D Gastaldi, G Paul, L Marchese, S Irico, E Boccaleri, S Mutke, L Buzzi, and F Canonico. Hydration products in sulfoaluminate cements: evaluation of amorphous phases by xrd/solid-state nmr. *Cement and Concrete Research*, 90:162–173, 2016.
- [19] MD Cohen. Theories of expansion in sulfoaluminate-type expansive cements: schools of thought. *Cement and Concrete Research*, 13(6):809–818, 1983.
- [20] A. Telesca, M. Marroccoli, M. L. Pace, M. Tomasulo, G. L. Valenti, and P. J.M. Monteiro. A hydration study of various calcium sulfoaluminate cements. *Cement and Concrete Composites*, 53:224–232, 2014. ISSN 09589465. doi: 10.1016/j.cemconcomp.2014.07.002. URL <http://dx.doi.org/10.1016/j.cemconcomp.2014.07.002>.
- [21] M Morioka. Hydration reaction of caliumsulphoaluminate-type expansive additive. *Cement Science and Concrete Technology*, 52:2–7, 1998.

- [22] Irvin A Chen, Craig W Hargis, and Maria CG Juenger. Understanding expansion in calcium sulfoaluminate–belite cements. *Cement and Concrete Research*, 42(1):51–60, 2012.
- [23] Nguyen Duc Van, Hyeonggil Choi, and Yukio Hama. Modeling early age hydration reaction and predicting compressive strength of cement paste mixed with expansive additives. *Construction and Building Materials*, 223:994–1007, 2019.
- [24] Hyeonggil Choi, Myungkwan Lim, Ryoma Kitagaki, Takafumi Noguchi, and Gyuyong Kim. Restrained shrinkage behavior of expansive mortar at early ages. *Construction and Building Materials*, 84:468–476, 2015.
- [25] Hyeonggil Choi, Myungkwan Lim, Heesup Choi, Takafumi Noguchi, and Ryoma Kitagaki. Modelling of creep of concrete mixed with expansive additives. *Magazine of concrete research*, 67(7):335–348, 2015.
- [26] Hyeonggil Choi and Takafumi Noguchi. Modeling of mechanical properties of concrete mixed with expansive additive. *International Journal of Concrete Structures and Materials*, 9(4):391–399, 2015.
- [27] T.C. Powers and T.L. Brownyard. Studies of the physical properties of hardened Portland cement past, Part 9: General summary of findings on the properties of hardened Portland cement paste. *J. American. Con. Inst.*, 18(3):972–992, 1947.
- [28] Y. Otabe and T. Kishi. Evaluation of strength development based on hydrate formation in initial pore volume. *Japan Concrete Institute Annual Paper*, 1(27):571–576, 2005.
- [29] K.K. Schiller. Strength of porous materials. *Cement and Concrete Research*, 1(4):419 – 422, 1971. ISSN 0008-8846. doi: [https://doi.org/10.1016/0008-8846\(71\)90035-4](https://doi.org/10.1016/0008-8846(71)90035-4). URL <http://www.sciencedirect.com/science/article/pii/0008884671900354>.
- [30] ASTM ASTM C305-20. Standard practice for mechanical mixing of hydraulic cement pastes and mortars of plastic consistency. Technical report, ASTM, 2020.
- [31] Karen Scrivener, Ruben Snellings, and Barbara Lothenbach. *A practical guide to microstructural analysis of cementitious materials*. Crc Press, 2018.
- [32] Ippei Maruyama and Go Igarashi. Cement reaction and resultant physical properties of cement paste. *Journal of Advanced Concrete Technology*, 12(6):200–213, 2014.

- [33] D. L Bish and SA Howard. Quantitative phase analysis using the rietveld method. *Journal of Applied Crystallography*, 21(2):86–91, 1988.
- [34] I. Maruyama et al. Rate of Hydration of Alite and Belite in Portland Cement. *Journal of Structural and Construction Engineering (Transactions of AIJ)*, 75(650):681–688, 2010. ISSN 1340-4202. doi: 10.3130/aijs.75.681.
- [35] Peter Hewlett and Martin Liska. *Lea’s chemistry of cement and concrete*. Butterworth-Heinemann, 2019.
- [36] M. Arai et al. *Chemistry of Cement Materials*. Dai-Nippon Tosho Publishing Co., Ltd., Tokyo, 1984.
- [37] D.P. Bentz. Three-dimensional computer simulation of portland cement hydration and microstructure development. *Journal of the American Ceramic Society*, 2(80), 7 1997.
- [38] R.H. Bogue. *Chemistry of Portland Cement*. 2 edition, 1955.
- [39] P. Catharin. Heat of hydration and strength development. *Betonwerk+ Fertigteil-Technik*, pages 539–544, 1978.
- [40] W. et al Lerch. Heat of hydration of portland cement pastes. *Part of Bureau of Standards Journal of Research*, pages 645–664, 1934.
- [41] E.S. Newman et al. Heat of hydration and transition of calcium sulfate. *Part of Bureau of Standards Journal of Research*, (20):825–836, 1938.
- [42] S. Skalamprinos et al. Enthalpy of formation of ye’elimite and ternesite. *J Therm Anal Calorim*, (131):2345–2359, 2018.
- [43] H.F.W. Taylor. *Cement Chemistry*. 2 edition, 1997.
- [44] H. Woods et al. Effect of composition of portland cement on heat evolved during hardening. *Ind. Eng. Chem.*, (11):1207–1214, 1932.
- [45] Mateusz Wyrzykowski, Giovanni Terrasi, and Pietro Lura. Expansive high-performance concrete for chemical-prestress applications. *Cement and Concrete Research*, 107:275–283, 2018.
- [46] Olivier Coussy. *Poromechanics*. John Wiley & Sons, 2004.
- [47] Olivier Coussy. Poromechanics of freezing materials. *Journal of the Mechanics and Physics of Solids*, 53(8):1689–1718, 2005.

- [48] Michael Steiger. Crystal growth in porous materials—i: The crystallization pressure of large crystals. *Journal of crystal growth*, 282(3-4):455–469, 2005.
- [49] Florian Osselin, Antonin Fabbri, Teddy Fen-Chong, Jean-Michel Pereira, Arnault Lassin, and Patrick Dangla. Poromechanics of salt nucleation within an unsaturated reservoir rock. In *Poromechanics V: Proceedings of the Fifth Biot Conference on Poromechanics*, pages 772–781, 2013.
- [50] RM Espinosa, L Franke, and G Deckelmann. Model for the mechanical stress due to the salt crystallization in porous materials. *Construction and Building Materials*, 22(7):1350–1367, 2008.
- [51] Rosa M Espinosa-Marzal, Andrea Hamilton, Megan McNall, Kathryn Whitaker, and George W Scherer. The chemomechanics of crystallization during rewetting of limestone impregnated with sodium sulfate. *Journal of materials research*, 26(12):1472–1481, 2011.
- [52] Xuerun Li, Yu Zhang, Xiaodong Shen, Qianqian Wang, and Zhigang Pan. Kinetics of calcium sulfoaluminate formation from tricalcium aluminate, calcium sulfate and calcium oxide. *Cement and concrete research*, 55:79–87, 2014.
- [53] GH Nancollas. The crystal growth of sparingly soluble salts. *Croatica chemica acta*, 45(1):225–231, 1973.
- [54] F Schaube, L Koch, A Wörner, and H Müller-Steinhagen. A thermodynamic and kinetic study of the de- and rehydration of $\text{Ca}(\text{OH})_2$ at high H_2O partial pressures for thermo-chemical heat storage. *Thermochimica acta*, 538:9–20, 2012.
- [55] Carl W Correns. Growth and dissolution of crystals under linear pressure. *Discussions of the Faraday society*, 5:267–271, 1949.
- [56] Piyush Chaunsali and Paramita Mondal. Influence of calcium sulfoaluminate (CSA) cement content on expansion and hydration behavior of various ordinary portland cement-CSA blends. *Journal of the American Ceramic Society*, 98(8):2617–2624, 2015.
- [57] Piyush Chaunsali. *Early-age hydration and volume change of calcium sulfoaluminate cement-based binders*. PhD thesis, University of Illinois at Urbana-Champaign, 2015.
- [58] Ellis M Gartner, Fulvio J Tang, and Stuart J Weiss. Saturation factors for calcium hydroxide and calcium sulfates in fresh portland cement pastes. *Journal of the American Ceramic Society*, 68(12):667–673, 1985.

- [59] F-J Ulm, G Constantinides, and Franz H Heukamp. Is concrete a poromechanics materials?—a multiscale investigation of poroelastic properties. *Materials and structures*, 37(1):43–58, 2004.
- [60] Report on expansion (for structure) from taiheiyo cement group.
- [61] Koichi Maekawa and Chikako Fujiyama. Rate-dependent model of structural concrete incorporating kinematics of ambient water subjected to high-cycle loads. *Engineering computations*, 2013.
- [62] Yuya Takahashi, Shimpei Ogawa, Yasushi Tanaka, and Koichi Maekawa. Scale-dependent asr expansion of concrete and its prediction coupled with silica gel generation and migration. *Journal of Advanced Concrete Technology*, 14(8):444–463, 2016.
- [63] Afshin Mohammadi, Ebrahim Ghiasvand, and Mahmoud Nili. Relation between mechanical properties of concrete and alkali-silica reaction (asr); a review. *Construction and Building Materials*, 258:119567, 2020.
- [64] Farshad Rajabipour, Eric Giannini, Cyrille Dunant, Jason H Ideker, and Michael DA Thomas. Alkali–silica reaction: current understanding of the reaction mechanisms and the knowledge gaps. *Cement and Concrete Research*, 76:130–146, 2015.
- [65] George W Scherer. Structure and properties of gels. *Cement and Concrete Research*, 29(8):1149–1157, 1999.
- [66] Xiaoqiang Hou, R James Kirkpatrick, Leslie J Struble, and Paulo JM Monteiro. Structural investigations of alkali silicate gels. *Journal of the American Ceramic Society*, 88(4):943–949, 2005.
- [67] Asghar Gholizadeh Vayghan, Farshad Rajabipour, and James L Rosenberger. Composition–rheology relationships in alkali–silica reaction gels and the impact on the gel’s deleterious behavior. *Cement and Concrete Research*, 83:45–56, 2016.
- [68] Y Takahashi, K Shibata, M Maruno, and K Maekawa. Uniaxial restraint tests under high-stress conditions and a chemo-hygral model for asr expansion. In *CONCREEP 10*, pages 1061–1065. 2015.
- [69] Yuya Takahashi, Koki Shibata, and Koichi Maekawa. Chemo-hygral modeling of structural concrete damaged by alkali silica reaction. In *Proceedings of the 1st Ageing of Materials & Structures 2014 Conference*, pages 424–431, 2014.

- [70] Yuya Takahashi, Yasushi Tanaka, and Koichi Maekawa. Chemo-hygral model for asr expansion and its effects on fatigue lives of bridge slabs. In *COMPLAS XIII: proceedings of the XIII International Conference on Computational Plasticity: fundamentals and applications*, pages 944–955. CIMNE, 2015.
- [71] Yuya Takahashi, Shimpei Ogawa, Yasushi Tanaka, and Koichi Maekawa. Scale-dependent asr expansion of concrete and its prediction coupled with silica gel generation and migration. *Journal of Advanced Concrete Technology*, 14(8):444–463, 2016.
- [72] Fuyuan Gong, Yuya Takahashi, and Koichi Maekawa. Strong coupling of freeze-thaw cycles and alkali silica reaction-multi-scale poro-mechanical approach to concrete damages. *Journal of Advanced Concrete Technology*, 15(7):346–367, 2017.
- [73] M Ish-Shalom and Arnon Bentur. Properties of type k expansive cement of pure components iii. hydration of pure expansive component under varying restraining conditions. *Cement and Concrete Research*, 5(2):139–152, 1975.
- [74] M Tsujino, R Yuasa, and H Hashida. Method of test for restrained expansion of expansive concrete using a cylindrical mold. *Concr. J*, 52:519–527, 2014.
- [75] Duc Van NGUYEN, Emika KUROIWA, Jihoon KIM, Hyeonggil CHOI, and Yukio HAMA. Influence of restrained condition on mechanical properties, frost resistance, and carbonation resistance of expansive concrete. 2020.
- [76] Milos Polivka. Factors influencing expansion of expansive cement concretes. *Special Publication*, 38:239–250, 1973.
- [77] Yukikazu Tsuji. Method of predicting chemical prestress. *The Cement Association of Japan*, 27:189–192, 1973.
- [78] Akira Oshio, Yoshinobu Goto, Tomohiro Imai, and Yoshitaka Ohmori. Basic experiments for uniaxially restrained high strength expansive cement concrete. *The Cement Association of Japan*, 27:179–181, 1973.